THE UNIVERSITY OF CALGARY

Investigation of Interfacial Mass Transfer in Vapour Extraction Process

by

Arash Boustani

A THESIS

SUBMITTED TO THE FACULTY OF GRADUATE STUDIES

IN PARTIAL FULFILLMENT OF THE REQUIREMENTS FOR THE

DEGREE OF MASTER OF SCIENCE IN CHEMICAL ENGINEERING

DEPARTMENT OF CHEMICAL AND PETROLEUM ENGINEERING

CALGARY, ALBERTA

MAY, 2001

ABSTRACT

Vapex (vapor extraction) is a relatively new process for the recovery of heavy oil and bitumen that involves the injection of a vaporized solvent to reduce the viscosity of the oil. The diluted oil is then allowed to drain into a production well under the influence of gravity. It is a potentially economic process that can be applied to reservoirs that are not suitable for thermal recovery method. In addition, the process has the potential to sequester greenhouse gases, and is capable of in situ upgrading of heavy oil.

The primary objective of this research was to identify the main processes governing the interfacial mass transfer of solvent into bitumen. The influence of convective dispersion and concentration-dependent-diffusivity on mass transfer in Vapex was examined. This research began with experiments in Hele-Shaw cell to verify the validity of the existing analytical models of Vapex. Experiments in Hele-Shaw cell revealed that a convective dispersion due to momentum variation is created which in turn enhances the mass transfer of solvent into bitumen.

The research was then extended to experiments in Sandpack to investigate the role of convective dispersion in porous media. Due to the existence of sand particles making up the porous media, the nature of the dispersion is different than that in Hele-Shaw cell. Results of the sandpack experiments conducted in this work and the experiments reported by others revealed that the dispersion in Vapex was considerably more pronounced than what would be predicted from the correlations reported in the literature. A new correlation incorporating the viscosity ratio and the Peclet number was developed and validated against the available experimental results.

ACKNOWLEDGEMENTS

I would like to extend my deepest gratitude to my supervisor, Dr. Brij B. Maini, for providing me the opportunity to work on this project. I highly appreciate his continuous support, encouragement and guidance throughout this work. His unconditional availability and desire to share his scientific knowledge and experience were exceptional elements for nourishing the passion to carry out this research.

I would also like to greatly appreciate Dr. Roger Butler for his technical input and generosity in providing some of the experimental equipment used in these experiments.

Thanks are also extended to Dr. Anil Mehrotra, Dr. Tony Settari, Dr. Mehran Pooladi Darvish, Dr. Carolyn Hyndman and Dr. Swapan Das for their technical input and suggestions and their valuable time throughout this work.

I would like to thank the helpful and friendly support of Mr. Paul Stanislav and Mr. Clarence Urness. I would also like to thank all the staff of electronics and engineering technical staff for preparation and installation of devices used in our experiments.

I am very grateful to Dr. Anil Mehrotra, Amber Spence, Sharon Hutton, Dolly Parmar, Rita Padamesy and Linda Peshke for their excellent administrative support throughout the duration of my graduate studies.

The financial support of the Department of Chemical & Petroleum Engineering and The Engineering for Environment of the University of Calgary and AOSTRA for sponsoring this research is highly appreciated.

Finally, I would like to thank my family, friends and fellow graduate students for their moral support and understanding during my studies.

TABLE OF CONTENTS

LIST OF TABLES

LIST OF FIGURES

Nomenclature

a	Constant in Archie's equation	
a	Vapex parameter (Das)	
a	Capillary diameter (Taylor Dispersion)	(L)
b	Hele-Shaw cell spacing	(L)
A	cross-sectional area of diffusion	(L^2)
C_{s_max}	Maximum solvent concentration at solute-solvent interface	(L^3/L^3)
C_{s_min}	Minimum solvent concentration for oil to become mobile	(L^3/L^3)
C_b	Concentration of bitumen in diluted bitumen	(L^3/L^3)
C_s	Concentration of solvent in diluted Bitumen	(L^3/L^3)
C_s	Solvent concentration	(L^3/L^3)
d_p	Particle (grain) diameter in packed cell	(L)
$dc_s/d\xi$	Concentration gradient for solvent within diffusion layer	(1/L)
D_{eff}	Effective molecular diffusion coefficient	(L^2/t)
D_{app}	Apparent molecular diffusion coefficient	(L^2/t)
D_o	Intrinsic molecular diffusion coefficient	(L^2/t)
d_p	Particle diameter making up the sandpack	(L)
F	Formation electrical resistivity factor	
g	Gravitational acceleration	(L/t^2)
h	Drainage height	(L)
j	Diffusion flux (Fick)	(L/t)
k	Permeability of medium	(L^2)
K_t	Transverse dispersion coefficient	(L^2/t)

K_l	Longitudinal dispersion coefficient	(L^2/t)
m	Cementation factor in Archie's equation	
N_{pe}	Peclet number	
Ns	Vapex mass transfer parameter (Butler)	
P	Pressure	(M/Lt^2)
Q	Production rate	$(L^3/t/L)$
Q_b	Bitumen flow rate per cell thickness	(L^2/t)
Q	Dimensional oil flow rate	(L^3/t)
$\tilde{q}$	Mass of diluted bitumen per unit volume per unit time	$(M/L^3/t)$
r	Radial distance from the centre of the capillary tube	(L)
S_o	oil saturation	
S_{or}	residual oil saturation	
t	Time, sec	(t)
T	Absolute temperature	(T)
u	Convective fluid velocity in static diffusion cell	(L/t)
U	Solvent/bitumen interface velocity	(L/t)
V	Convective fluid velocity	(L/t)
v	Velocity as a function of Hele-Shaw cell spacing	(L/t)
V_A	Solvent volume fraction	
V_B	Bitumen volume fraction	
V_a	Molar volume of solvent at the normal boiling point	$(L^3/Mole)$
x	Distance in X-direction	(L)

χ_A	Compositional parameter of solvent	
χ_B	Compositional parameter of bitumen	
μ	Viscosity of diluted oil	(M/L/t)
μ_A	Viscosity of solvent at the mixing temperature	(M/Lt)
μ_B	Viscosity of bitumen at the mixing temperature	(M/Lt)
$\rho_{Diluted}$	Density of diluted bitumen	(M/L^3)
ρ_A	Density of solvent (Shu-Lederer)	(M/L^3)
ρ_B	Density of bitumen (Shu-Lederer)	(M/L^3)
$\Delta\rho$	Density of pure bitumen minus density of pure solvent	(M/L^3)
ΔX	Thickness normalized flowing surface area in Z direction	(L)
ΔZ	Thickness normalized flowing surface area in X direction	(L)
ξ	Unit length of concentration gradient in thin-film theory	(L)
α	Multiplier controlling the dependency of β on viscosity ratio	
β	Dimensionless dispersion multiplier in porous media	
γ	Dimensionless dispersion multiplier in Hele-Shaw cell	
Ω	cementation factor (Das)	
ϕ	Porosity	
θ	Angle of inclination from horizon	
θ	Exponent controlling the dependency of β on viscosity ratio	
σ	Inhomogeneity index for porosity distribution in Peclet number	

Subscripts

s	Solvent
b	Bitumen
eff	Effective
X	in X Direction
Y	in Y Direction
Z	in Z Direction
t	transverse
l	longitudinal

CHAPTER ONE
INTRODUCTION

1.1 General Description

Several experimental studies have shown that the extraction of heavy oil and bitumen using vaporized hydrocarbon solvents (Vapex) is a technically viable alternative to thermal recovery methods (Butler & Mokrys 1989, Butler & Mokrys 1991, Butler & Mokrys 1993, Mokrys & Butler 1993, Das 1995, Das & Butler 1998, Das 1998). In this process, a mixture of solvent vapor is injected into the reservoir via a horizontal well and the diluted low viscosity oil is produced by gravity drainage into a horizontal production well. The solvent is also recovered and recycled. The schematic illustration of this process is shown in Figure-1.1.

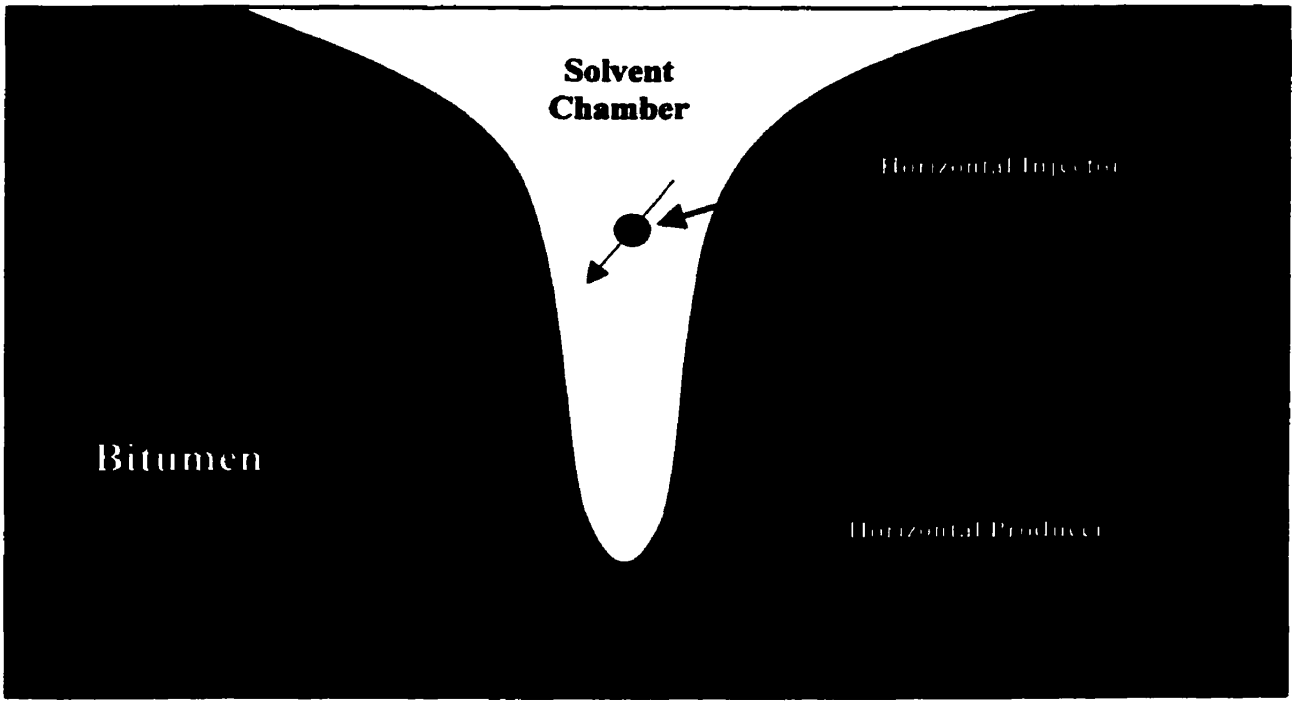

Figure-1.1: Schematic illustration of the Vapex process.

Due to its higher energy efficiency, in-situ upgrading, lower environmental pollution, lower capital costs etc. vapor extraction is superior to steam processes. The process is also suitable for offshore operations, for thin, low permeability reservoirs and those underlain by large aquifers, which are not amenable to current thermal recovery processes (Das 1998, Das & Butler 1998, Nghiem et al. 2000).

In spite of its apparent great potential (based on laboratory results), some important aspects of the process are not fully understood to make reliable predictions of the field scale behavior. The most important factor among these is the rate of mass transfer across the gas-liquid interface. Majority of the analytical models used currently is based on the assumption of diffusion into a stagnant liquid layer with constant molecular diffusivity and tends to grossly under-predict the rate of solvent dissolution.

Laboratory experiments have shown that the oil production rates in physical model tests using reservoir sand can be several times higher than the rate predicted by the simple diffusion model (Das & Butler, 1998). Possible reasons for this enhancement could be:

- The increase in molecular diffusivity with solvent concentration (due to decreased oil viscosity).
- Increase in the gas/oil interfacial area due to presence of a saturation transition zone at the interface.
- Enhanced mass transfer due to convective dispersion in porous media.

Propane and butane are perceived to be the most promising solvents to yield the highest recovery rates for Vapex (Das, 1995). However, there is a relative merit in assessing the feasibility of utilization of Green House Gases (GHG) like CO_2 in the Vapex process. Atmospheric concentration of GHGs has substantially increased as a consequence of fossil fuel combustion and other industrial activities. It is thought that increasing GHGs would increase the energy input to the earth and hence global warming is thought to occur.

Injection of greenhouse gases into subsurface strata is perceived to be one of the alternative techniques to minimize atmospheric emissions of greenhouse gases. However, due to uncertainties associated with estimation of recovery rates in Vapex, the implications of utilization of Vapex process for sequestration of greenhouse gases are yet to be determined.

1.2 Objectives of the Research

1- Investigation of basic mass transfer mechanisms controlling the recovery rate in Vapex.

2- Development of an improved mathematical model for better prediction of recovery rates in Vapex.

3- Assessment of feasibility of utilization of Green House Gases (GHG) such as CO_2 in the Vapex process.

1.3 Thesis Structure

This thesis is prepared in 8 chapters. Chapter 2 serves as a general introduction to the vapor extraction (VAPEX) mechanism and historical evolution of the process. The basic principles of mass transfer used for mathematical modeling of Vapex in Hele-Shaw cell and porous media by earlier research are discussed in detail. Moreover, this chapter highlights the discrepancy between the estimated recovery rates by the existing analytical models and the recovery rates measured by experiments in porous media.

Chapter 3 describes the role of diffusion and convective dispersion in enhanced mass transfer in porous media. Incorporation of longitudinal and transverse dispersion can improve the quality of the estimated recovery rates by Vapex in porous media. This chapter also compares the existing analytical models for estimation of molecular diffusion coefficients of solvents in bitumen.

Chapter 4 reviews the development of mass transfer theories for bituminous systems and highlights the strong dependency of diffusion on solvent concentration, over the entire concentration range.

Chapter 5 presents an investigation of interfacial mass transfer for Vapex process through experiments in Hele-Shaw cell. The experiments in this section highlight the differences between the existing analytical models, for estimation of diffusion coefficients and their impact on the estimated recovery rates. Moreover, the results of the experiments suggest that convective dispersion is a viable mechanism for enhanced mass transfer in Vapex, even in the Hele-Shaw cell environment.

Investigation of interfacial mass transfer for Vapex in porous media is presented in Chapter 6. This chapter utilizes the results of experiments in various sandpack models to establish a relationship between the enhanced mass transfer and parameters controlling dispersion and diffusion process in porous media.

Chapter 7 presents an overview of the historical emissions of greenhouse gases in Canada and Alberta, and investigates the feasibility of utilization of greenhouse gases and particularly CO_2 for improved oil recovery in Vapex.

Conclusions, important observations and recommendations for future tests are presented in chapter 8.

CHAPTER TWO
LITERATURE REVIEW

Injection of various miscible solvents for improved recovery of conventional oil has been investigated for several years. However, utilization of solvents for recovery of heavy oil is a relatively new subject. Allen et al. (1974) presented a huff & puff technique that injects propane or butane into a cell of Athabasca tar sand in cycles.

VAPEX process (Vapor Extraction) was introduced into the literature by Butler et al. (1989), as an alternative technique for recovery of heavy oil and bitumen. This process, which is a solvent-leaching gravity drainage mechanism, reduces the viscosity of heavy oil by the addition of a solvent into the bitumen as shown in Figure-2.1. The solvent in this process behaves similar to steam in Steam Assisted Gravity Drainage (SAGD) and the diluted bitumen to the heated bitumen (Butler et al. 1981, Butler & Stephens 1981, Butler 1994), as shown in Figure-1.1. Solvent is injected through a horizontal well into the reservoir. A horizontal producer is drilled right below the injector. Similar to SAGD, a vapour chamber is formed around and above the injector that grows in time as more oil is produced. The diluted oil flows within the diffusion layer and toward the producer, under the influence of gravity. Vaporised solvent results in a larger density difference and hence a greater driving force is created.

Butler and Mokrys (1989) carried out their first set of experiments in a Hele-Shaw cell to confirm that such system is a direct analog of the SAGD process. Experiments were run at room temperature and atmospheric pressure, utilizing toluene as solvent and Athabasca and Suncor Coker-Feed as bitumen. Dissolution of solvent resulted in a significant viscosity reduction for both bitumen samples as shown in Figure-2.1. However, viscosity reduction was higher for the bitumen of a higher original viscosity. They also observed that as time progresses, the drainage height decreases, convection currents within the cell slow down and the interface transforms into a smooth S-shaped flat curve.

They conducted several experiments at different cell permeabilities (cell spacing). Their results confirmed the theoretical relationship between the drainage rate and the square root of cell permeability. They also observed that the drainage rate is a linear function of square root of bitumen height as shown in Figure-2.2.

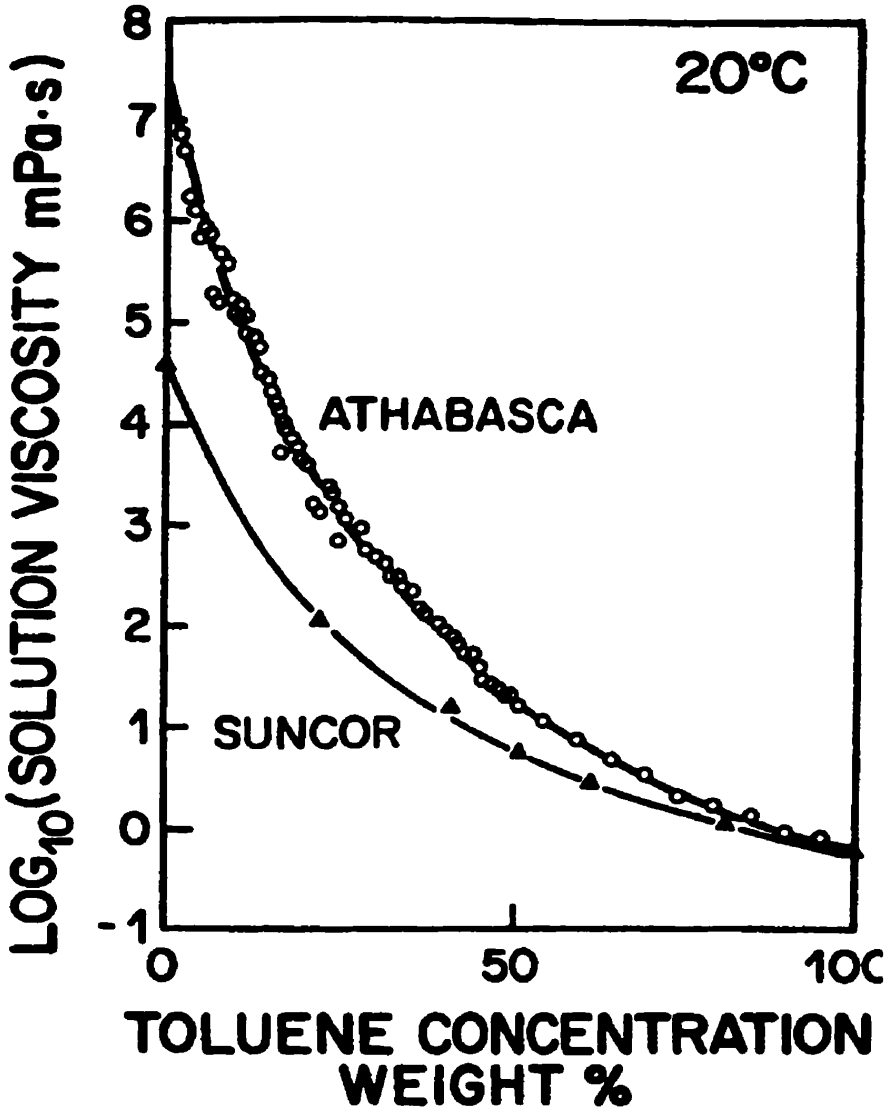

Figure-2.1: Reduction of bitumen viscosity by toluene.
(After Butler & Mokrys, 1989)

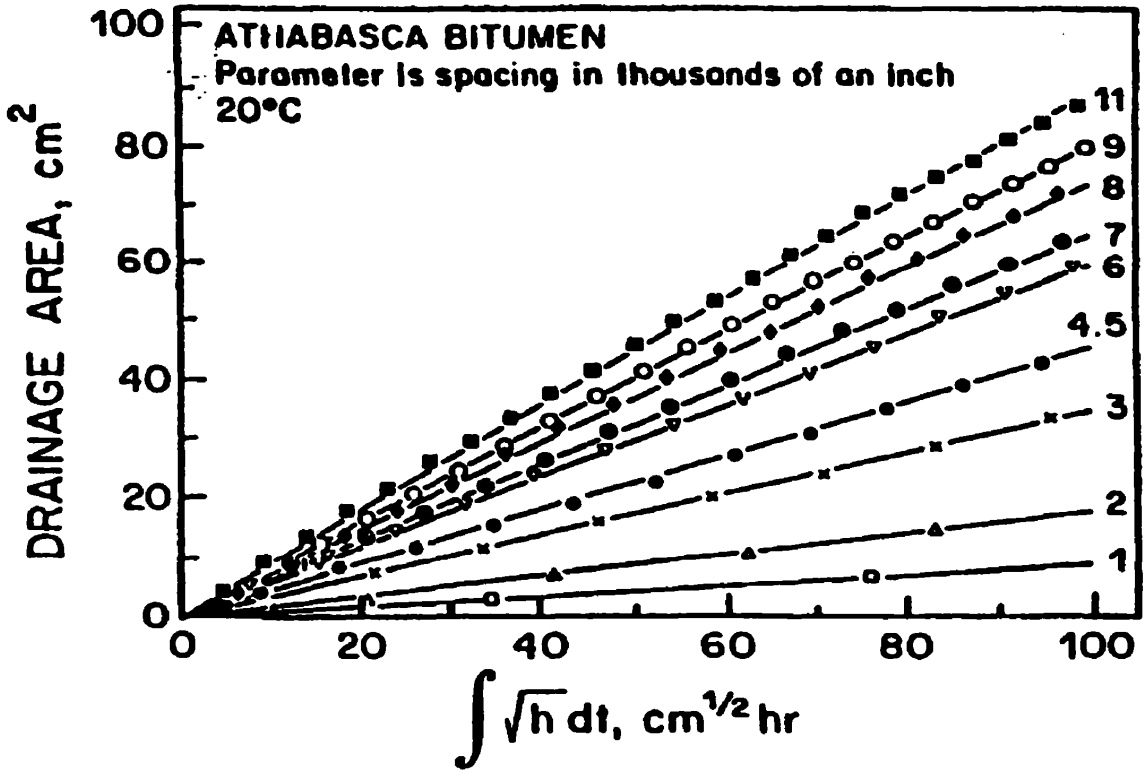

Figure-2.2: Bitumen drainage rate vs. cell height.
(After Butler & Mokrys, 1989)

A theoretical model was developed by Dunn et al. (1989) to investigate the effect of CO_2 and ethane injection for recovery of bitumen under gravity drainage in glass bead packed cells. This approach was mainly tailored around the SAGD process. The recovery rate with CO_2 was considerably higher than that with ethane. However, the recovery rate was still not as attractive as with propane or butane, which were tested later by Butler and Das (1995) and Das (1995). Instead of the thin film theory (explained in subsequent sections), Dunn et al. considered the concentration distribution across a unit element from C_{s_max} (maximum solvent concentration at solvent-bitumen interface) to C_s=0 at infinity. Although the mathematical formulation for concentration distribution is more rigorous and is considered to be more accurate, this approach is not significantly better than the thin film

theory. Dunn et al. adopted an approach similar to SAGD (constant thermal diffusivity vs. temperature) and neglected the strong concentration dependency of molecular diffusivity. Assumption of a constant thermal diffusivity in thermal recovery is valid due to the practical range of temperatures involved in such processes.

Butler and Mokrys (1991) extended their earlier experiments on VAPEX to simultaneous injection of solvent and hot water. The driving force behind this idea was mainly to improve the efficiency of recovery by bridging the two processes of VAPEX and SAGD. It was noted earlier that without the injection of hot water, the latent heat due to condensation of vapor would cause some warming (Butler & Mokrys, 1989). However, the associated viscosity reduction was still too low to cause an appreciable improvement. Instead, Butler and Mokrys (1991) suggested an intermediate heating in the range of 40-70°C. This would be perceived economically more attractive in comparison to conventional SAGD process, due to lower heating costs and smaller heat losses. Several experiments were run in a packed cell of glass beads at different temperatures. At the start of each experiment, hot water was injected alone and shortly after, oil production dropped to zero. At that point, propane vapor was injected, while maintaining hot water injection. Figure-2.3 presents cumulative oil production before and after propane injection. Note that the cumulative oil production after propane injection is almost ten times of that prior to propane injection (hot water only).

Figure-2.4 shows that the relationship between the rate of recovery upon injection of propane and the vapor chamber temperature is linear. Butler and Mokrys (1991) attributed the increased oil recovery to recycling of the solvent, by re-vaporization of propane under the presence of hot water, at the bottom of the cell. This process is schematically illustrated in Figure-2.5. Although, these results seemed to be better than earlier experiments, the low drainage rates and high solvent/oil ratio were not promising enough for an economically viable project.

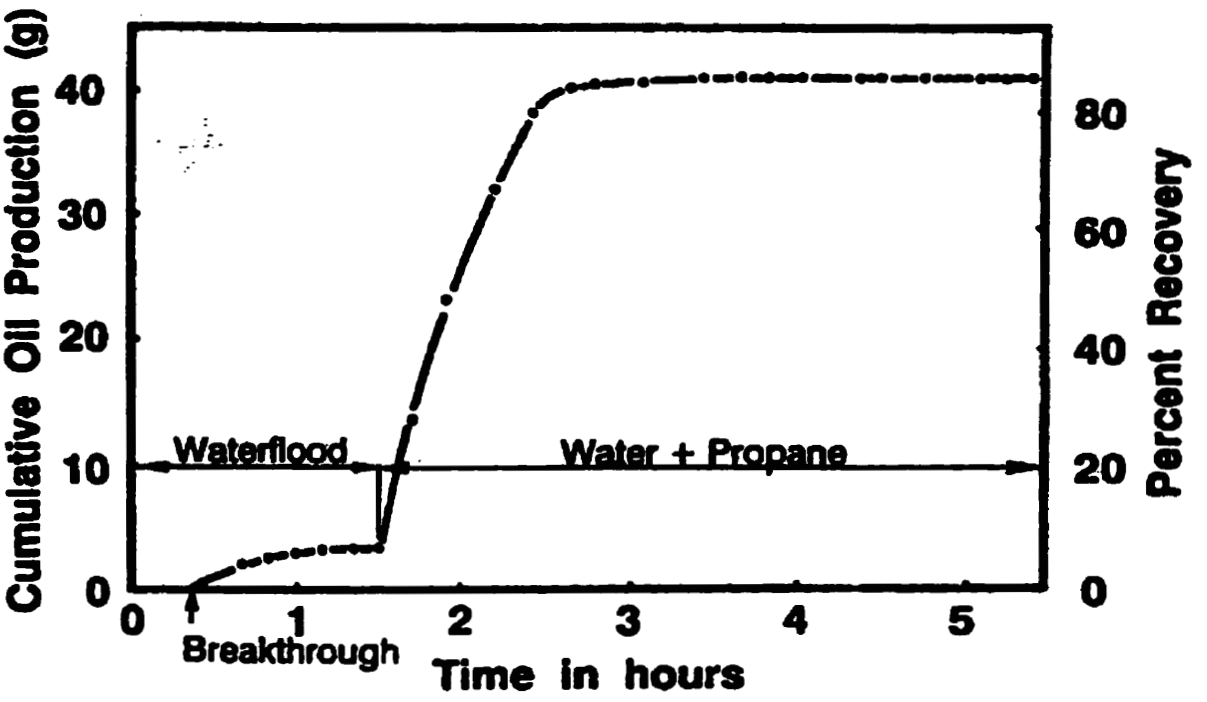

Figure-2.3: Cumulative oil production by hot water injection in vapex. (From Butler & Mokrys, 1991)

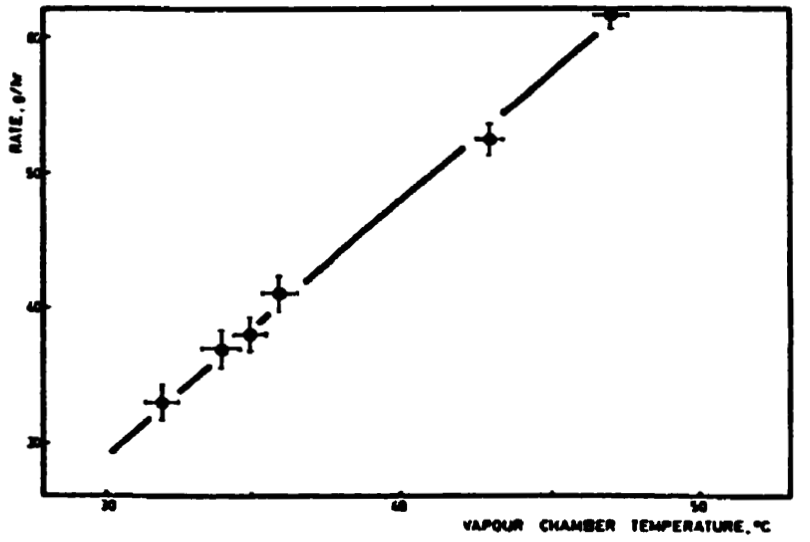

Figure-2.4: Experimental oil production data vs. temperature in vapex . (From Butler & Mokrys, 1991)

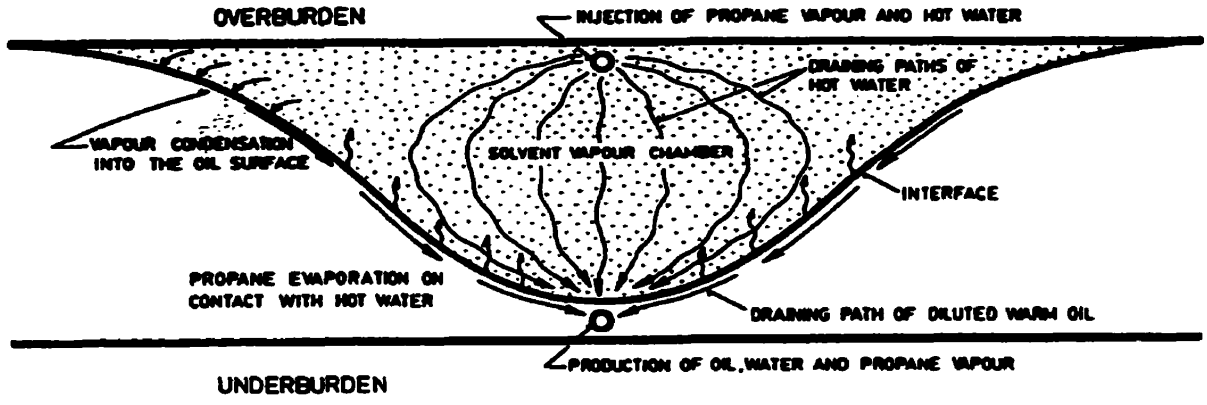

Figure-2.5: Schematic illustration of vapex/hot-water process.

(From Butler & Mokrys, 1991)

Butler and Mokrys (1993) carried out their research on potential problem areas of VAPEX, using a large physical model. In this work, the emphasis was on asphaltene precipitation, rates, recoveries and gas/oil ratios. Experiments with hot water and propane injection were repeated as before and cumulative oil recovery exhibited more or less the same trend as those in the previous experiments, as shown in Figure-2.6.

Asphaltene deposition resulted in in-situ upgrading of oil. The injected propane near its dew point mixes preferentially with the lighter components of the crude, while the heavier residues are left behind as asphaltene deposits. As an example, the viscosity of Tangleflags oil was reduced to 20% of its original value by propane injection. The glass beads were consolidated in a series of parallel dark stripes by precipitation of asphaltene on their surfaces. However, such deposits did not hinder the flow of oil.

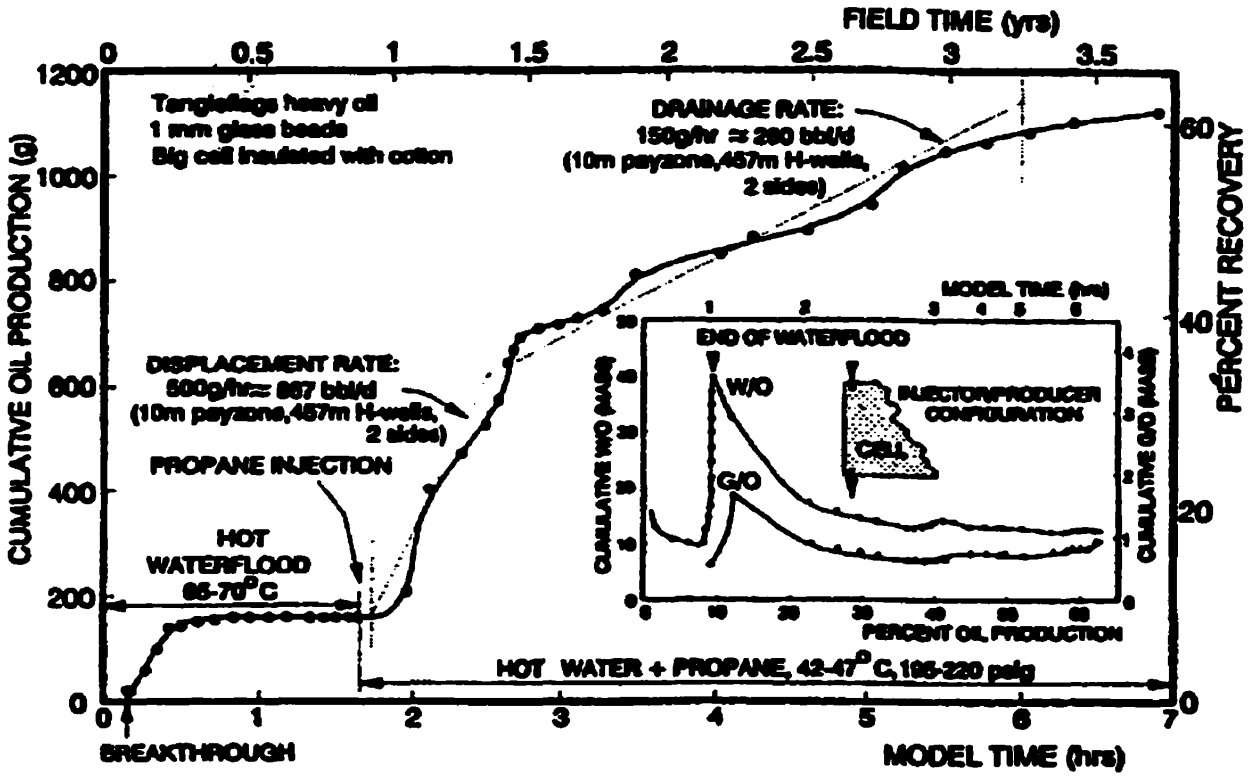

Figure-2.6: Performance of Vapex / Hot-water process, for Tangleflags crude.

(From Butler & Mokrys, 1993)

Perhaps, the reduced viscosity of oil partially compensated a lowered permeability of the consolidated beads, resulting in a drainage that appeared to be unimpaired. Injection of gaseous solvent resulted in minimum asphaltene drop out. This in-situ upgrading of heavy oil has potentially significant cost saving benefits during transportation and surface processing of the crude. They suggested that the addition of some non-condensable gas to the solvent might reduce asphaltene precipitation while maintaining a high recovery rate.

To assess the feasibility of Vapex process without hot water injection, Butler & Mokrys (1993) conducted a set of experiments in the absence of water. Interestingly, dry propane injection resulted in higher projected field rates in comparison to hot water-propane injection. The packed-cell experiments (Butler & Mokrys, 1991) with hot water-propane in a cell with height of 7cm had resulted in a reported field production of Q=0.1035 bbl/day/ft. On the other hand, dry propane injection in packed cell (Butler & Mokrys, 1993) with a cell height of 21.7cm resulted in a scaled rate of Q=0.1825 bbl/day/ft. Mathematical model (that will be explained in subsequent sections) had shown that production rate is approximately proportional to the square root of drainage height, i.e.

$$\frac{Q_1}{Q_2} = \sqrt{\frac{H_1 k_1}{H_2 k_2}} \qquad (2.1)$$

Direct comparison of the reported recovery rates with respect to the height and permeability of the cell suggest that hot water does not have a significant impact on the rate of recovery of the VAPEX process. The poor performance of hot water could be partly caused by water-shielding effect, as noted by Das and Butler (1996). In that regard, the scaling criteria used by Butler and Mokrys (1991) to transform laboratory results into field scale equivalents might not hold in the presence of hot water.

Suitability of ethane as an alternate solvent was examined through similar procedures with identical crude (Butler & Mokrys, 1993). The cumulative oil recovery was about half of that for typical propane run and the viscosity of the recovered oil remained unaffected. Moreover, the magnitude of viscosity reduction by injection of pentane was the same as that for propane.

Das (1995) developed the earlier mathematical model for diffusional mass transfer in porous media, accounting for system porosity and residual saturation in the swept zone. He also introduced the concept of Vapex Parameter "a", for quantitative measure of the relative rates at different conditions. Similar to Butler's N_s parameter, Vapex parameter

incorporates all the reservoir parameters (excluding the reservoir height) and physical properties of the solvent-bitumen pair at the desired temperature and pressure. Mathematically, the Vapex parameter is defined as:

$$a = \sqrt{2kg\phi^{\circ}\Delta S_{o}N_{s}} \qquad (2.2)$$

Das (1995) carried out his preliminary studies in Line Source Hele-Shaw cell using saturated propane. He noticed asphaltene precipitation and drainage of diluted oil in a series of single steps. Asphaltenes were deposited on the wall of the cell as parallel ribbons, whenever solvent condensation occurred, under operating pressure and temperature. He noticed that asphaltene precipitation does not reduce the flow of oil. Indeed, he noted that asphaltene drop out results in in-situ upgrading of the oil and an increase of up to 50% in recovery speed. He noticed that production rates are proportional to the square root of permeability. He also investigated the impact of pressure cycling on recovery rates, by imposing sudden changes on injection pressure. The back-calculated Vapex parameter from cycles at higher pressure were almost twice larger than those at lower pressure. He concluded that higher pressure results in higher solvent solubility and hence higher recovery speed, provided that the vapor chamber is filled with a non-condensable gas. Presence of non-condensable gas assures maximum density difference between the vapor chamber and the diluted oil and hence gravity drainage is maximized.

Das (1995) continued his work by carrying experiments in sandpack. He noticed that extraction rate in porous media is 3 to 5 times faster than the predicted values by analytical models. He attributed the increased recoveries in porous media due to extended interfacial area of contact, increased solubility, capillary imbibition and surface renewal. Interestingly, the recovery rates in porous media, similar to Hele-Shaw cell, exhibited a linear relationship with the square root of permeability, as shown in Figure-2.7.

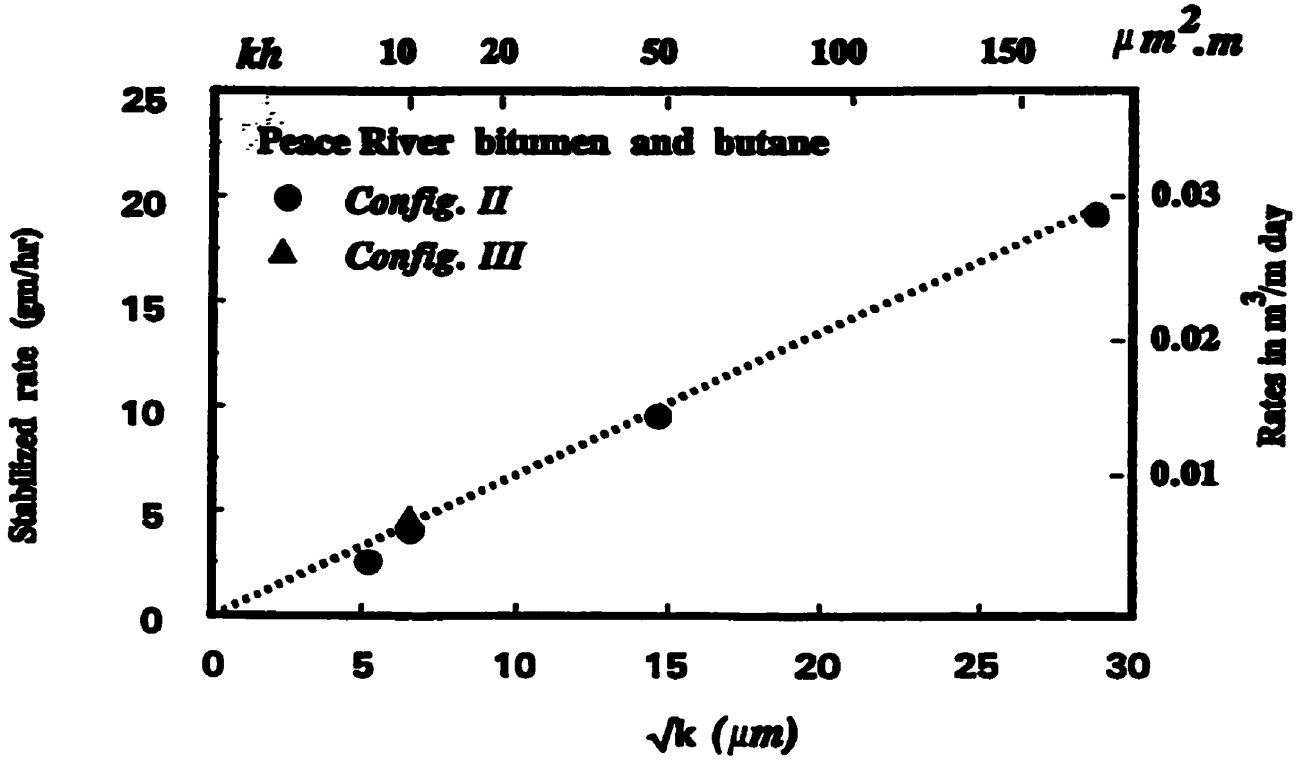

Figure-2.7: Experimental stabilized flow rate versus cell permeability. (After Das, 1995)

Das (1995) also investigated the upward leaching of the oil by injection of solvent at the lower side of the cell containing a layer of bottom water. In this scenario, the injected solvent moves through the less viscous water easily and spreads itself under the oil and higher contact area is created. Due to counter current flow of solvent (moving upward) and oil (falling down), more mixing will occur and recovery rates are higher. He also noticed that extraction rates for Peace River bitumen and Lloydminster heavy oil are comparable, while the original viscosity of the two oils differs by more than an order of magnitude.

2-1 Analytical Model of Vapex in Hele-Shaw Cell

The mathematical model developed by Butler and Mokrys (1989) is based on extraction of bitumen by solvent in a Hele-Shaw cell model, adopting a thin film mass transfer formulation. The model consists of two parallel plates separated by a distance b, representing a porosity of ϕ=1.0 and permeability of $k=b^2/12$. The corresponding mass balance in the diffusion boundary layer under steady-state condition is given by a one dimensional diffusion equation as:

$$-D\frac{dc_s}{d\xi}=U\,c_s \qquad (2.3)$$

c_s = Solvent concentration (volume fraction)

ξ = Perpendicular distance from interface

D = Molecular diffusion coefficient for solvent

U = Velocity of advancing interface, perpendicular to diffusion boundary layer

$dc_s/d\xi$ = Concentration gradient for solvent within diffusion layer

A small portion of bitumen-solvent interface is shown in Figure-2.8. Solvent concentration at the outermost edge of the diffusion layer (towards solvent) is at its maximum ($C_s= C_{max}$ at ξ=0), while solvent concentration at the innermost edge (towards bitumen) is at its minimum ($C_s= C_{min}$ at $\xi=\xi_{max}$), for oil to become mobile. It is also assumed that dissolved gas concentration profile ahead of the interface and within the bulk of the bitumen is near steady state (i.e. $\partial c/\partial t = 0$). Assumption of a steady-state solvent mass transfer into the bitumen in a closed system might not hold, as the concentration gradient is dynamically changing in time. It is important to mention that this model assumes zero residual oil saturation (S_{or}=0) in the zone swept by solvent.

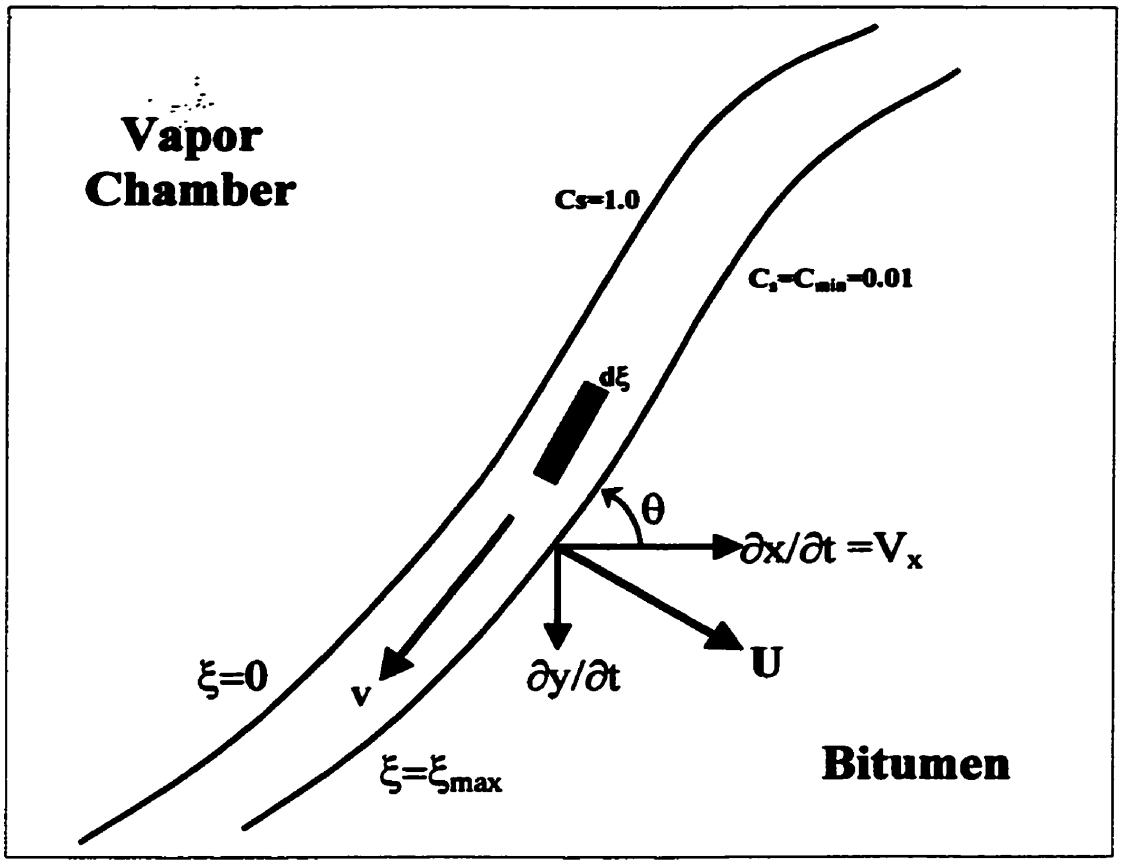

Figure-2.8: Vertical cross section of Vapex model through solute/solvent interface.

(After Butler & Mokrys, 1989)

One of the main assumptions used to simplify the solution for this model is a steady-state pressure gradient in the direction of flow within the diffusion layer. In that regard, the following simplified form of Brinkman equation (Bird et al., 1966) is used:

$$\Delta\rho\, g \sin\theta = V\mu/k + \mu d^2v/dw^2 \qquad (2.4)$$

In the above formulation, 'V' is the average velocity vector along the interface, v is the parabolic velocity profile within the thickness of the cell and 'w' is variable distance within the Hele-Shaw cell spacing. The left-hand side of the above equation is the gravitational force and the first term on the right-hand side is viscous drag force. The second term in

right-hand side accounts for viscous forces due to variation of velocity gradient in the direction perpendicular to inner surface of Hele-Shaw cell. Butler and Mokrys (1989) neglected the second order differential, d^2v/db^2, for closely spaced plates of Hele-Shaw cell, where flow strictly remains laminar. For most practical permeabilities encountered in oil reservoirs, this assumption is correct and analogous to Darcy flow.

They assumed that flow of diluted oil exclusively takes place in the diffusion layer with a volume fraction of solvent dissolved in it. Therefore, bitumen flow rate is expressed as:

$$Q_b = \int_0^{\xi_{max}} V\,(1-C_s)\;d\xi \qquad (2.5)$$

They considered that at $\xi = 0$ (the lower limit of integral) solvent concentration is at its maximum value C_{max} , and is equal to the solubility limit of solvent within bitumen at the prevailing pressure and temperature. At the other end of the thin-film where $\xi = \xi_{max}$ (the upper limit of integral), solvent concentration is at its minimum C_{min} value where oil becomes mobile. The above assumption would be valid only for bitumen systems where the oil is immobile without the solvent (Das & Butler 1996). Should the oil in question be of some limited mobility, these assumptions need to be modified. Even if the dependency of viscosity as a function of temperature and concentration is incorporated properly, the volumetric oil flow rate without addition of solvent should be deducted from the recovery rate with solvent, to determine the net flow rate due to the solvent. Combining equations (2.3), (2.4) and (2.5) gives:

$$Q_b = \frac{kg\sin\theta}{U}\int_{c_{min}}^{c_{max}} \frac{\Delta\rho D(1-C_s)}{\mu C_s}\;dC_s = \frac{kg\sin\theta}{U}N_s \qquad (2.6)$$

Where,

$$N_s = \int_{c_{min}}^{c_{max}} \frac{\Delta\rho D(1-C_s)}{\mu C_s}\;dC_s \qquad (2.7)$$

Since N_s is directly related to physical characteristics of the solvent-bitumen system, Butler & Mokrys (1989) mention that at constant pressure and temperature, N_s should be constant. Das (1995) calculated the Vapex parameter (a modified form of N_s) for numerous experiments in Hele-Shaw cell. The results of this calculation shown in Figure-2.9 indicate that Vapex parameter indeed remains constant within the limit of experimental error.

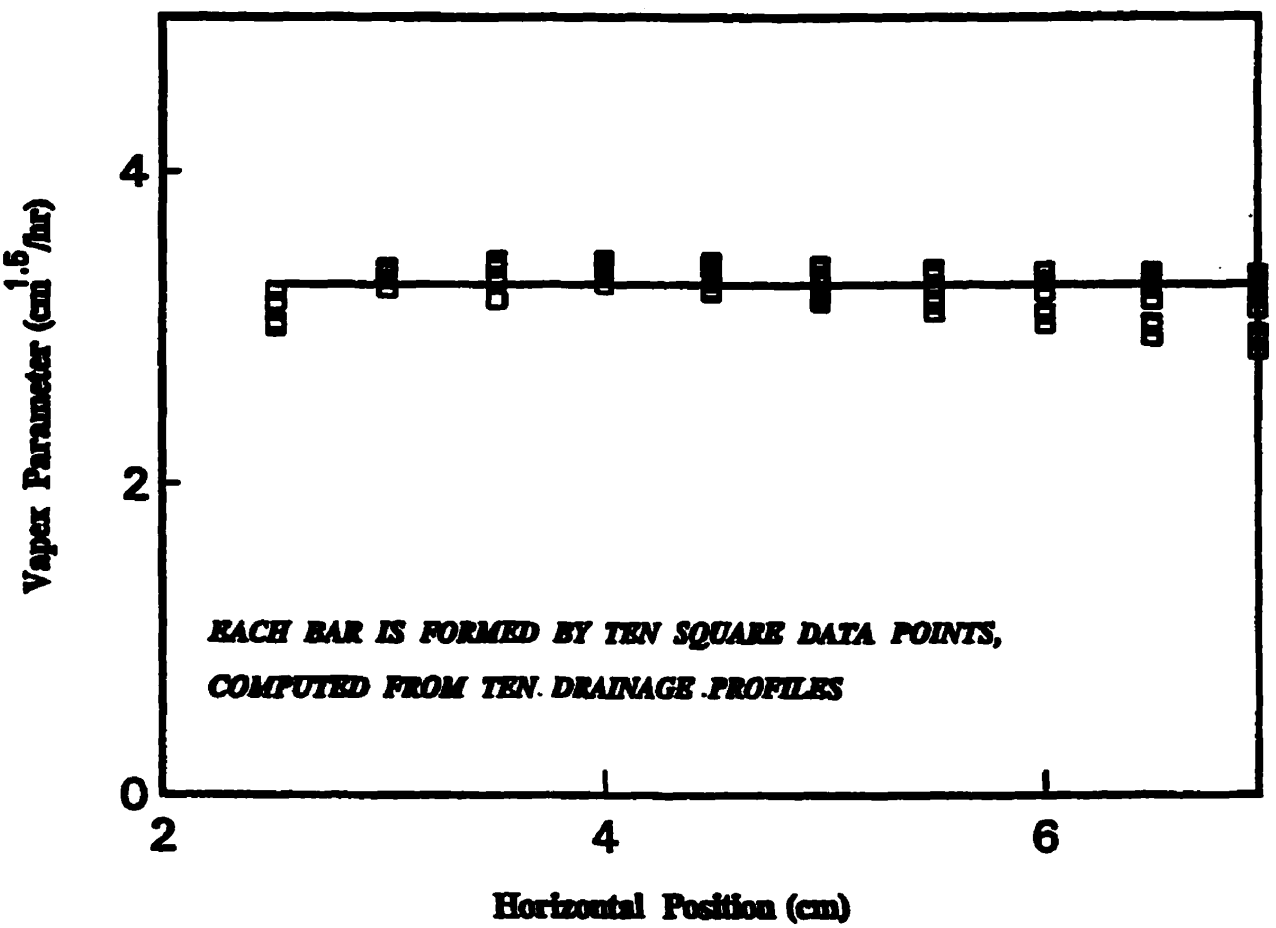

Figure2.9: Computed values of Vapex parameter for different positions and times. (After Das, 1995)

Figure-2.10 represents the relationship between oil production and boundary layer position. The crosshatched area represents the cumulative oil produced during time "t" at ordinate "y" and mathematically represented through the following relationship:

$$\int_0^t Q\,dt = \phi\,\Delta S_o \int_y^h X dy \qquad (2.8)$$

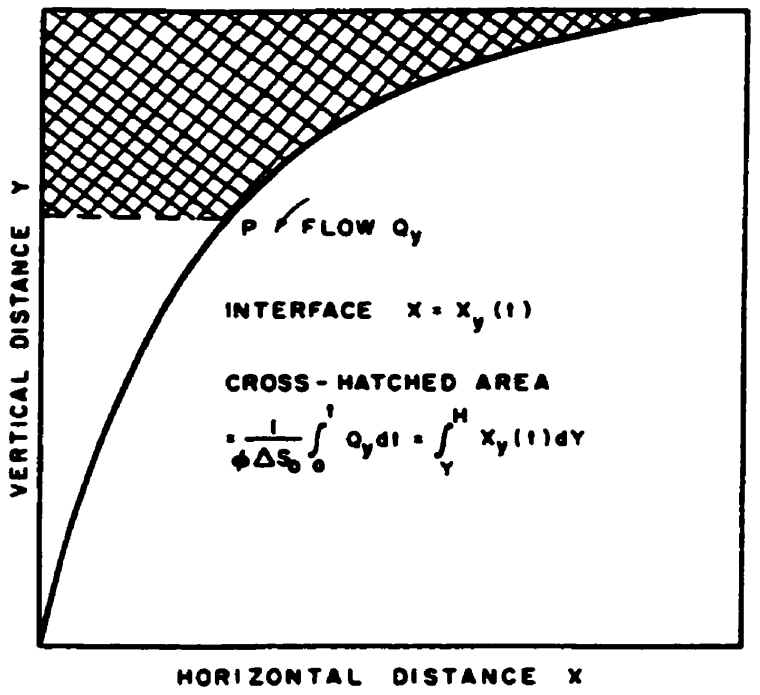

Figure-2.10: Schematic presentation of cumulative recovery vs. interface position. (After Butler & Mokrys, 1989)

Rearranging equation 2.8 by taking its derivative with respect to time "t" and distance "y" respectively yields:

$$\partial Q/\partial y = -\phi \Delta S_o\, \partial X/\partial t \qquad (2.9)$$

Finally, Butler and Mokrys express the geometric relationship between principal velocity vector U, and the advance of boundary layer in X-direction as

$$U = \partial X/\partial t \sin\theta \qquad (2.10)$$

Combining equation (2.6), (2.9) and (2.10) results in:

$$Q = - kg\phi\Delta S_o N_s / (\partial Q/\partial y) \qquad (2.11)$$

Where, $0 < Y < h$

$0 < Q < Q$

Equation (2.11) can be integrated with respect to the above boundary conditions to obtain flow rate as:

$$Q = \sqrt{2kg\phi\Delta S_o N_s (h - y)} \qquad (2.12)$$

Note that in equation 2-10, for any value of θ, the interface velocity U would be smaller than $\partial X/\partial t$. In other words, it implies that $\partial X/\partial t$ is the principal vector of velocity. However, in reality U is the main vector with two projections in X and Y direction. This complication arises from the fact that Butler and Mokrys tend to simplify the model by solving it in one dimension only. In that regard, they had no other choice but assuming that growth of the vapor chamber and hence the advance of boundary layer is exclusively in X-direction. Under such assumption, $\partial X/\partial t$ becomes the principal vector of velocity and its projection U, perpendicular to interface becomes smaller. It is noteworthy, that similar analogy is used in SAGD formulation (Butler, 1994).

Laboratory experiments of SAGD and Vapex in Hele-Shaw cell resulted in slightly lower rates of recovery as opposed to the predicted values by Butler's model. Over-estimation of velocity component in the X-direction (as noted above) and assumption of a steady-state process can possibly contribute to such discrepancy. Butler (1994) reduced the constant term "2" in equation 2.12 to "1.3" to improve the quality of history match. Had the solution been developed in 2-D, it is very likely that there would have been no need for the

above-mentioned modification and correction for the location of interface curves by the TANDRAIN assumption (Butler and Stephens, 1981). Figure-2.11 presents the typical location of the boundary layers before and after Tandrain correction.

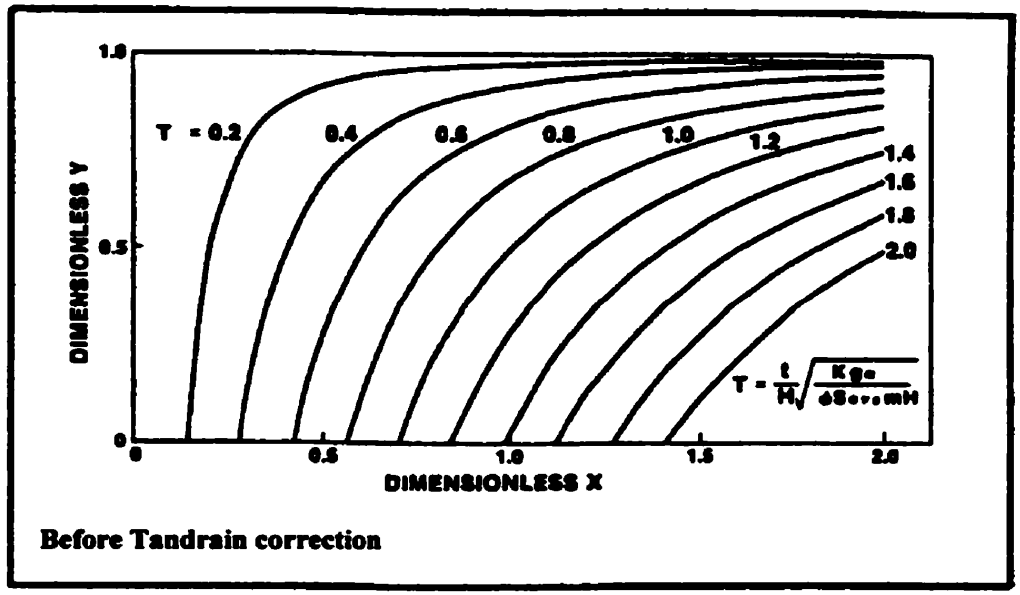

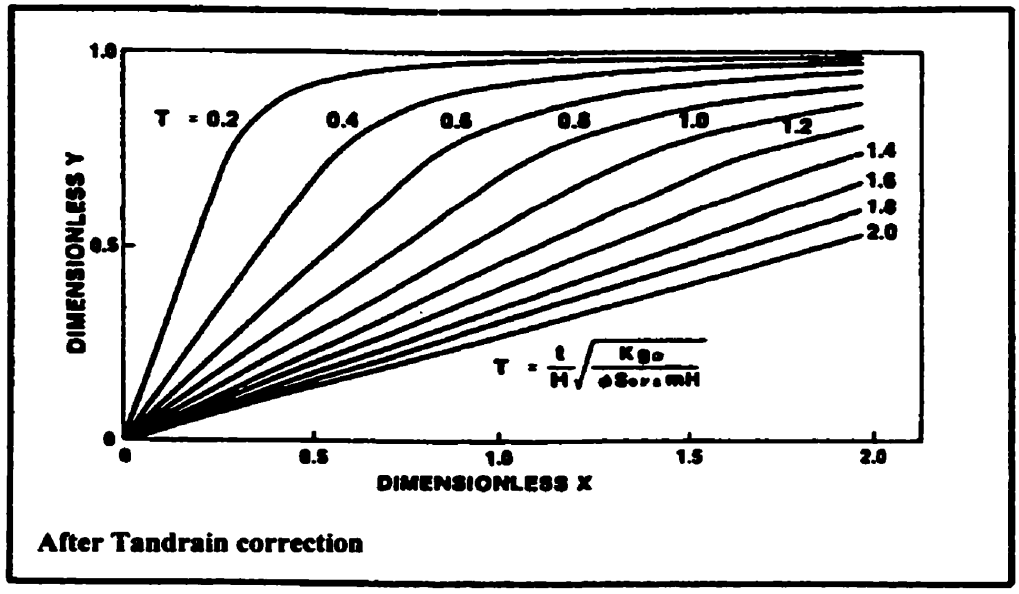

Figure-2.11: Position of solute/solvent interface, before and after Tandrain correction (After Butler & Stephens, 1981)

2-2 Analytical Model of Vapex in Porous Media

Earlier mathematical models for Vapex were based on Hele-Shaw cell performance. To obtain meaningful predictions for field conditions, a scaling procedure was outlined by Butler & Mokrys (1991) and adopted by other authors to convert the Hele-Shaw cell results to reservoir condition (Butler 1991, Das & Butler 1995, Jiang 1997). The predicted production rates were not promising enough to be viable for field implementation. However, there was still a great need to develop the relevant equations for porous media.

Das (1995) modified the earlier VAPEX model, incorporating an apparent diffusion coefficient D_{app} of solvent in bitumen in presence of porous media and a cross sectional area 'A', at solvent bitumen interface. Therefore, equation 2.3 was reformulated as:

$$-A\, D_{app}\, dc_s/d\xi = A\, \phi\, U\, c_s \qquad (2.13)$$

Das related the intrinsic molecular diffusion D_o to apparent diffusion coefficient D_{app} in porous media by following relationship:

$$D_{app} = D_o\, \phi^{\,m} \qquad (2.14\text{-a})$$

Where "m" is the cementation factor which is a measure of consolidation of rock. Other sources in literature (Perkins and Johnston, 1963) indicate that this relationship is rather as follows:

$$D_{app} = D_o / F\, \phi \qquad (2.14\text{-b})$$

F is the formation electrical resistivity factor. Formation electrical resistivity factor, as suggested by Archie (1942) is related to porosity, cementation factor "m" and the constant "a" by the following equation:

$$F = a / \phi^m \qquad (2.15)$$

Satisfactory results are obtained using equations with a=0.81 and m=2 in sands and a=1 and m=2 in compacted formations. Within their normal ranges of application these exponents are slightly different from the so-called Humble formula where a=0.62 and m=2.15. Other values of cementation factor are shown in Table-1 (Archie, 1942) as a function of rock lithology. The values of formation factor F, in this table are computed based on assumption of an average porosity of ϕ=0.30 and coefficient of a=1.

Table-2.1: Experimental values of cementation factor vs. rock lithology.

Rock Description	m	F [1]	1/Fϕ
Unconsolidated rocks (loose sands, oolitic limestone)	1.3	4.78	0.70
Very slightly cemented (Gulf coast type of sands, except Wilcox)	1.4-1.5	5.4-6.1	0.62-0.55
Slightly cemented (most sands with 20% porosity or more)	1.6-1.7	6.9-7.7	0.49-0.43
Moderately cemented (highly consolidated sands, 15% porosity or less)	1.8-1.9	8.7-9.9	0.38-0.34
Highly cemented (low porosity sands, quartzite, limestone, dolomite of intergranular porosity, chalk)	20.-2.2	11.1-14.1	0.30-0.24

1- Assuming a=1 and ϕ=0.30

As the cementation factor increases, the grains making up the rock become more consolidated and hence, the apparent diffusion coefficient based on Equation-2.14b will be successively smaller than molecular diffusion coefficient. Note that all the experiments for Vapex are conducted in unconsolidated sandpacks, where the value of m is considerably smaller than for consolidated reservoir rocks. In that regard, the apparent diffusion coefficient in sandpack is only about 70% of the intrinsic molecular diffusion coefficient, i.e. 1/Fϕ=0.7. This concept is schematically illustrated in Figure-2.12.

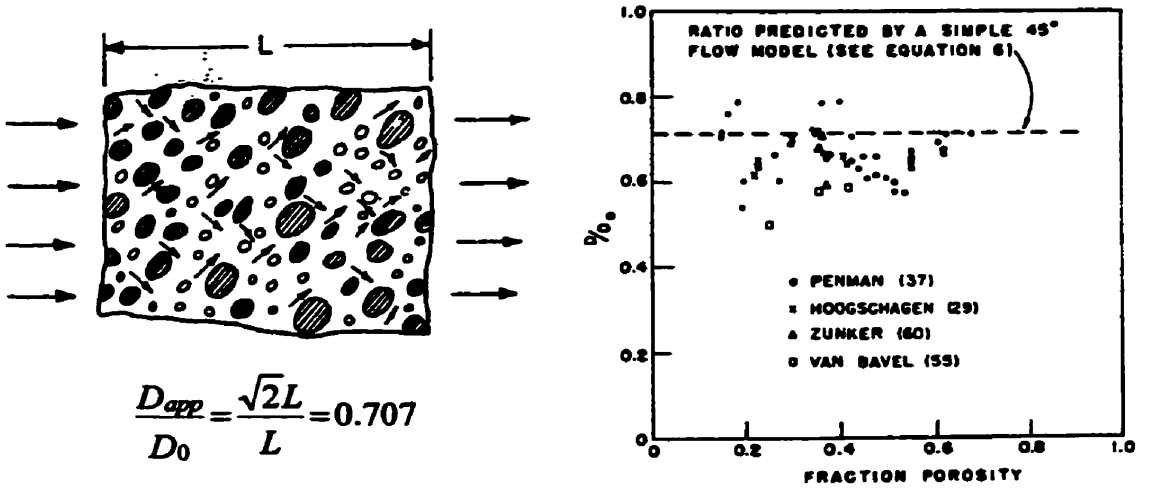

Figure-2.12: The effect of a tortuous path on apparent diffusion coefficient.

Inserting the coefficients for compacted formation (a=1 and m=2) into equation (2.14-b) results in:

$$D_{app} = D_o \phi \qquad (2.14\text{-c})$$

The difference between equation 2.14-a and 2.14-c can be explained by the statement by Perkins (1963) that *"In the oil industry, the apparent diffusion coefficient in a porous medium, D_{app}, is usually based on the average cross sectional area open for diffusion and the overall length"*. Therefore, Das could have excluded the ϕ term in equation 2.14-b, assuming that the molecular diffusivity term D has already accounted for porosity effect.

Das combines equation (2.14-a) and (2.13) to get

$$- D_o \, dc_s/d\xi = \phi^{(1-m)} U c_s \qquad (2.16)$$

The remainder of the derivation is similar to that of Hele-Shaw cell as explained before. Therefore, Das reformulates the recovery rate in porous media as:

$$Q = \sqrt{2k\ \phi^{m}\ g\ \Delta S_o N_s h} \qquad (2.17)$$

Development of the mathematical model of Vapex for porous media based on equation 2.14-c results in the following relationship:

$$Q = \sqrt{2k\ \phi\ g\ \Delta S_o N_s h} \qquad (2.18)$$

The above formulation assumes that the effect of porosity and tortuousity are explicitly incorporated in calculation of N_s parameter. Therefore, N_s parameter is calculated based on an effective diffusion coefficient in porous media, which is externally correlated to a pure molecular diffusion coefficient and convective dispersion multipliers in porous media. The methodology used to incorporate the diffusion and dispersion effects is explained in detail in subsequent chapters.

2-3 Influence of Porous Media on Vapex Process

To study the effect of porosity on Vapex process, Das and Butler conducted a series of experiments in a packed cell of glass beads and Ottawa sand utilizing Butane as solvent. The results indicated that flow rates obtained from packed cells were up to an order of magnitude higher than values predicted from a Hele-Shaw cell model modified for porous media (Das 1995, Das and Butler 1995, Das and Butler 1998, Das 1998). They suggested several factors contributing to increased recovery rate in porous media. These factors are:

a- improved interfacial contact (both at the leading front of the boundary layer and in the 2-phase region behind it),

b- increased rate of solubility and effective diffusivity

c- enhanced surface renewal by capillary imbibition and development of transient mass flux at the bitumen interface (vapor non-wetting)

d- enhancement during the rising of the solvent chamber (mixing by counter-current flow)

However, the above-mentioned factors have not been incorporated systematically into a reliable mathematical model for prediction of recovery rates in Vapex.

One of the main differences between Hele-Shaw cell and sand packed models is that residual oil saturation in the extracted Vapex chamber in Hele-Shaw cell is zero, whereas in packed model this value might not be zero. Moreover, a transition zone (hereafter referred to as 2-phase region) is formed from the onset of the minimum solvent saturation at bitumen interface (Leading Front), towards the extracted zone at maximum solvent saturation due to capillary forces. This concept is schematically illustrated in Figure-2.13.

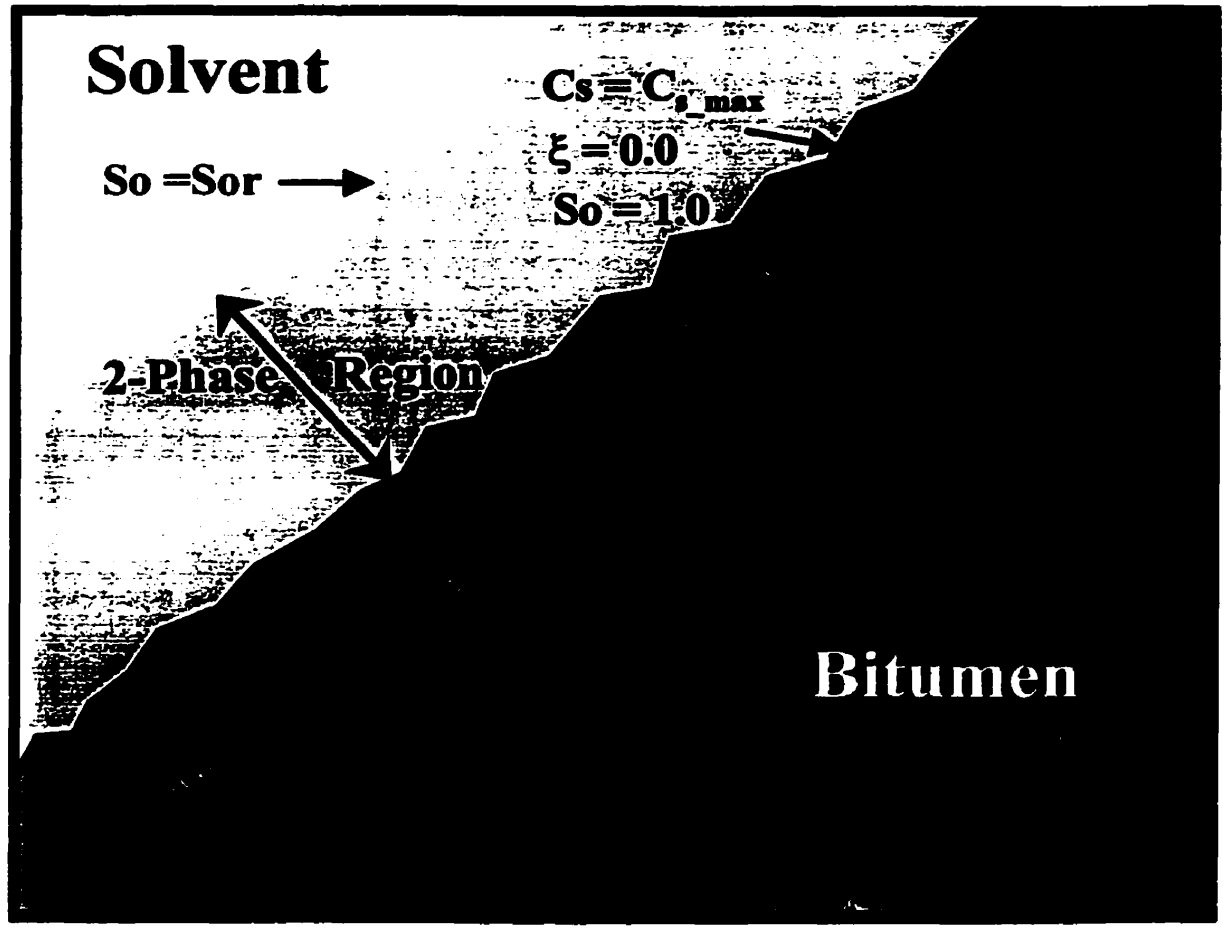

Figure-2.13: Schematic illustration of mass transfers for Vapex in porous media.

Das and Butler (Das 1995, Das and Butler 1998) noted that the extent of the gas-liquid interface becomes more dispersed in finer sands. They suggested that as the solvent-bitumen interface moves away, the oil left behind is still in contact with solvent in the chamber. Therefore, after a long residence time the solvent concentration increases, the surface tension decreases and in turn, the gravity forces exceed the capillary forces and hence the diluted residual oil falls.

Das and Butler (1995, 1998) also suggested that enhancement of the process at the leading front is due to increased rate of surface renewal by capillary imbibition. Based on this theory, as soon as oil is diluted, it is drawn away from the interface by the adjacent capillary pore in the extracted sand matrix. The bitumen surface is refreshed and a renewed transient diffusion flux (higher than steady-state flux) is established. This procedure repeats in cycles. Das (1995) suggests that solvent does not need to penetrate a long distance to access fresh bitumen. Therefore, in an attempt to close the aforementioned discrepancy between the analytical and experimental data, they include the combined effect of all those parameters into an effective diffusion coefficient D_{eff}. Finally, they managed to reconstruct the desired history match on recovery rates, utilizing effective diffusion terms, up to an order of magnitude higher than apparent diffusivity D_{app}, where:

$$-D_{eff}\, dc_s/d\xi = U\, c_s \qquad (2.19)$$

To examine the impact of surface tension on enhanced surface renewal, Das (1995) computed the surface tension of mixture of Peace River bitumen with propane and butane using modified Brock-Bird correlation (1955) by HYSIM® software. The calculated surface tension of this mixture as shown in Figure-2.14, decreases from 34 to 13 dyne/cm (60% reduction) as the mass fraction of solvent increases from zero to 0.25. However, he did not elaborate to relate these results with a mathematical model for prediction of enhanced recovery rates. Therefore, it would be an interesting task to cross correlate the effect of capillary pressure with recovery rate, over a wide range of porosity.

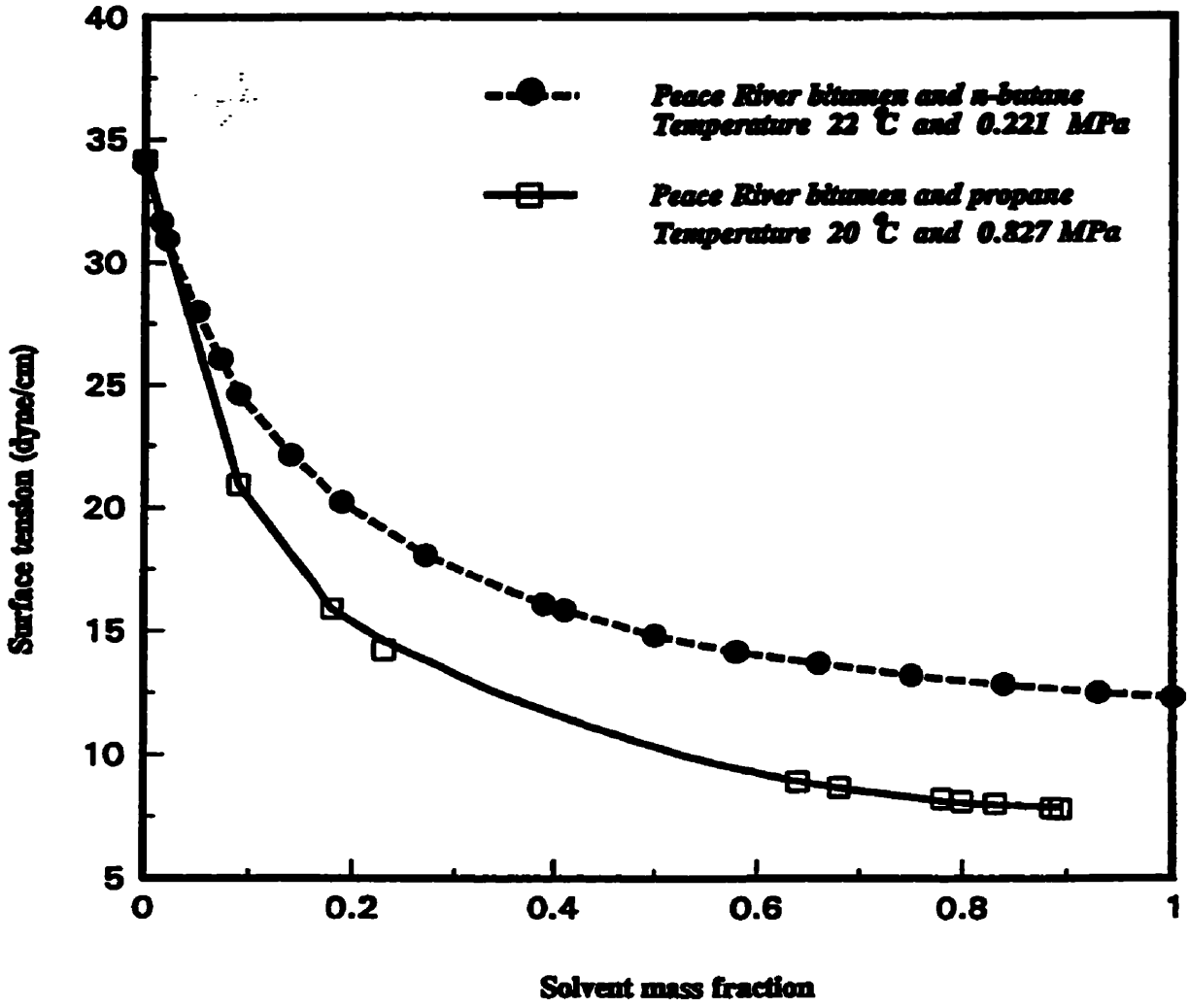

Figure-2.14: Surface tension vs. solvent concentration.

(From Das, 1995)

CHAPTER THREE
THE ROLE OF DIFFUSION AND DISPERSION IN VAPEX

Performance of the Vapex process is directly related to the amount of solvent dissolving into bitumen. In a steady state process, the rate of recovery in the transition zone (2-phase region) needs to be balanced with that in the leading front of the boundary layer. Unless the leading boundary layer delivers the expected amount of oil into the 2-phase region, the combination of all the processes within the 2-phase region would not be able to produce more than the delivered oil volume by the leading front. This means that enhancement of mass transfer at the leading front is a priory for improved recovery rate in the 2-phase region. In other words, mass transfer of the solvent at the leading boundary layer is the limiting factor of interfacial mass transfer. Therefore, the combination of all the processes in the 2-phase region only tends to influence the thickness of the transition zone, rather than influencing the rate of mass transfer.

It is noteworthy that, with the exception of molecular diffusion and transverse dispersion that are present almost everywhere in the system, the remaining mechanisms are predominantly prevailing only within the 2-phase region. Particularly, interfacial tension and capillary forces become a material issue in the force balance of a two-phase region only. At the leading front, mass transfer exclusively occurs in a single-phase environment where interfacial tension and capillary forces are absent. Therefore, the parameters controlling the mass transfer at the leading front appear to be diffusion and dispersion only.

3-1 Dispersion Process

Earlier estimates based on a mass transfer model, which is only comprised of molecular diffusion alone, could not explain the desired high recovery rates in porous media (Dunn et al. 1989, Das and Butler 1995, Das 1995, Das and Butler 1998). Therefore, it appears that at least a secondary mechanism (like convective dispersion) should be incorporated into the mass transfer model to address the observed high recovery rates in porous media. Almost

all investigators initially overlooked the enhanced mass transfer in Vapex due to dispersion phenomena.

Dunn et al. (1989) had pointed out the possibility of increased recovery due to dispersion. Although the application of dispersion coefficient improved the rate of recovery of their analytical model by almost an order of magnitude, they were not able to address the 460 times discrepancy with respect to some of their experimental results. Part of this discrepancy might be due to the fact that they used a constant diffusion coefficient, independent of solvent concentration. Depending on the solubility limit of the solvent under prevailing pressure and temperature, the estimated diffusion coefficients as a function of concentration can change by almost two orders of magnitude. Complications due to existence of connate water as the second phase and/or human error are other possibilities that might have caused such a large discrepancy.

Lim et al. (1996) used an effective diffusivity, 2-3 orders of magnitude higher than molecular diffusivity to history-match their experimental results in sandpacks. They mentioned that the mechanism relating to an increase in diffusivity is not well understood. But, they had pointed out physical dispersion as one of the most viable processes governing the enhanced mass transfer in porous media.

Nghiem et al. (2000) developed an Equation of State compositional simulation model for prediction of asphaltene dropout and assessment of downhole upgrading capability of bitumen by Vapex. They incorporated molecular diffusion and convective dispersion into their material balance. They used a constant dispersivity coefficient, as a direct multiplier to the phase velocity (rather than Peclet number) in their numerical modeling. They mentioned that the mixing mechanism is effectively controlled through a total dispersion coefficient. They also showed through sensitivity analysis that larger dispersion coefficients result in higher mixing. However, they did not elaborate on the criteria for selection of the most appropriate coefficient.

Although arbitrary multipliers might provide a good history match to some laboratory experiments, they might fail to provide a reasonable match for different solute-solvent pair or formations of different lithological characteristics. Therefore, a more rigorous and systematic approach in selection of such multipliers is necessary to provide a more reliable estimation of the recovery rates. This aspect of the dispersion is of significant importance, since the economic prospect of the project is directly controlled by the recovery speed.

3-2 Longitudinal and Transverse Dispersion

The mass transfer in Vapex, similar to other mass transfer processes in porous media, is comprised of two components, the longitudinal and transverse dispersion. Longitudinal dispersion develops along the direction of the bulk flow in systems where both solute and solvent are flowing in the same direction. Downward movement of diluted oil along the interface will cause longitudinal dispersion in the same direction and transverse dispersion, perpendicular to the direction of bulk flow and into the bitumen. This process is schematically illustrated in Figure-3.1.

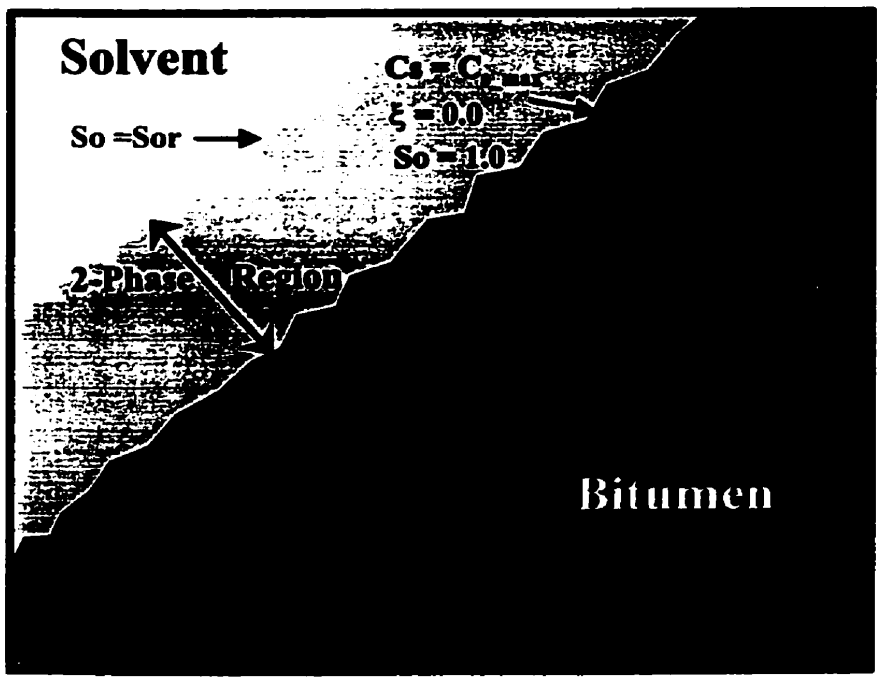

Figure-3.1: Development of longitudinal and transverse dispersion vs. bulk flow.

Transverse dispersion was earlier perceived to be the sole mechanism controlling the improved delivery of solvent into the bitumen bulk in Vapex process (Personal conversations with Dr. Ashok Singhal, Petroleum Recovery Institute (PRI), Calgary-Canada, July 1999). However, later on it was realized that indeed both longitudinal and transverse dispersion are actively present in 2-D models of Vapex experiments.

Blackwell (1962) conducted a series of experiments in a sand-packed column to investigate the microscopic dispersion, where one fluid is displaced from a porous media by a second fluid, which is miscible in the first. In this work, transverse dispersion coefficients were measured for a range of flow rates, grain sizes, fluid viscosities and column lengths. They compared the results of experiments by plotting the experimental dispersion coefficients divided by molecular diffusion, K_t/D_o vs. mass transfer Peclet number, d_pU/D_o. The results of these experiments presented in Figures 3.2 to 3.4 indicate that transverse dispersion is independent of column length and fluid viscosity and rather a strong function of fluid velocity and average particle radius.

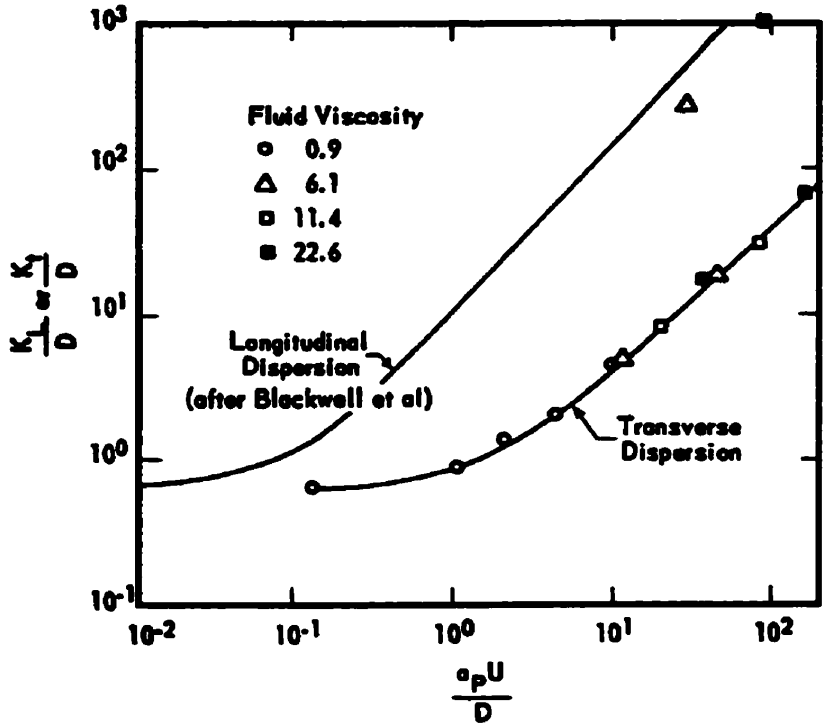

Figure-3.2: Examination of effect of viscosity on dispersion in 40-200-mesh sand. (After Blackwell, 1962)

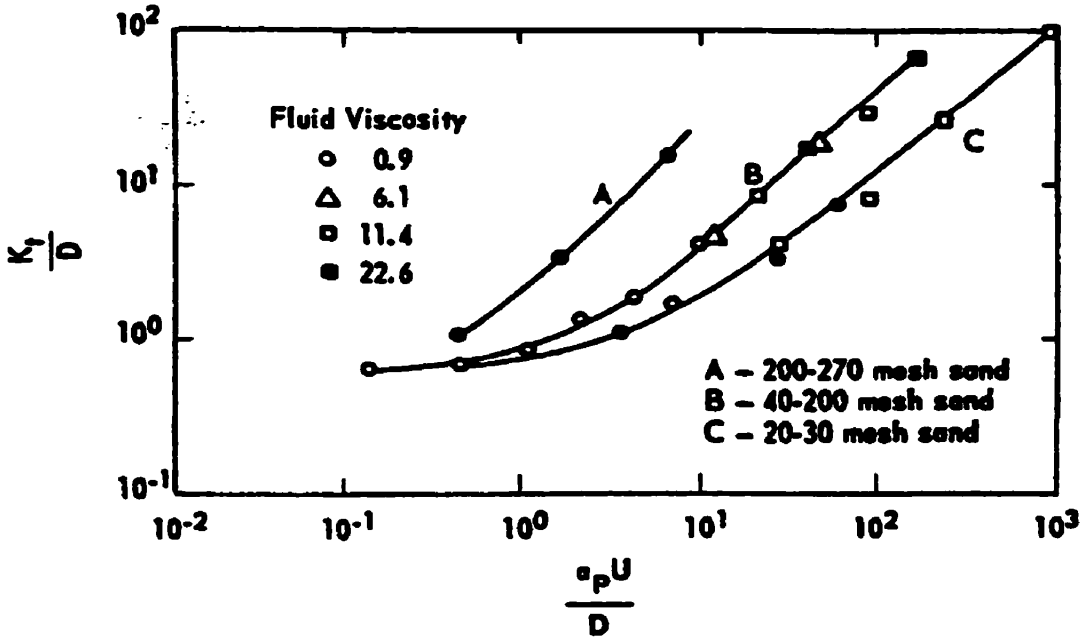

Figure-3.3: Examination of effect of sand size on transverse dispersion coefficient. (After Blackwell, 1962)

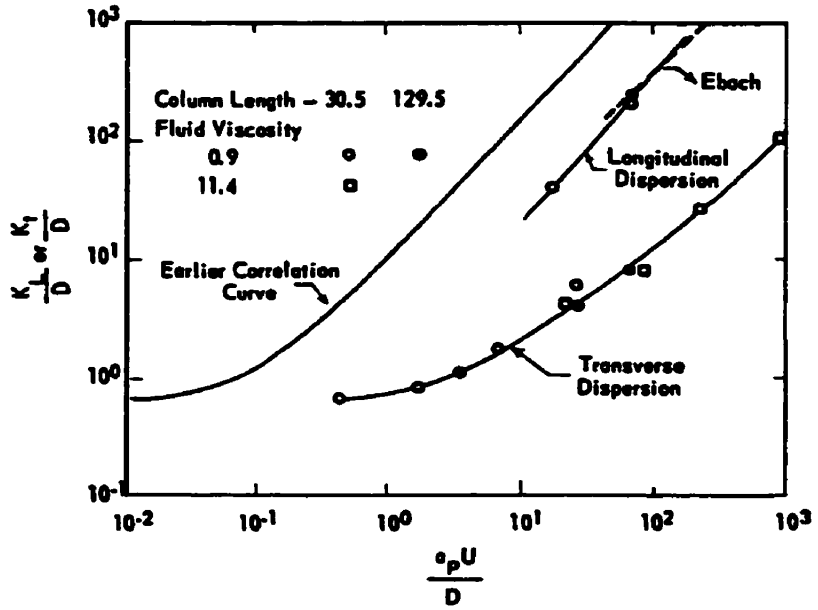

Figure-3.4: Examination of effect of column length on dispersion in 20-30-mesh sand. (After Blackwell, 1962)

Magnetic Resonance Imaging (MRI) of the Vapex process (Fisher et al. 2000) as shown in Figure-3.5, indicates existence of a funnel-shaped zone of oil with dissolved gas in a 2-D model. Enlargement of the zone of increased gas concentration towards the lower side of the model is caused partly by the expected increase in the volume of flow with increasing distance from the top of the model and partly by the fixed location of the production well. It indicates that as the diluted oil moves down the interface, the vertical velocity decreases and the horizontal velocity vector increases slightly.

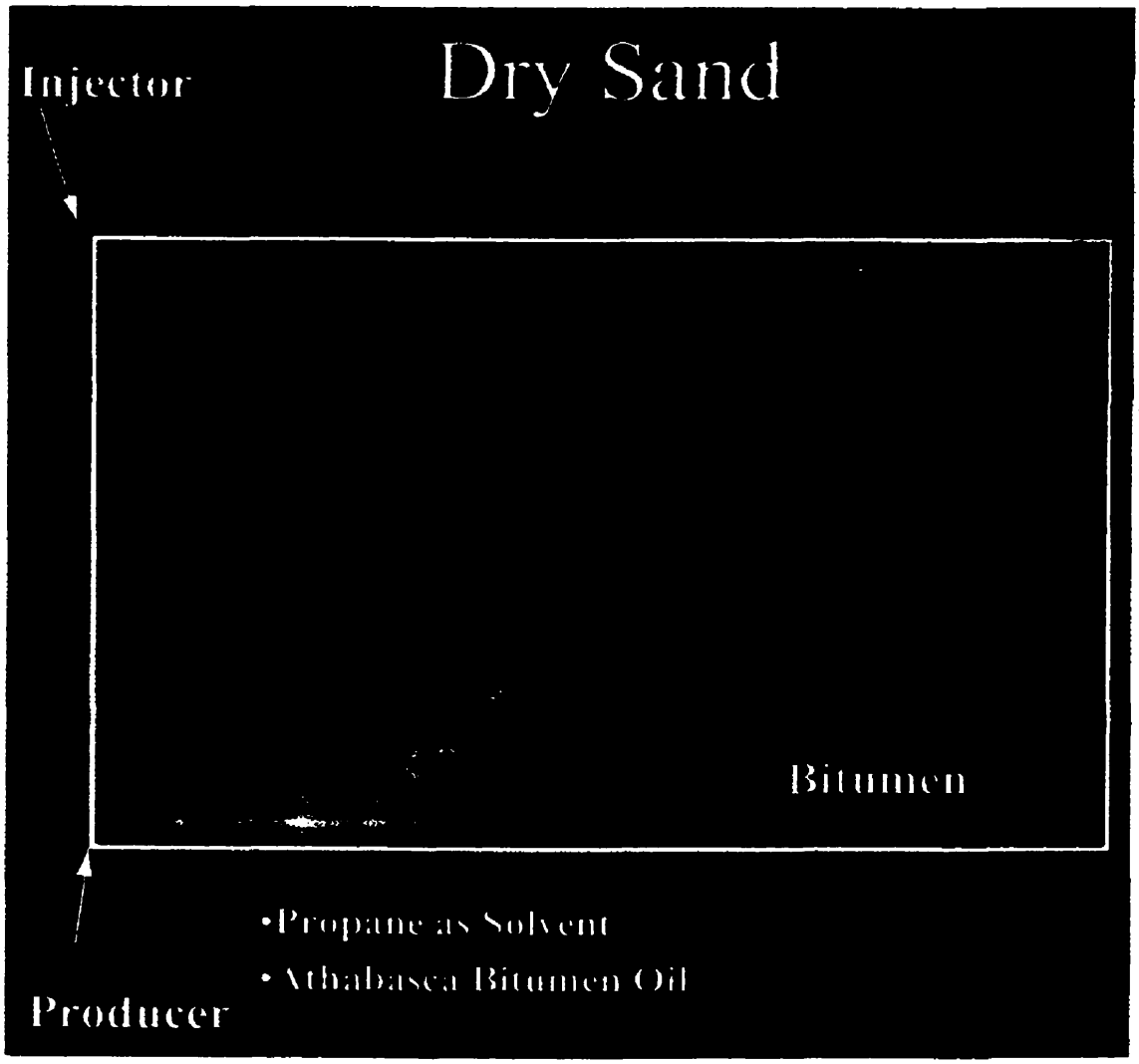

Figure-3.5: MRI image of Vapex using Athabasca bitumen and propane, T=17 °C. (After Fisher et al., 2000)

In a region where both diffusion and dispersion are present, the overall mass transfer is the summation of both diffusion and dispersion components. Perkins & Johnston (1963) present relationships for estimation of overall mass transfer under the influence of longitudinal and transverse dispersions as shown in Equation-3.1 and 3.2 respectively.

$$\frac{K_l}{D_o} = \underbrace{\frac{1}{F\phi}}_{\text{Molecular Diffusion}} + \underbrace{0.5\,\frac{V d_p \sigma}{D_o}}_{\text{Convective Dispersion}}; \qquad \text{where } \frac{V d_p \sigma}{D_o} < 50 \tag{3.1}$$

$$\frac{K_t}{D_o} = \underbrace{\frac{1}{F\phi}}_{\text{Molecular Diffusion}} + \underbrace{0.0157\,\frac{V d_p \sigma}{D_o}}_{\text{Convective Dispersion}}; \qquad \text{where } \frac{V d_p \sigma}{D_o} < 10^4 \tag{3.2}$$

where,

K_t = transverse dispersion coefficient

K_l = longitudinal dispersion coefficient

d_p = particle diameter

σ = inhomogeneity factor

D_o = molecular diffusion coefficient

V = convective fluid velocity in the direction of bulk flow

The first term of both the above equations corresponds to molecular diffusion component of mass transfer as a function of formation factor and system porosity. The second term is the dispersion component, expressed in terms of the product of Peclet number N_{Pe}, and a multiplier. The Peclet number is a dimensionless parameter, which in the mass transfer theory is expressed as a function of particle diameter, bulk fluid velocity and molecular diffusion coefficient. The particle diameter is primarily used to characterize the size of the flow channels in the porous media. Although a characteristic radius, more directly related to the actual pore size distribution is desirable, the average particle radius is determined readily by sieve analysis and appears to adequately characterize the size of the flow channels for many types of porous media (Blackwell, 1962). The inhomogeneity index σ,

is a constant value for a given media and expresses the degree of variation in pore size distribution. For typical random packs, σ is usually about 3.5 (Perkins and Johnston, 1963). However, σ may be larger for poorly packed beads or a bit smaller for larger beads. The two multipliers of the above dispersion components (0.5 and 0.0157) are numbers that previous investigators have found during laboratory investigation of dispersion phenomena in unconsolidated sand or bead packs (Aris and Amundson 1957, Blackwell 1962, Perkins and Johnston 1963).

The above relationships indicate that in a system where petrophysical parameters (Archie's constant 'a', cementation factor 'm', porosity 'ϕ') are available and the dependency of molecular diffusion coefficient and mixture viscosity to solvent concentration are known $\{D_o=f(C_s)$ and $\mu=f(C_s)\}$, velocity distribution in a 2-D model can be used to compute the corresponding longitudinal and transverse dispersion coefficients.

In the absence of a 2-D model, the only mass transfer mechanisms, which are capable to deliver solvent to the bulk of the bitumen, would be molecular diffusion and transverse dispersion. In reality, enhanced mass transfer due to longitudinal dispersion increases the concentration of solvent along the interface. The increased concentration at any level along the interface provides more solvent to be transported to the bulk of bitumen under the influence of transverse dispersion. In that regard, no matter how small is the convective velocity, the larger coefficient of longitudinal dispersion makes its presence on the overall mass transfer noticeable. Therefore, in a 2-D model, the influence of longitudinal and transverse dispersion is necessary. As the shape of the interface changes in time, the orientation of the velocity-vector V, and its projections in X and Z-directions change. Therefore, utilization of a two dimensional model provides a better representation of dispersive mass transfer.

Note that in the absence of velocity terms, K_l and K_t would be reduced to their minimum values, equivalent to D_{app} term in equation 2.14-b. Moreover, it should be emphasized that the diffusion coefficients in the above equation are exclusively the intrinsic diffusion coefficients of solute in solvent, rather than overall diffusion coefficients. The overall diffusion coefficient incorporates both the pure molecular diffusional mass transfer as well as the transport term due to diffusion-induced-convection. However, since in our model the convective velocities are formulated separately, the intrinsic diffusivities should be used instead. This concept is explained in more detail in Chapter-4.

3-3 Diffusion Coefficient in Vapex

It is important to mention that mass transfer theories utilize "Solute" & "Solvent" terminologies in a different context than that used in oil industry. In mass transfer theories, Bitumen (comprising the bulk of the mixture and accommodating the molecules of propane at smaller mass fraction) for example, would be referred to as Solvent, whereas propane would be the Solute. However, in the context of this work we maintain the consistency with the established norm in oil industry and refer to propane as the solvent.

There are several theories for estimation of diffusion coefficients for liquids and gases in the literature. Predictive theories of diffusion are not as well developed for liquids as they are for gases (Schmidt, 1989). Many of these theories are built around the kinetic phenomena in liquids. However, because of the arbitrary assumptions involved in treatment of kinetic forces, none of these theories are quite satisfactory in predicting the correct diffusivities for bitumen systems (Oballa & Butler, 1989).

Correlations on the basis of molecular theory use the Stokes equation to determine the force on a sphere of a molecule immersed in a fluid. In dilute solutions of spheres in Newtonian fluids, the force acting on spheres moving through the fluid is directly proportional to the number of spheres in solution and inversely to the viscosity of the fluid they move through. In that regard, the dependency of diffusivity to concentration can be expressed as $D= \alpha\mu^{-\beta}$,

where viscosity dynamically changes as a function of concentration. In this relationship, coefficients of α & β depend on the characteristics of the solute/solvent pair. Table-3.1 summarizes some of the correlations for estimation of molecular diffusion coefficients.

Table-3.1: Comparison of correlations for estimation of liquid diffusivities.

$D = 7.4 \times 10^{-8} (\Phi M)^{0.5} T \mu^{-1} V_a^{-0.6}$	Wilke & Chang (1955) All Solutes
$D = RT/3\pi\mu d$	Reid et al. (1987)
$D = \alpha\mu^{-\beta}$	Hayduk & Cheng (1971)
$D = \alpha\mu^{-2/3}$	Hiss & Cussler (1973)
$D = 0.0591 \times 10^{-9} \mu^{-0.545}$	Hayduk et al. (1973) * Propane, Peace River Bitumen
$D = 1.306 \times 10^{-9} \mu^{-0.46}$	Das & Butler (1996) * Propane, Peace River Bitumen
$D = 4.131 \times 10^{-9} \mu^{-0.46}$	Das & Butler (1996) * Butane, Peace River Bitumen
$D = 13.3 \times 10^{-8} T^{1.47} V_a^{0.71} \mu^{(10.2/V_a - 0.791)}$	Hayduk & Minhas (1982) ** Normal Paraffin Solute/Solvent

* - Units are: D= (m^2/s) ; μ = (Ps)
** - Units are: D= ($c\ m^2/s$) ; μ = (cp)

Many authors assume that the product of viscosity (μ) and diffusivity (D) is a constant, which might be a valid assumption for ideal mixtures. But as soon as there is deviation from ideality (e.g. concentrated solutions), this relationship does not hold anymore.

Schmidt (1989) summarized a number of correlations for estimation of binary diffusion coefficients in concentrated solutions. Almost all these correlations are defined as a function of diffusivity at infinite dilution. In the absence of experimental data at infinite dilution, it is possible to use binary diffusion coefficients of diluted solutions and predict the diffusivity at concentrated range. However, Schmidt noted that there are several

different possibilities for this approach and most of the existing correlations have not been tested yet.

Where theoretical correlations fail to provide reliable estimates, experimental approach can be used to measure molecular diffusivity. In general, the end user should examine the relevant assumptions controlling the validity of each correlation in regard to the particular case under his/her investigation.

Figure-3.6 presents the estimated molecular diffusion coefficient of propane into Panny heavy oil as a function of solvent concentration based on three different correlations. Note that the estimated diffusivities by Das and Butler (1996) are more than an order of magnitude higher than those estimated by Hayduk et al (1973) and Hayduk & Minhas (1982) correlations. The primary reason for this difference is that Das and Butler used α and β coefficients (through an optimization procedure) that provide a better history match to their experiments in Hele-Shaw cell. In that regard, any additional mechanism that could have affected the experimental rates of Vapex in Hele-Shaw cell is overlooked.

It is noteworthy that the coefficients proposed by other researchers were derived from a large database of experiments that were primarily dedicated to measurement of molecular diffusion coefficient. Needless to say, utilization of arbitrary coefficients might result in estimation of inappropriate diffusion coefficients. Therefore, in the absence of additional information, there is a greater likelihood that the coefficients of α and β by Hayduk at al. and Hayduk and Minhas provide a more reliable estimate of true diffusive characteristic of solute/solvent pair.

Prior to any further discussion on this topic, it is important to review the following terminologies in the mass transfer theory.

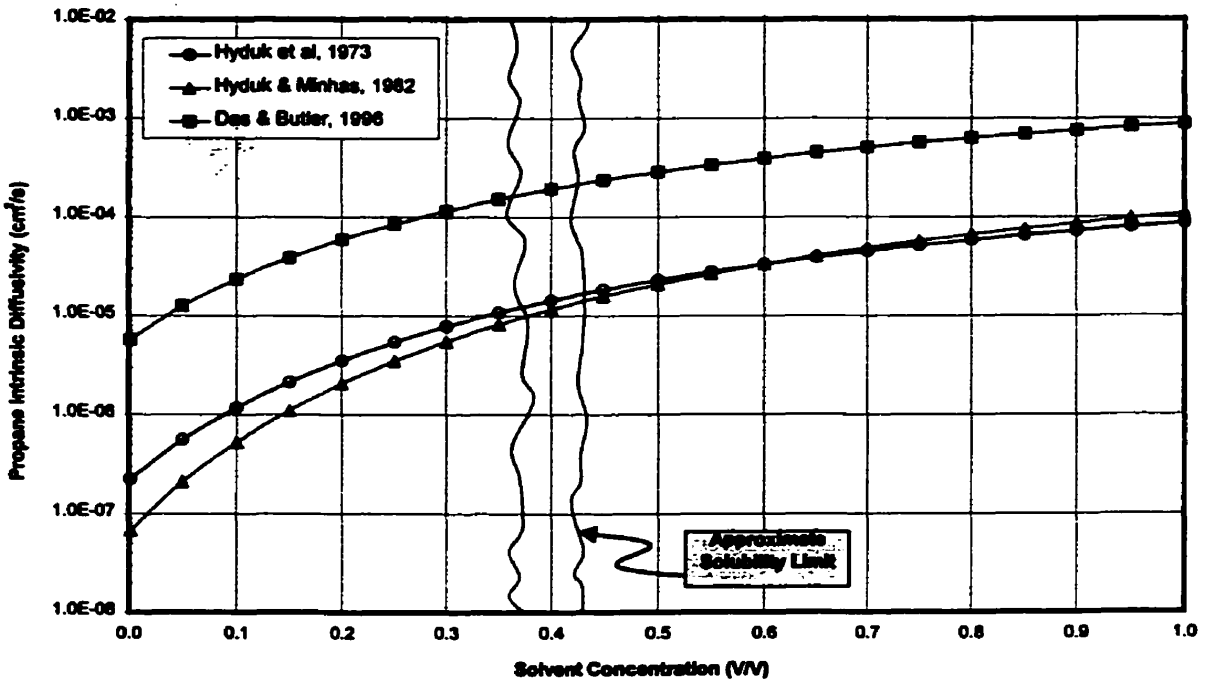

Figure-3.6: Dependency of intrinsic diffusivity on propane concentration, Panny oil.

Self-Diffusion Coefficient: Refers to diffusion of a single component within itself due to the Brownian motion of the molecules.

Intrinsic Diffusion Coefficient: In concentrated solutions and/or solutions that the molecular sizes of solute and solvent are significantly different, convective currents are created. Under such circumstances, the overall mixing of the two components (overall transport) is both under the influence of the induced convection and a pure molecular diffusion term, the so-called intrinsic molecular diffusion coefficient. In some experimental measurements of diffusion, the combined effect of the two processes is measured in terms of an overall diffusion coefficient. Therefore, introduction of intrinsic diffusion coefficient helps to separate these two effects.

Overall Diffusion Coefficient: The overall diffusion coefficient represents the net result of diffusion process and the bulk flow rate of the solvent/solute mixture. The bulk flow is

created due to convective forces created under the influence of concentration gradients, in concentrated solutions. Introducing the idea of intrinsic diffusion coefficient can separate these two (experimentally dependent) mass transfer coefficients.

Apparent Diffusion Coefficient: The apparent diffusion coefficient in porous media is usually based on the average cross-sectional area open to diffusion and the distance traveled by the molecules. Due to the tortuous paths in porous media, the actual average distance that molecules move is larger than the net distance between the two points. Therefore, apparent diffusion coefficient is smaller than the intrinsic diffusion coefficient. This concept is schematically illustrated in Figure-3.7.

The multiplier relating the intrinsic diffusion coefficient to apparent diffusion coefficient is controlled by system tortuousity, as shown by equation 2.14-b. This multiplier can be determined externally, if the corresponding petrophysical parameters as listed in Table-2.1 are known. In the Hele-Shaw cell where porosity is 100%, tortuousity is zero and the apparent diffusion coefficient is equal to intrinsic molecular diffusion coefficient.

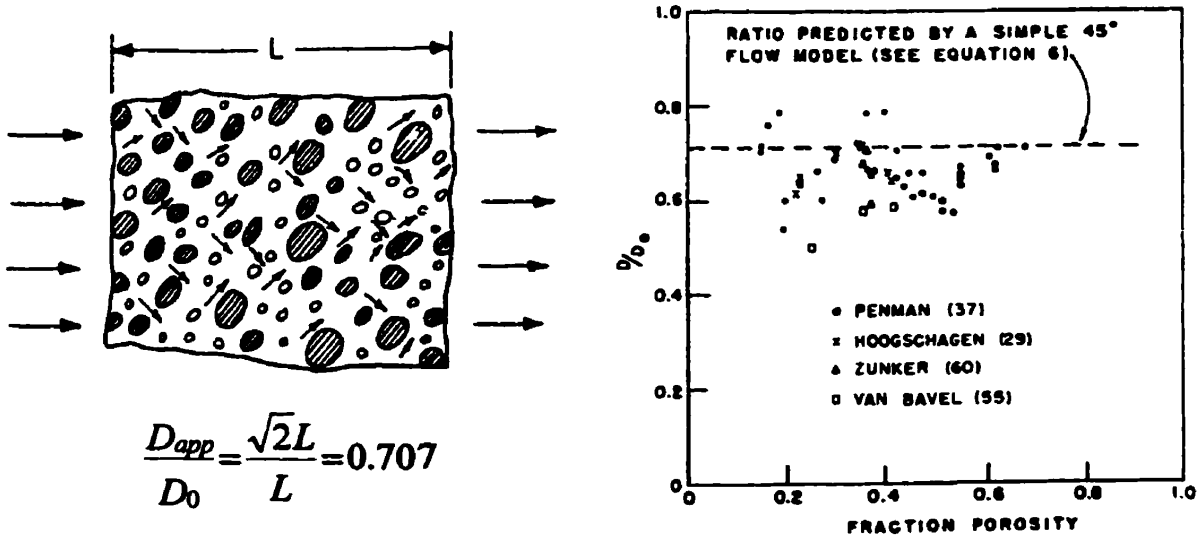

Figure-3.7: The effect of a tortuous path on apparent diffusion coefficient. (After Carman, 1939)

Effective Diffusion Coefficient: The recovery rates from experimental tests in porous media were observed to be higher than the estimated values from molecular diffusion coefficients. Therefore, effective diffusion coefficient was introduced to incorporate the combined effect of all the parameters that can potentially result in higher mass transfer in Vapex in porous media. At low fluid velocities where Peclet number is almost zero the longitudinal and transverse dispersion effects are absent and therefore, the effective diffusion coefficient becomes equal to apparent diffusion coefficient.

CHAPTER FOUR

MODELING AND MESAUREMENT OF DIFFUSION COEFFICIENT IN CONCENTRATED SOLUTIONS

Several investigators have expressed numerical values for diffusivity of different substances in bitumen and heavy oils. However, the reported values appear to be constant and independent of solvent concentration (Fu & Phillips 1978, Schmidt et al. 1982, Schmidt 1989, Riazi 1996, Zhang et al. 1998). Moreover, many of the quantitative examination of the diffusion process are conducted either in the regions of high or low solvent concentration (Schmidt, 1989). The primary objective of this section is to review the development of mass transfer theories for bituminous systems and highlight the strong dependency of diffusion coefficient on solvent concentration, over the entire concentration range.

Hutcheon et al. (1952) presented a methodology for measurement of inter-diffusion of polyvinyl acetate with a series of solvents at intermediate concentration. They mentioned that in systems where solute and solvent have considerable difference in molecular size, the rate of true diffusion should be much slower for larger molecules (e.g. bitumen and polymer) than that for smaller molecules (e.g. solvent). However, as the solvent molecules diffuse into the polymer, its volume increases and as a result produces an apparent diffusion of the polymer species into the solvent phase. In their experiments, they placed the solute and solvent in a transparent static diffusion cell, as shown in Figure-4.1, and determined the rate of overall diffusion by measurement of refractive index with a monochromic light passing through the cell. The concentration of solvent is determined from the relationship between the refractive index and concentration, as a function of cell coordinate.

Hutcheon et al. (1952) showed that intrinsic diffusion coefficient of polymer could be neglected in their experiments. This enabled them to calculate the intrinsic diffusion coefficient of the solvent. They observed that the overall (mutual) diffusion coefficient

attains a maximum value at intermediate polymer concentrations (as shown in Figure-4.2), whereas intrinsic diffusion coefficient is continuously increasing.

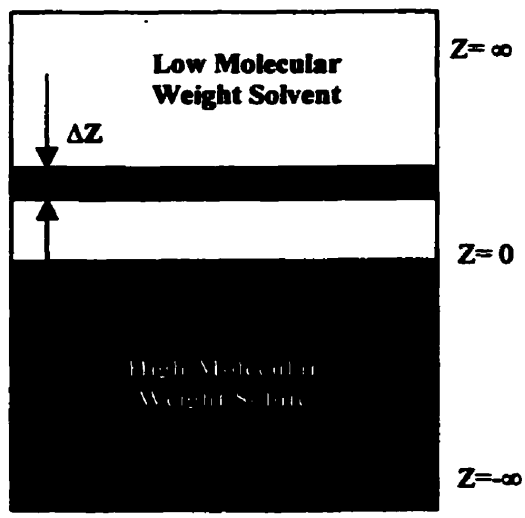

Figure-4.1: Static diffusion cell.

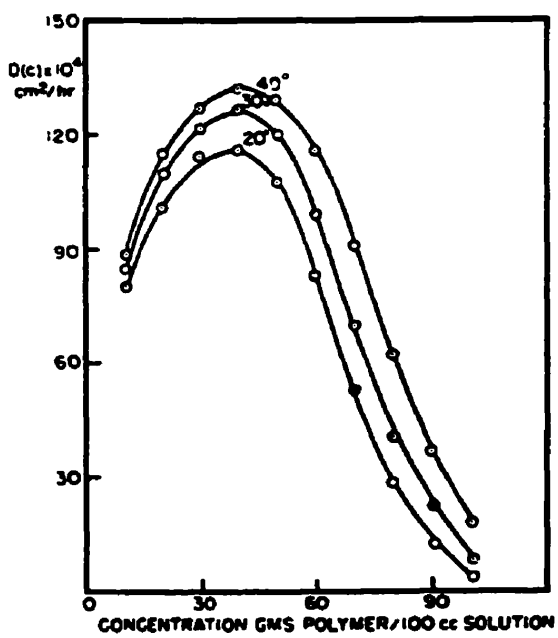

Figure-4.2: Mutual diffusion coefficient for acetone-polyvinyl acetate as a function of concentration and temperature, (After Hutcheon et al., 1952)

Hayes and Park (1955) conducted a set of experiments for measurement of diffusion of benzene in rubber. Similarly, they observed maximum values of overall diffusion coefficient at intermediate concentrations, as shown in Figure-4.3. However, they noted that variation of the viscosity with concentration is very much larger than variation of diffusion coefficient.

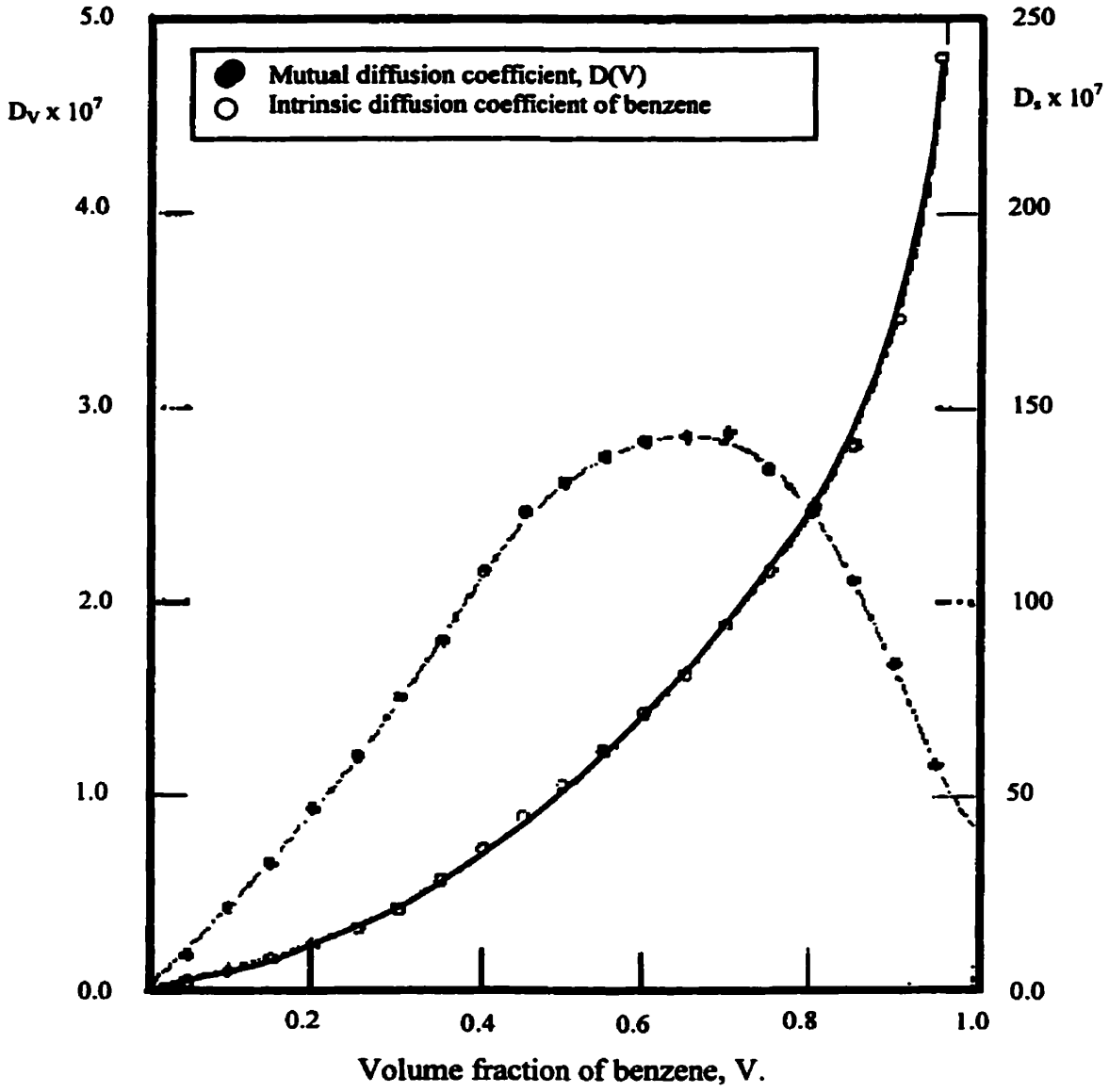

Figure-4.3: Mutual and intrinsic diffusion coefficient of benzene in rubber. (After Hayes & Park, 1955)

Oballa and Butler (1989) adopted the same methodology and applied it for measurement of diffusion in bitumen-toluene systems, utilizing a vertical cell with closely spaced flat windows. Concentration distributions were measured by means of pulsed laser beam in vertical direction. The results of the experiments indicated strong dependency of diffusion coefficients on concentration.

Figure-4.4 presents the measured overall diffusion coefficient from a series of experiments by Oballa & Butler. The perfect overlay of all the points from different runs on a single curve suggests that overall diffusion coefficient is not depended on cell spacing. They utilized the self-diffusion coefficient values (from literature) and back calculated the intrinsic diffusion coefficients for bitumen and solvent, as shown in Figure-4.5.

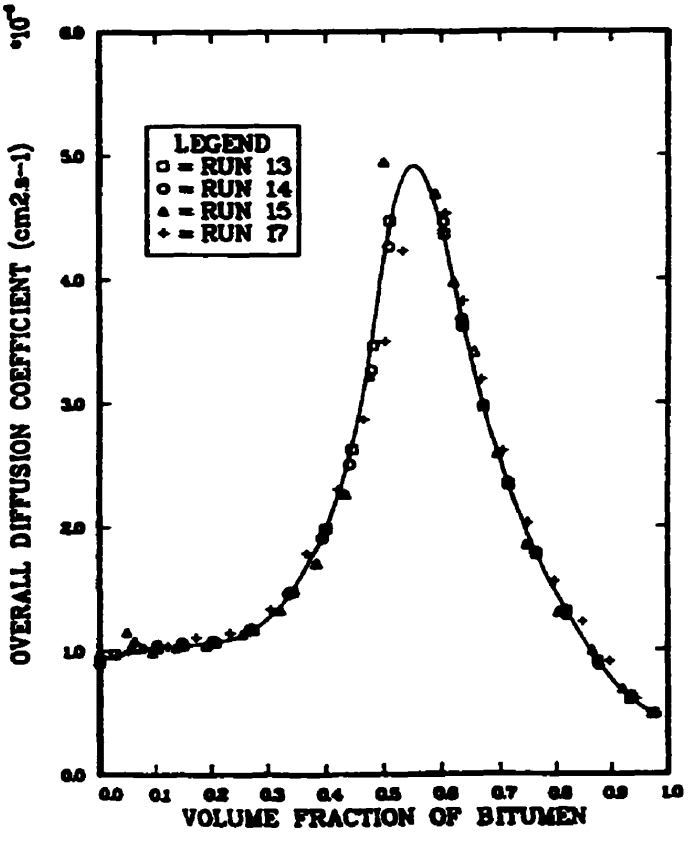

Figure-4.4: Overall diffusion coefficient for toluene-bitumen system. (After Oballa & Butler, 1989)

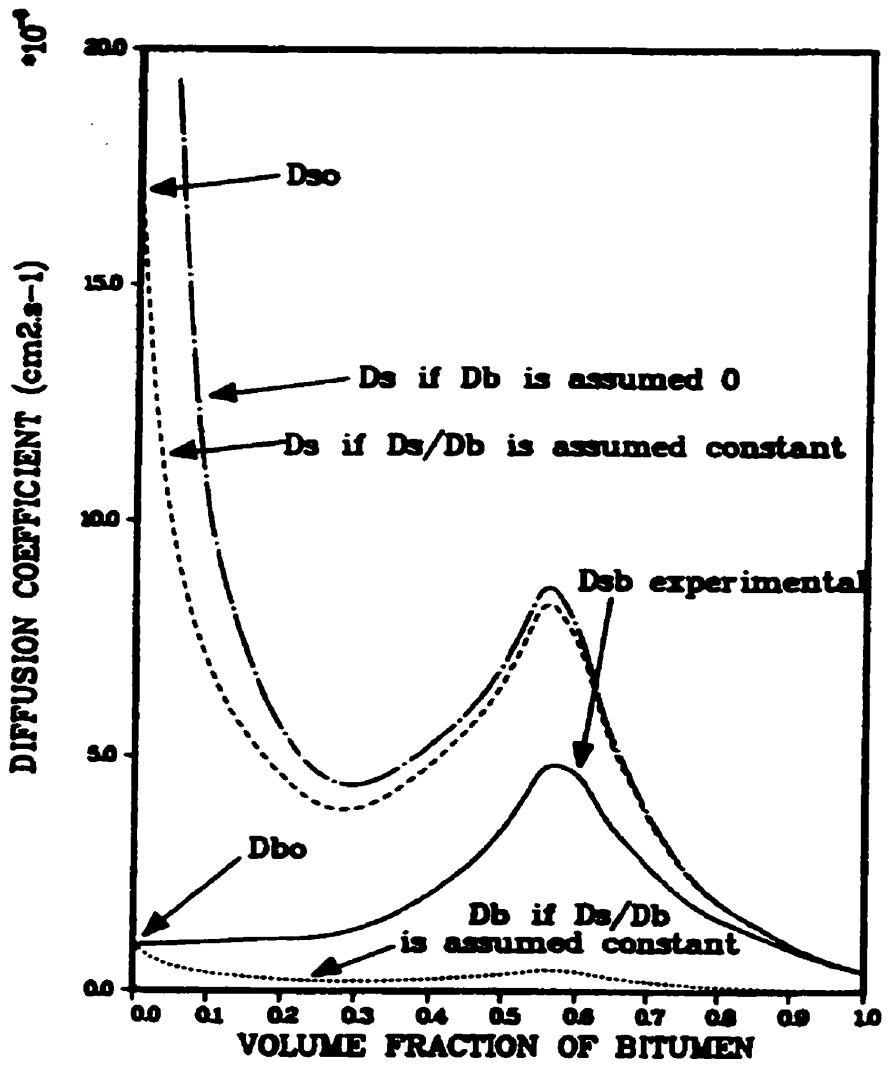

Figure-4.5: Intrinsic Diffusivity of toluene in bitumen (After Oballa & Butler, 1989).

Oballa and Butler observed peak intrinsic diffusivities at intermediate concentrations. This behavior was contrary to the expected trend, and they attributed that to formation of transient asphaltene structures. Existence of asphaltene as the third phase violates the assumption of a binary diffusion process. However, a later work for measurement of intrinsic diffusivity of CO_2 in bitumen by Upreti (2000), reproduced similar behavior at intermediate concentrations.

In this work, Upreti injected known amount of gas into a closed vessel at constant temperature. The gas, which is placed on top of a bitumen sample, gradually diffused into the bitumen. Due to diffusion of gas into the bitumen, the total moles of free gas in the space above the bitumen decreased. The reduced moles of free gas are measured in terms of transient pressure decay in time. Since the surface area of the vessel is known, it is possible to relate this pressure decay to intrinsic molecular diffusivity of the gaseous solvent.

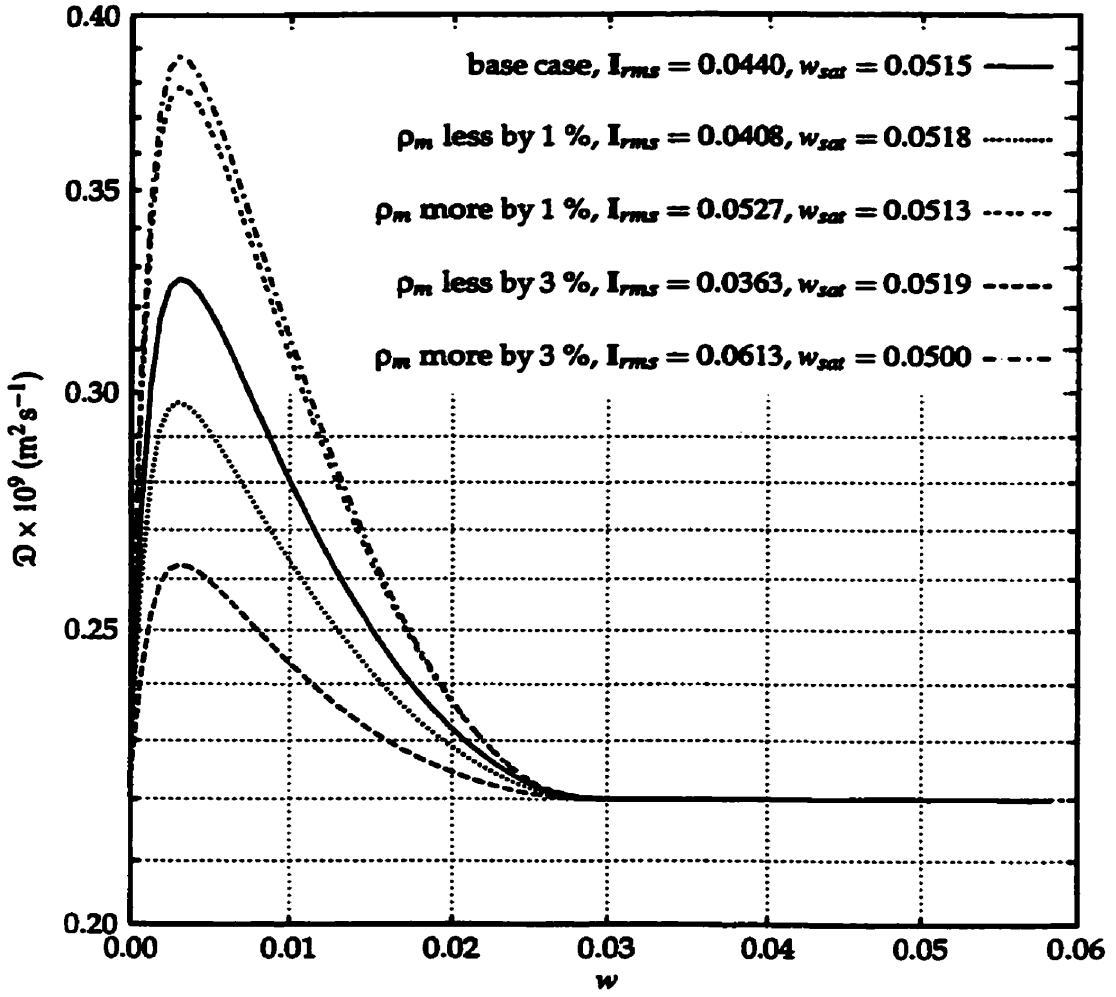

Figure-4.6: Intrinsic Diffusivity of CO_2 in Athabasca bitumen at 4 MPa. (After Upreti, 2000)

Figure-4.6 presents the calculated intrinsic molecular diffusivities vs. CO_2 concentration by Upreti. Note that the peak diffusivity in this plot is developed at concentrations around C=0.003 (w/w). Considering the large molecular weight of the bitumen used in the experiments, its likely that this number corresponds to concentrations close to C=0.01 (V/V). This number is considerably smaller than the solvent concentration of 45% (V/V) for peak intrinsic diffusivity in Oballa & Butler's work. The main difference between the two systems is that toluene-bitumen are completely miscible, whereas CO2-bitumen have limited solubility. Therefore, the observed concentration at peak intrinsic diffusivity is either due to the solubility limit of solvent into bitumen, or is indicative of a wide variation of behavior of intrinsic diffusion coefficient at intermediate concentrations, for different solute-solvent pairs.

It is important to mention that the asymptotically increasing values of intrinsic diffusivity vs. solvent concentration, as suggested by analytical correlations of Table-3.1, are different than the trends obtained by Oballa (1989) and Upreti (2000). On the other hand, the propane solubility hardly exceeds concentrations in excess of 25% by mass (Das & Butler, 1996) (40 % by volume). Therefore, there is a great likelihood that for the practical ranges of solvent concentration, analytical correlations might exhibit identical trend to experimental values and provide a reasonable estimate of molecular diffusion coefficients.

Earlier, on the discussion of dispersion effects in porous media, it was seen that the magnitude of intrinsic diffusion coefficient could considerably affect the dispersive mass transfer through computation of Peclet number. Therefore, the validity of observed peak diffusivity over the complete concentration range should be examined further. This can be of greater importance for Miscible processes where solvent concentration can be as high as 100%.

The remainder on this chapter deals with reviewing the development of analytical relationships used for calculation of intrinsic diffusion coefficients from experimentally measured overall diffusivities.

4-1 Intrinsic Diffusion Coefficient

During diffusion of solvent into bitumen, the small molecules of solvent tend to diffuse faster than the macromolecules of bitumen. As a result of diffusion of solvent into bitumen, the pressure within the bitumen system increases and causes a bulk flow of bitumen into the solvent-rich section (Hutcheon et al., 1952). In a static diffusion cell, the net flow of solvent in the Z direction is the sum of the diffusional flux of solvent $-D_s \partial Cs/\partial Z$ and the flux of solvent carried by the bulk flow $u.C_s$. To satisfy volume conservation, this net flow must be equal to the flow of bitumen transferred by diffusion and bulk flow as follows:

$$-D_s\frac{\partial C_s}{\partial Z}+u_z\cdot C_s = D_b\frac{\partial C_b}{\partial Z}-u_z\cdot C_b \qquad (4.1)$$

The left-hand side (LHS) of equation 4.1 is the net flux of solvent downward and the RHS corresponds to net bitumen flux upward. D_s and D_b are intrinsic diffusion coefficients for solvent and bitumen respectively and are generally functions of concentration. The first term in each side of this equation corresponds to diffusion mass flux whereas the second term corresponds to convective bulk flow. Equation 4.1 can be rearranged in terms of bulk flow velocity, assuming constant volume upon mixing (i.e. excess volume = 0.0) such that $C_s + C_b = 1.0$ (i.e. concentrations are volume fraction).

$$u_z = (D_s - D_b)\frac{\partial C_s}{\partial Z} \qquad (4.2)$$

From equation (4.2) it becomes obvious that in systems with identical intrinsic molecular diffusion coefficients, the diffusion-induced-convection velocity is nearly zero. However, in solvent-bitumen system where the difference between the molecular size of solute and solvent is large, intrinsic diffusion coefficient of solvent is substantially higher than that of solute and hence the velocity term is significant. It is important to mention that in a particular system, both diffusion coefficients (D_b and D_s) as well as velocity "u" will be functions of concentration. Incorporating the diffusion and convection terms into the

volume balance across a unit element ΔZ, results in the following one-dimensional pseudo-steady-state equation.

$$\frac{\partial}{\partial Z}\left(D_s\frac{\partial C_s}{\partial Z}-u_z\cdot C_s\right)=\frac{\partial C_s}{\partial t} \tag{4.3}$$

If individual values for intrinsic diffusion coefficients (D_s and D_b) or the inter-relationship between D_s and D_b are known for a solvent/solute pair, it is possible to proceed with the solution of the problem. However, neither of them is usually known. Therefore, laboratory techniques are used to measure the overall diffusivity and utilize analytical correlations to determine the intrinsic diffusion coefficient.

4-2 Dependency of Intrinsic to Overall Diffusivity

In a static diffusion cell, as shown in Figure-4.1, the plane of Z=0 is the sharp interface between the two components at zero time. As time goes by, the fluids tend to move to the other side and hence diffuse into each other. Due to volume conservation in the system, the sum of both flows must be equal to zero. In that regard, the diffusion coefficient of solvent into bitumen (D_{os}) is equal to the diffusion coefficient of bitumen into solvent D_{ob}.

$$D_{os} = D_{ob} = D_{bs}. \tag{4.4}$$

The term D_{bs} is the overall diffusion coefficient of either component (bitumen or solvent) and is perceived as a material property, dependent on system composition, temperature and pressure. The volume balance for pseudo-steady-state diffusion of solute/solvent in a static cell with fixed volume can be expressed as:

$$A.j_s|_z - A.j_s|_{z+\Delta z} = \text{Volume Accumulation} = A.\Delta Z\ \partial C_s/\partial t \tag{4.5}$$

Dividing both sides by unit volume (A.ΔZ) and taking the limit as ΔZ➔0 yields:

$$\frac{\partial C_s}{\partial t} = -\frac{\partial j_s}{\partial Z} = \frac{\partial j_b}{\partial Z} \tag{4.6}$$

Incorporating the Fick's law of diffusion as $j_s = -D_{ss}\frac{\partial C_s}{\partial Z}$ and equation 4.4 results in:

$$\frac{\partial C_s}{\partial t} = -\frac{\partial j_s}{\partial Z} = \frac{\partial j_b}{\partial Z} = \frac{\partial}{\partial Z}(D_{ss}\frac{\partial C_s}{\partial Z}) \tag{4.7}$$

Combining equation (4.7) and (4.3) results in:

$$\frac{\partial}{\partial Z}(D_{bs}\frac{\partial C_s}{\partial Z}) = \frac{\partial}{\partial Z}(D_s\frac{\partial C_s}{\partial Z} - u_s C_s) \tag{4.8}$$

Therefore,

$$D_{bs}\frac{\partial C_s}{\partial Z} = D_s\frac{\partial C_s}{\partial Z} - u_s C_s \tag{4.9}$$

Combining equation (4.2) and (4.9) results in

$$D_{bs}\frac{\partial C_s}{\partial Z} = D_s\frac{\partial C_s}{\partial Z} - C_s(D_s - D_b)\frac{\partial C_s}{\partial Z} \tag{4.10}$$

Canceling the concentration gradients $\partial C_s/\partial Z$ from both sides of equation 4.10 results in:

$$D_{bs} = D_s - C_s(D_s - D_b) \tag{4.11}$$

Since concentration is expressed as volume fraction, where C_b=1-C_s, then:

$$D_{bs} = D_s(1 - C_s) + D_b C_s = D_s C_b + D_b C_s \tag{4.12}$$

From equation 4.12 the following end-point boundary conditions can be considered:

@ $C_s = 0.0$ ➔ C_b=1.0 and hence D_{bs}=D_s (i.e. overall diffusion is controlled by solvent)

@ $C_s = 1.0$ ➔ C_b=0.0 and hence D_{bs}=D_b (i.e. overall diffusion is controlled by bitumen)

This implies that the value of the overall diffusion coefficient is equal to the intrinsic diffusion coefficient of solvent in pure bitumen and equal to intrinsic diffusion coefficient of bitumen in pure solvent. Oballa and Butler (1989) suggest that the concentration dependence for both intrinsic and self-diffusion coefficients are similar. Therefore, the ratio of D_s/D_b will be constant and expressed as:

$$\text{i.e. } \frac{D_s}{D_b} = \frac{D_{so}}{D_{bo}} \tag{4.13}$$

By substituting equation 4.12 into the above equation, we can derive a relationship to calculate intrinsic diffusion coefficient for bitumen, as a function of overall diffusivity:

$$D_b = \frac{D_{bs}}{\frac{D_{so}}{D_{bo}} C_b + C_s} \tag{4.14}$$

The above formulation provides an easy way of determining the intrinsic diffusivity of solute and solvent, from a set of laboratory experiments dedicated to the measurement of overall diffusivity in concentrated solutions.

Although laboratory techniques for measurement of diffusivity provide more accurate information at intermediate concentrations, they are extremely labor intensive and time consuming. In addition, some uncertainties (e.g. peak intrinsic diffusivity at intermediate concentrations) are still surrounding the validity of these procedures for bituminous systems. Moreover, neither of the above work is directly carried with respect to the solvents of our interest (propane & butane). Therefore, until such uncertainties are alleviated, the interfacial mass transfer in Vapex will be investigated with respect to the existing analytical correlations.

CHAPTER FIVE
INTERFACIAL MASS TRANSFER IN HELE-SHAW CELL

We started our preliminary investigation of interfacial mass transfer in Vapex through experiments in Hele-Shaw cell. The primary motive behind this starting point was that complications due to tortuousity, inhomogeneity, capillarity etc., do not exist in Hele-Shaw cell. Hele-Shaw cell is comprised of two smooth and transparent plates of glass or Plexiglass that are placed parallel to each other with a small separation between them. The separation between the two parallel plates determines the permeability of the cell through the following relationship:

$$k = \frac{b^2}{12} \tag{5.1}$$

The constant spacing between the two plates is achieved by either placing a metallic shim of known thickness (in the case of plate glass) or machining and polishing one of the plates of the cell with high precision instruments (in the case of plexiglass).

5.1 Experimental Set-up and Procedure

Figure-5.1 presents the schematics of the laboratory set-up used in these experiments. The Hele-Shaw cell is filled with oil and held in upright position by a frame inside the pressure vessel. Three sides of the Hele-Shaw cell are totally sealed. Gas can diffuse and enter the cell through the fourth (vertical) edge of the cell, which remains open and emulates a line-source environment. The Hele-Shaw cell used in these experiments has an inner height of 7.4 cm and a width of 7.6 cm. The spacing between the two plates is 10 thou[1], corresponding to a cell permeability of 254-μm (5376 Darcy).

[1] – Thou, τ = 1/1000 inch

The pressure vessel is made-up of a thick aluminum body that can withstand up to 10-MPa pressure. The two ends of the pressure vessel have built-in glass windows, which permit light transmission through the cell for taking still photographs of the experiment.

The gas is injected into the vessel at constant pressure and temperature. The solvent gas used in these experiments is the commercial Propane, with an average purity of 98%. A pressure regulator was used downstream of the propane tank to assure that pressure remains below saturation pressure of the solvent during the experiments.

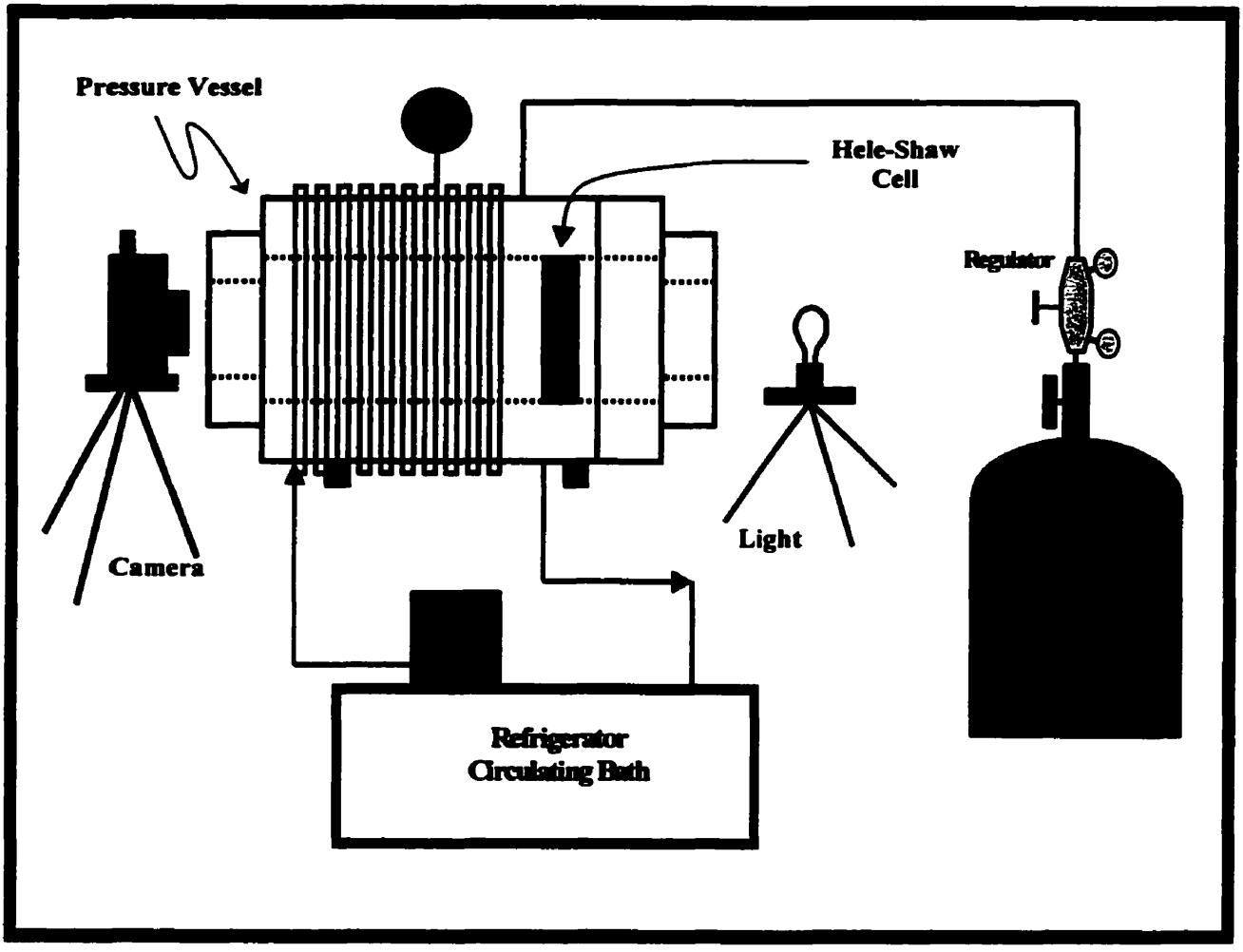

Figure-5.1: Schematics of the setup for Vapex experiments in Hele-Shaw cell.

A 15-m soft copper coil is wrapped around the vessel and connected to a circulating Glycol bath to maintain the temperature of the vessel at desired level throughout the experiment. The bath and vessel temperature were monitored and controlled to a tenth of a degree Celsius. A thermocouple was connected to the pressure vessel through a built-in port, for continuous monitoring of the temperature inside the vessel (not shown in diagram).

After filling the Hele-Shaw cell with oil, it was placed inside the pressure vessel such that the open edge of the cell was facing upward. The cell was left inside the vessel overnight to allow the entire system to be under thermal equilibrium, prior to the experiment. Shortly before the start of the test, the cell was rotated inside the vessel, such that the open edge of the cell becomes vertical. Solvent injection was started by opening the valve very slowly and adjusting the regulator, until the desired injection pressure was achieved. During the dry run experiments it was noticed that sudden opening of the valve might result in temporary cooling, due to Joules-Thomson cooling effect. The experiments that did not meet the requirements of thermal stability were excluded from the analysis.

The valve on the Propane tank was left open during the entire experiment to provide continuous supply of solvent (and constant pressure) during the consumption of Propane by diffusing into the bitumen.

A programmable digital camera (Kodak DC290) was used during the experiments to record still frames of the process. During each experiment, 160 frames were taken at 5-minute time intervals to assure that adequate number of data points is available for analysis. The camera was placed on a special pod on one side of the pressure vessel facing the Hele-Shaw cell, and an opaque light source was placed on the opposite side of the pressure vessel. The cross sectional area of the growing chamber was determined on each frame, through processing the frames by "ImagePro" image processing software.

5.2 Methodology

As the oil drains out of the cell, the gas enters and replaces the produced oil inside the Hele-Shaw cell and hence vapor chamber grows in time. The drainage rates are determined by calculating the rate of growth of the vapor chamber. Knowing the cell height and permeability, it is possible to back calculate the N_s parameter by inserting the measured recovery rates into equation 2.18. The N_s parameters were also computed analytically for comparison purposes using equation 2.7. Note that N_s parameter is primarily controlled by solvent concentration, viscosity and intrinsic diffusion coefficient of the solvent.

A methodology similar to that proposed by Das and Butler (1996) was utilized to express diffusion coefficient as a function of viscosity (Hayduk et al., 1973) and viscosity as a function of solvent concentration (Shu, 1984). Therefore, the N_s term was calculated analytically as a function of solvent concentration. The upper limit of solvent concentration was taken equal to the solubility limit of Propane at prevailing pressure and temperature (Das and Butler, 1996).

5.2.1 Viscosity Model

Shu (1984) presented a mixing rule for estimation of viscosity of liquid hydrocarbons, utilizing density and viscosity of solute and solvent at their corresponding concentration end-points to predict the mixture viscosity at intermediate concentrations. The technique proposed by Shu is primarily tailored around a technique, which was proposed earlier by Lederer (1933) as follows:

$$\ln \mu = x_A \ln \mu_A + x_B \ln \mu_B \qquad (5.2)$$

Where

μ_A = Viscosity of solvent at the mixing temperature, end-point viscosity-1

μ_B = Viscosity of bitumen at the mixing temperature, end-point viscosity-2

χ_A = Compositional parameter of solvent

χ_B = Compositional parameter of bitumen

and

$$\chi_B = 1 - \chi_A \tag{5.3}$$

Based on Lederer's theory, the compositional parameters are related to solvent concentration (or volume fraction, V_A) by the following equation:

$$\chi_A = \frac{\alpha V_A}{\alpha V_A + V_B} \tag{5.4}$$

Where,

V_A = Solvent volume fraction

V_B = Bitumen volume fraction

Shu presented a relationship for calculation of the parameter α by fitting a power-law relationship to a statistical data bank of viscosity data for different solute-solvent pairs. The result of this analysis indicate that α can be expressed as a function of end-point viscosity and density for solvent and bitumen as shown in the following equation:

$$\alpha = \frac{17.04\,\Delta\rho^{0.5237}\,\rho_A^{3.2745}\,\rho_B^{1.6316}}{\ln\left(\frac{\mu_A}{\mu_B}\right)} \tag{5.5}$$

Figure-5.2 presents the calculated mixture viscosity by Shu-Lederer correlation for bitumen and propane at several different temperatures. Note that mixture viscosities converge to a single value of $\mu_{\_mixture}$=0.1 (mPas) at propane end-point concentration. This behavior is well expected from the mixing rule theory. The corresponding values of solvent viscosity were determined based on modified square well viscosity model (Monnery et al., 1998) at the corresponding reduced temperature.

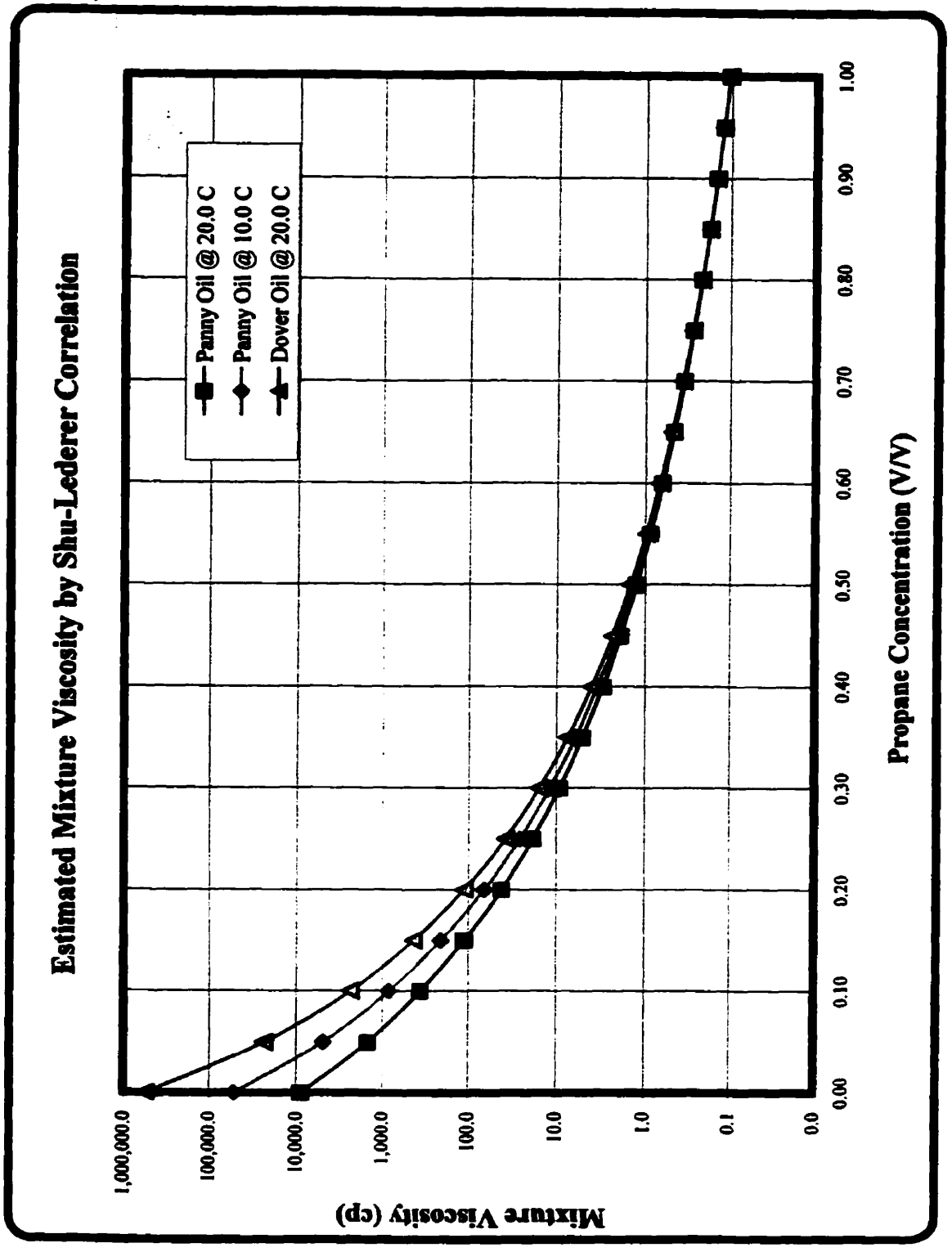

Figure-5.2: Calculated propane-butane mixture viscosity by Shu-Lederer correlation.

The density and viscosity data used for calculation of viscosity are presented in Table-5.1. Dover bitumen is extremely viscous and exhibits a viscosity of 543,800 mPas at room temperature. Figure-5.3 indicates that viscosity of bitumen samples decline exponentially as a function of temperature.

Table-5.1: Bitumen viscosity and density data

Sample	Bitumen Viscosity (mPas)	Bitumen Density (g/cm^3)
Dover @ 20 °C	543,800	1.027
Panny @ 10 °C	51,670	0.97
Panny @ 20 °C	8,971	0.97

5.2.2. Diffusivity Model

The model used for calculation of diffusion coefficient of solvent in butane is that of Hayduk and Minhas (1982) and shown is the following equation.

$$D = 13.3 \times 10^{-8} T^{1.47} V_a^{0.71} \mu^{(10.2/Va - 0.791)} \qquad (5.6)$$

Where,

T = Absolute temperature, °K

V_a = Molar volume of solvent at the normal boiling point, cm^3/mol

μ = Mixture viscosity at the corresponding solvent concentration, mPas

Therefore, in calculation of diffusion coefficient of solvent in bitumen, initially the dependency of viscosity on solvent concentration was determined, using Shu-Lederer correlation. Then, equation 5.6 was used to compute the diffusivity of solvent into bitumen at the corresponding concentrations. Table-5.2 summarizes the results of such calculation.

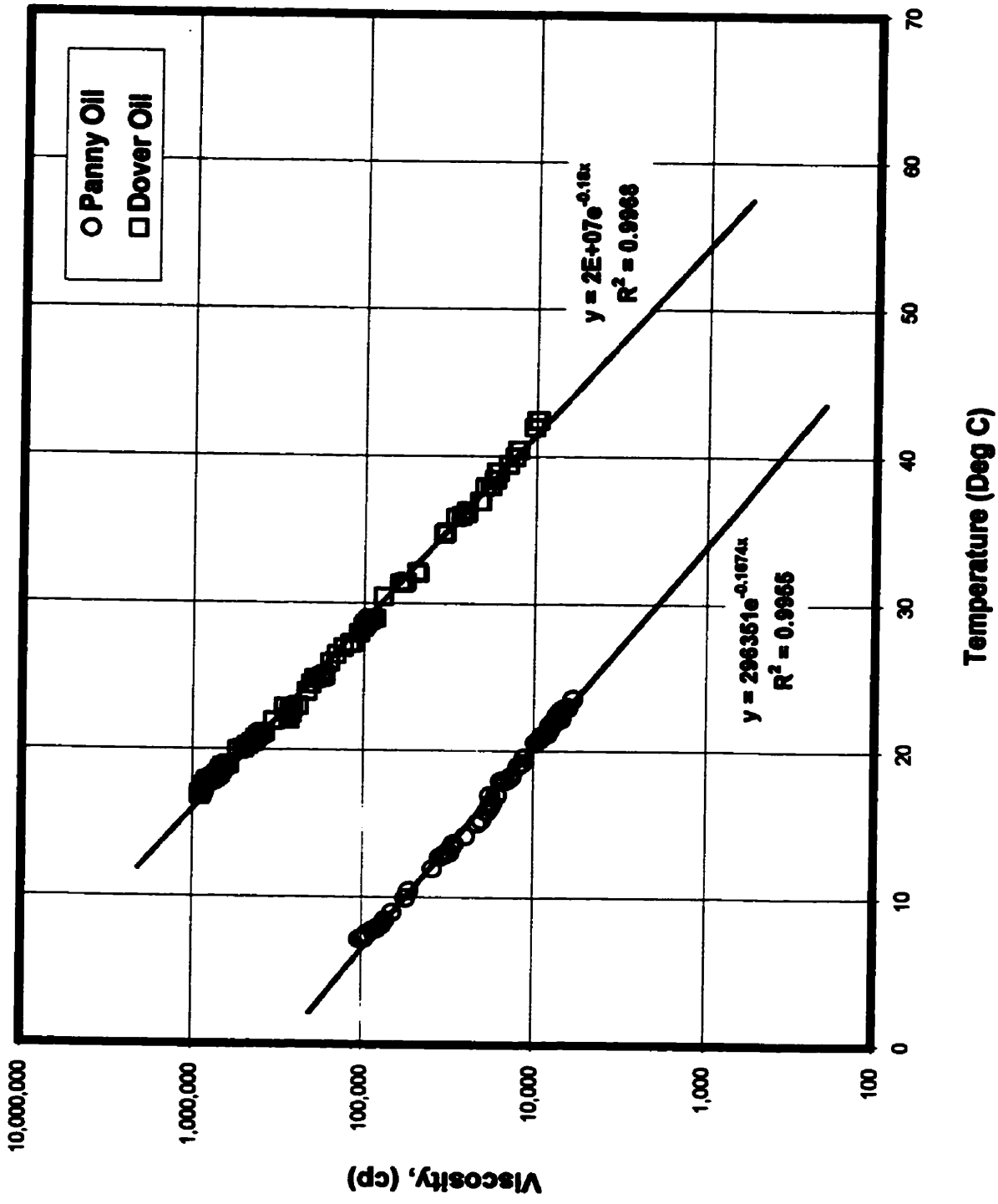

Figure-5.3: Viscosity of Panny and Dover oil as a function of temperature.

Table-5.2: Calculated intrinsic diffusivity of propane in Dover bitumen at 20 °C.

Bitumen Concentration, C_b (V/V)	Solvent Concentration, C_s (V/V)	Solvent Diffusivity [1], D_o (cm^2/s)	Mixture Viscosity @ 20 °C, $\mu_{mixture}$ (Pa.s)	Density Difference [2], $\Delta\rho$ (g/cm^3)
0.999	0.001	1.91E-08	543.80	0.936
0.950	0.050	1.06E-07	23.24	0.914
0.900	0.100	3.67E-07	2.39	0.891
0.850	0.150	9.37E-07	0.43	0.868
0.800	0.200	1.95E-06	0.112	0.845
0.750	0.250	3.50E-06	0.038	0.823
0.700	0.300	5.68E-06	0.016	0.800
0.650	0.350	8.50E-06	0.008	0.777
0.600	0.400	1.20E-05	0.004	0.754
0.550	0.450	1.61E-05	0.00234	0.731
0.500	0.500	2.07E-05	0.00146	0.708
0.450	0.550	2.59E-05	0.00097	0.685
0.400	0.600	3.16E-05	0.00068	0.662
0.350	0.650	3.76E-05	0.00049	0.640
0.300	0.700	4.40E-05	0.00037	0.617
0.250	0.750	5.08E-05	0.00028	0.594
0.200	0.800	5.77E-05	0.00022	0.571
0.150	0.850	6.49E-05	0.00018	0.548
0.100	0.900	7.22E-05	0.00015	0.525
0.050	0.950	7.96E-05	0.00012	0.502
0.000	1.000	8.71E-05	0.00011	0.480

1– Hayduk & Minhas Do-μ Correlation
2– Δρ = Mixture Density – Vapor Solvent Density

5.3. Data Analysis

The first set of experiments was conducted in Hele-Shaw cell with a cell spacing of 10 thou (254 μm), utilizing propane as solvent and UTF-Dover bitumen at room temperature (20 ± 0.5 °C). The time-lapse images of this experiment shown in Figure-5.4 indicate a very smooth and gradual growth of the vapor chamber. The cumulative production and drainage rate for three experiments in Hele-Shaw cell are shown in Figure-5.5 and 5.6 respectively. The production rates were computed by fitting a polynomial on the cumulative production curve and taking its derivative numerically. Minor variations between these experiments were most likely due to human error introduced, during analysis and calibration of "ImagePro" software.

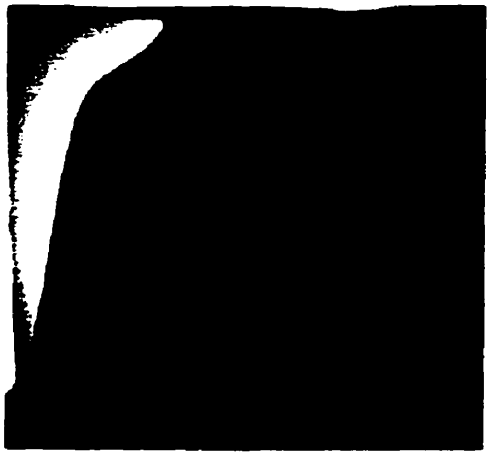

Δt=1.0 hrs

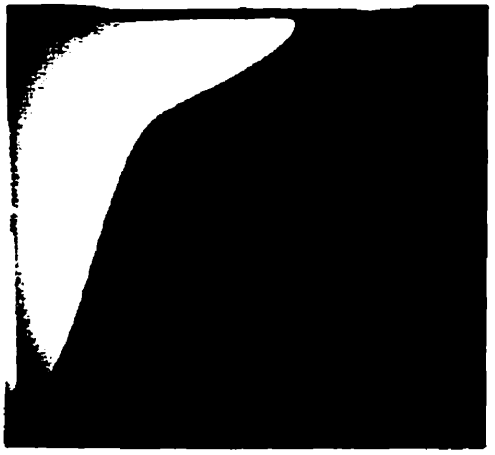

Δt=2.0 hrs

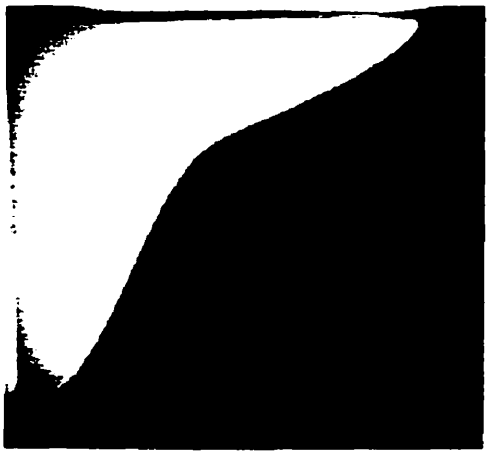

Δt=3.0 hrs

Figure-5.4: Time-lapse frames of Hele-Shaw Cell experiment; Propane/Dover-bitumen b=10 thou, T=20 °C, P=875 KPa

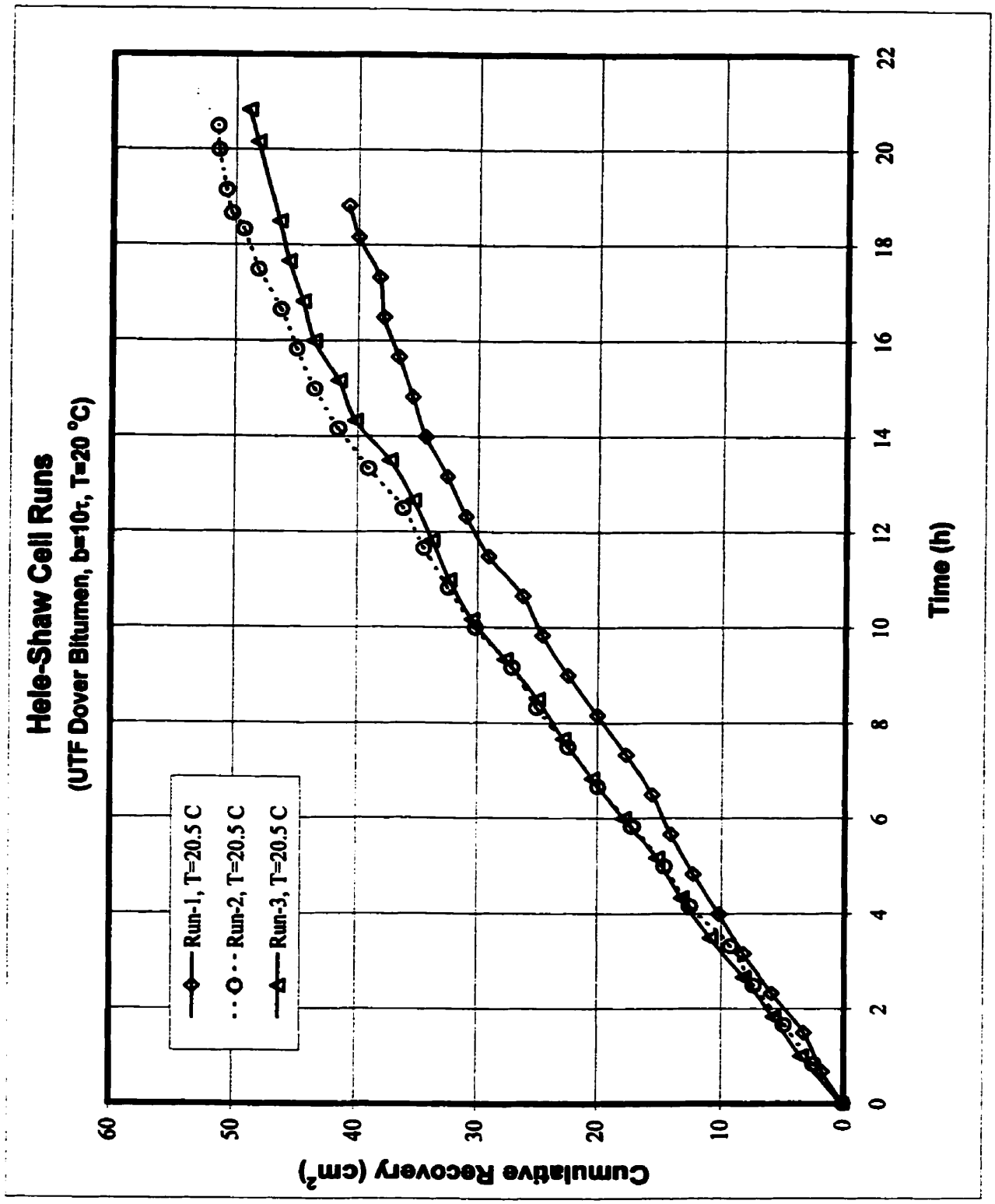

Figure-5.5: Cumulative oil for Hele-Shaw cell experiments, Propane/Dover-bitumen.

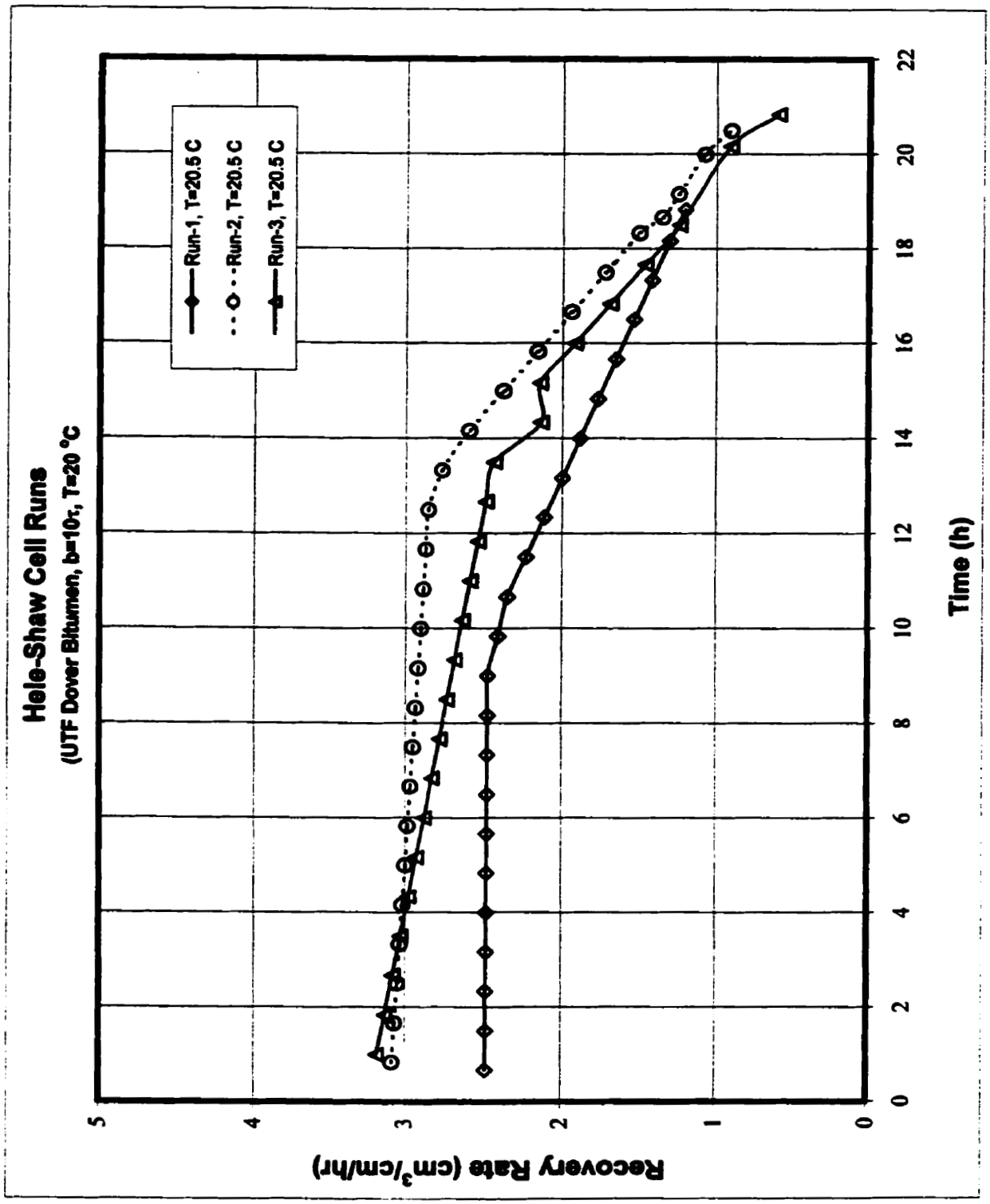

Figure-5.6: Production rates for Hele-Shaw cell experiments, Propane/Dover-bitumen.

The second set of experiments was conducted in the same cell with Northstar-Panny oil. This oil is more mobile and exhibits a viscosity of 8970 mPas at 20 °C. Selected time-lapse images of this experiment at room temperature are shown in Figure-5.7. Note that due to lower viscosity of original undiluted oil, the interface is not representing an S-shaped character as before. This is because the oil faraway from the interface is already mobile enough that it can flow without appreciable viscosity reduction by solvent and the S-shaped interface is not completely formed. The cumulative production and drainage rate for Panny oil experiments at 20 and 23 C are shown in Figure-5.8 and 5.9 respectively.

Finally, in order to examine the prospects of recovery by Vapex at the prevailing reservoir temperature, the third set of experiments were conducted at reduced temperature of 10 °C. The entire system temperature was lowered using the refrigerator-circulating bath and Hele-Shaw cell was left in the vessel overnight to establish thermal equilibrium. Figure-5.10 presents the selected images of these experiments. During the experiment the propane tank was left at room temperature and injection pressure was maintained at 875 KPa. The combination of high injection pressure and low cell temperature push the phase envelope of propane vapor into the saturation region and hence asphaltene precipitation occurs. The cumulative production and the corresponding recovery rates of this experiment are shown in Figure-5.11 and 5.12 respectively.

Table-5.3 summarizes the results of the Hele-Shaw cell experiments with a cell spacing of 254 μm. The flow rates presented in column-5 are the average stabilized flow rates during the early stages of each experiment and are perceived to provide a better representation of a steady-state-like process. Average values of N_s parameters were calculated from experiments conducted at identical temperature. Analytical values of N_s parameter were initially calculated using intrinsic molecular diffusion coefficient of propane and equation 2.7. Direct comparison of N_s parameters indicate that experimentally derived (back calculated) values are one to two orders of magnitude larger than those calculated analytically.

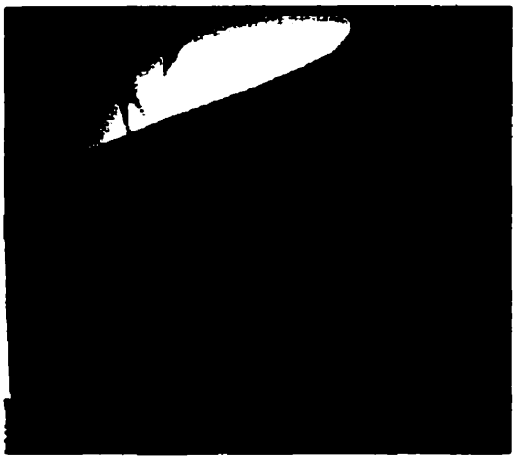

Δt=1.0 hrs

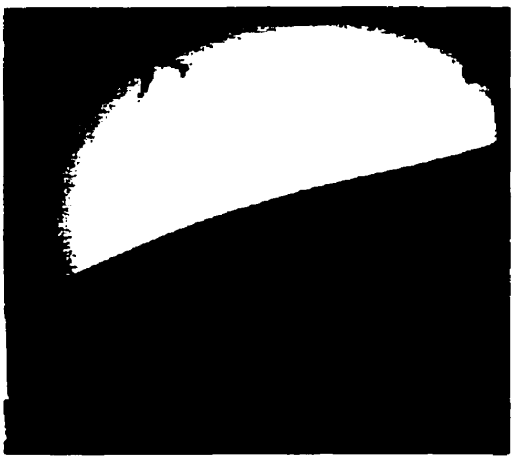

Δt=2.0 hrs

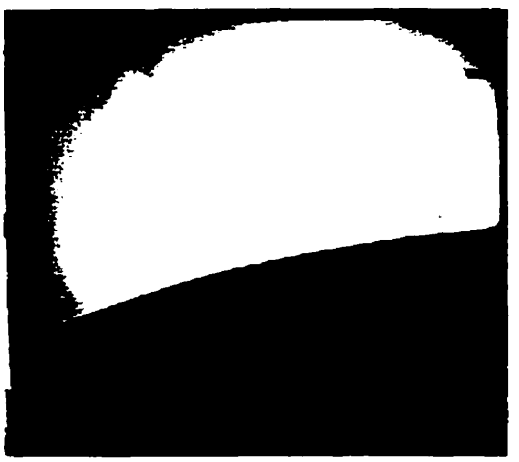

Δt=3.0 hrs

Figure-5.7: Time-lapse frames of Hele-Shaw Cell experiment; Propane/Panny-Oil b=10 thou, T=20 °C, P=875 KPa

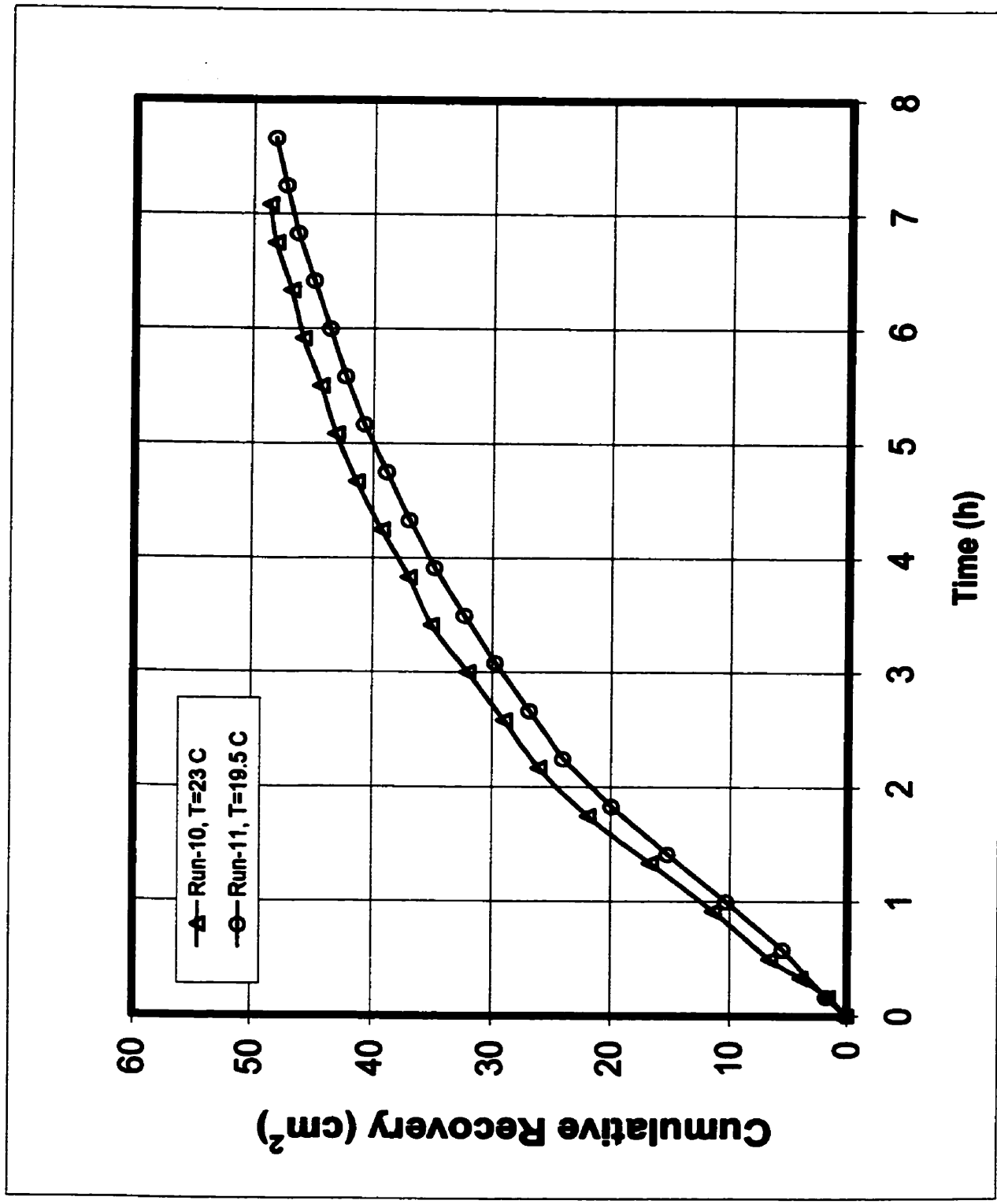

Figure-5.8: Cumulative production in Hele-Shaw cell, for Propane/Panny-Oil.

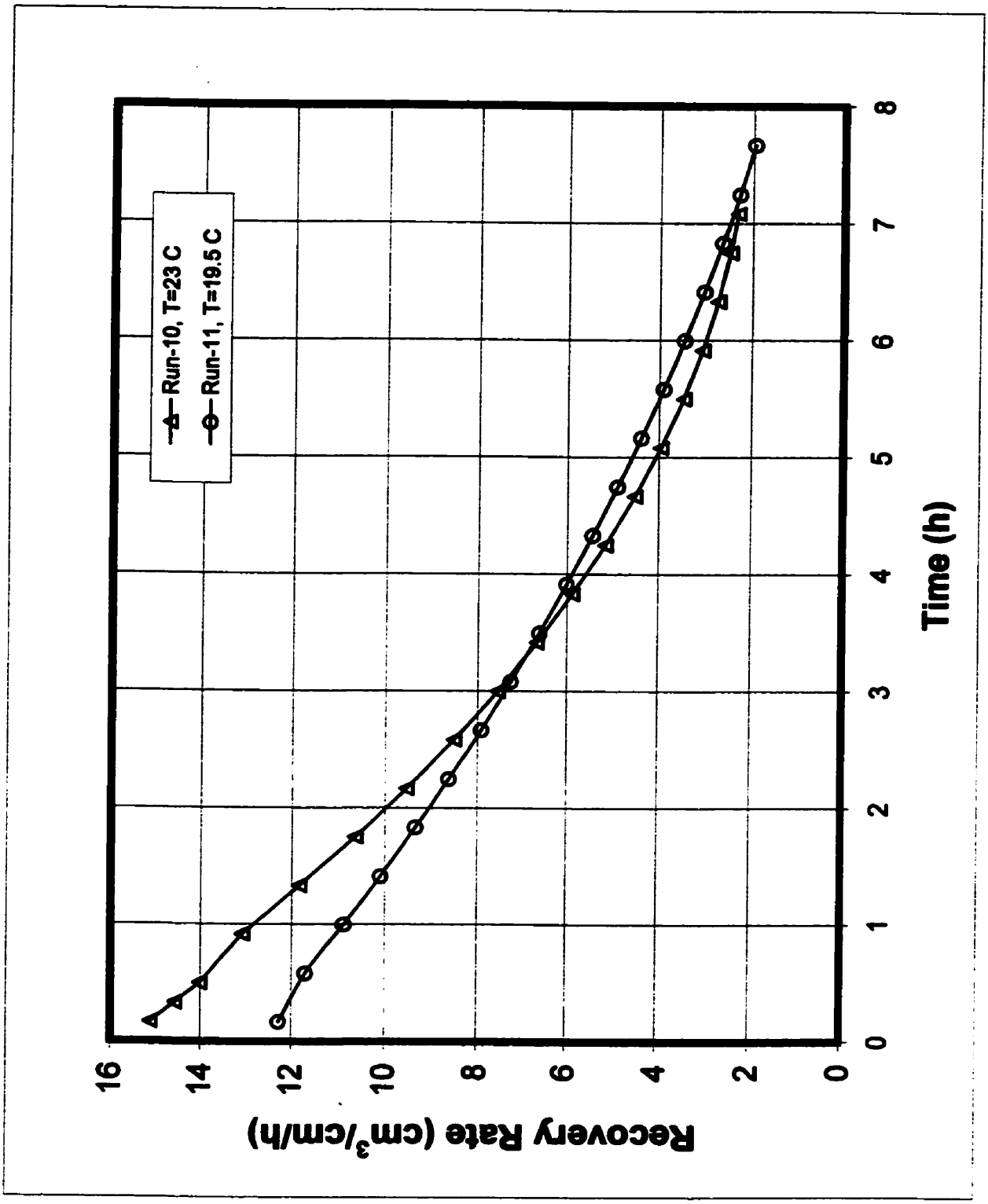

Figure-5.9: Recovery rate in Hele-Shaw cell, for Propane/Panny-Oil.

Δt=1.0 hrs

Δt=3.0 hrs

Δt=5.0 hrs

Figure-5.10: Time-lapse frames of Hele-Shaw Cell experiment; Propane/Panny-Oil b=10 thou, T=10 °C, P=875 KPa

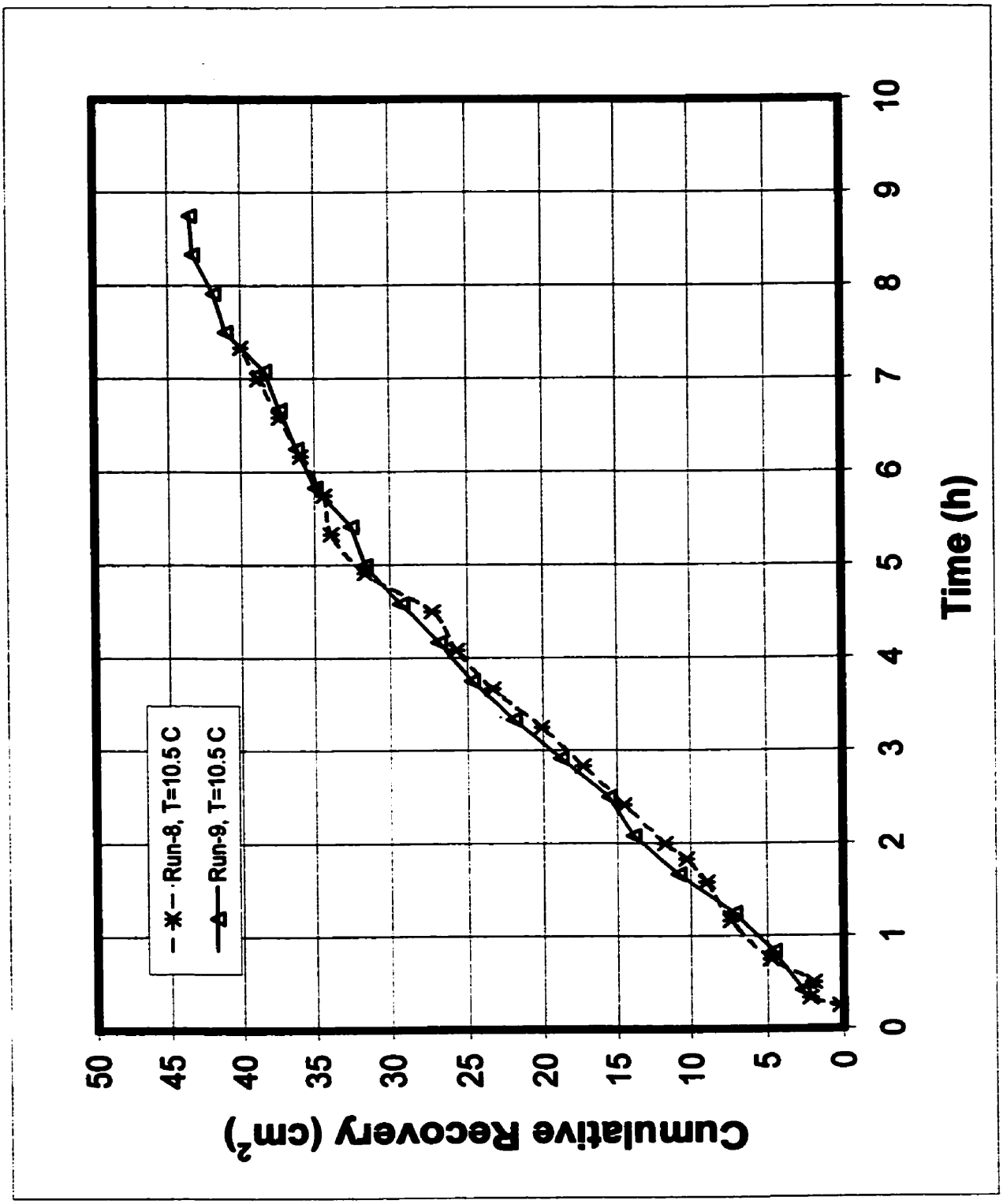

Figure-5.11: Cumulative oil, Hele-Shaw cell experiments; Propane/Panny-Oil, 10 °C.

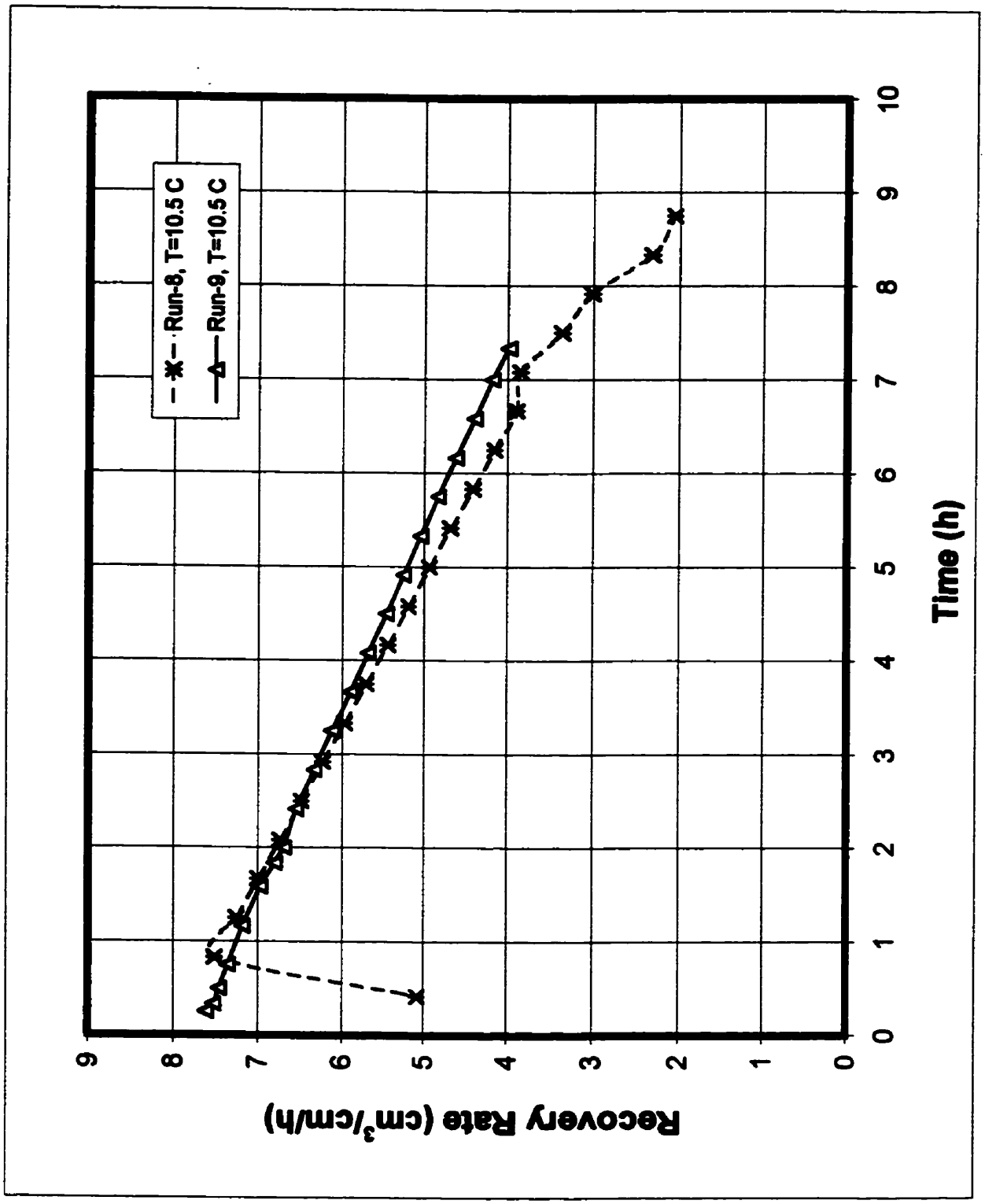

Figure-5.12: Production rate, Hele-Shaw cell experiments; Propane/Panny-Oil, 10 °C.

Table-5.3: Summary of calculated results for Propane/Bitumen experiments in Hele-Shaw cell (cell spacing b=10τ, k=5376 μm^2, cell width=7.6 cm, cell height=7.4 cm).

Run #	Oil	Undiluted Viscosity (mPa.s)	Temp °C	Max Rate (cm^3/cm/h)	Back Calculated N_s	Average N_s	Analytical N_s [1]	Analytical N_s [2]
1	Dover	543,800	20.5	2.47	8.00E-07	1.17E-06	2.99E-07	7.07E-07
2			20.5	3.08	1.24E-06			
3			20.5	3.33	1.45E-06			
7	Panny	51,676	10.5	6.9	9.02E-06	8.00E-06	4.04E-07	1.99E-06
8		51,676	10.5	7.52	7.42E-06			
9		51,676	10.5	7.6	7.57E-06			
10		5,918	23	15	2.95E-05	2.95E-05	5.87E-07	3.21E-06
11		10,800	19.5	12.28	1.98E-05	1.98E-05	5.41E-07	2.90E-06

1- Analytical Ns based on molecular diffusion coefficient only.
2- Analytical Ns based on Taylor dispersion & molecular diffusion coefficient.

In order to minimize the discrepancy between the analytical (column-7) and experimental values of N_s (column-8), we used an effective diffusion coefficient, incorporating the Taylor dispersion component. The computed N_s values incorporating dispersion effects are presented in column-9. Based on Taylor theory (1953), the non-uniform velocity distribution due to wall effect creates a momentum change between the center of the conduit and the wall, which in turn enhances the mass transfer in terms of dispersion.

When a slug of soluble matter is introduced into a fluid slowly moving through a capillary tube, it gradually spreads out (along the axis of the pipe) under the combined effects of molecular diffusion and a non-uniform velocity distribution. The parabolic velocity distribution is created due to momentum variation under the influence of the wall. Taylor showed that the concentration profile of the soluble matter is centered over the point moving at the mean speed of the flow, and is symmetrically distributed despite the asymmetry of the flow. This concept is schematically illustrated in Figure-5.13.

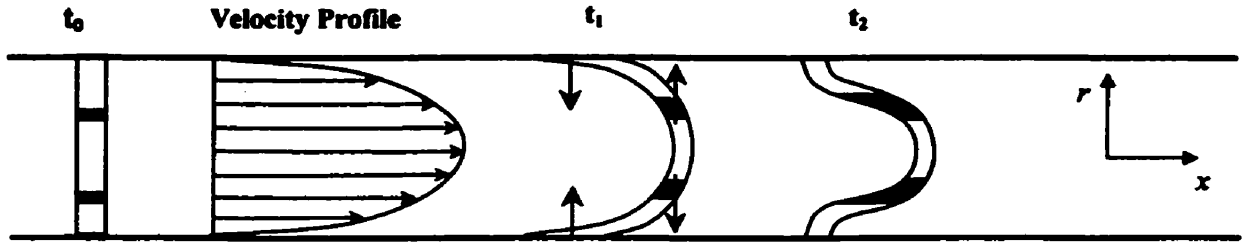

Figure-5.13: Variation of concentration distribution due to momentum change in capillary tubes (after Taylor, 1953).

In a circular pipe of radius a, the velocity V at distance r from the center of the pipe is written as a function of maximum fluid velocity u_0, at the axis as:

$$V = V_o\left(1 - r^2/a^2\right) \tag{5.7}$$

If the concentration C, is symmetrically distributed around the center line, concentration profile as a function of r, x and t can be written as:

$$D\left(\frac{\partial^2 C}{\partial r^2} + \frac{1}{r}\frac{\partial C}{\partial r} + \frac{\partial^2 C}{\partial x^2}\right) = \frac{\partial C}{\partial t} + V_o\left(1 - \frac{r^2}{a^2}\right)\frac{\partial C}{\partial x} \tag{5.8}$$

Taylor considered that the time necessary for appreciable change for concentration distribution to occur, under the influence of convective dispersion, is long compared with the 'time of decay' during which radial variations of concentration are reduced to a fraction of their initial value through the action of molecular diffusion. If concentration variations were independent of x, then any radial variations of concentration can rapidly disappear. He assumed that convection occurs across a plane, which moves at a constant speed, equal to half of the maximum fluid velocity, V_0.

$$x_1 = x - \frac{1}{2}V_o t \tag{5.9}$$

This assumption is theoretically valid for laminar flow. He determined an expression for estimation of rate of transfer of solute concentration as:

$$Q = -\frac{\pi a^4 V_o^2}{192 D} \frac{\partial C_m}{\partial x_1} \tag{5.10}$$

Therefore, the mixed zone will travel with the mean speed of the injected fluid and would be dispersed as if there were a constant dispersion coefficient *K*, such that:

$$K_l = D_o + \frac{V^2 a^2}{192 D_o} \tag{5.11}$$

The functional relationship between the velocity and the dispersion coefficient in the Hele-Shaw geometry will be different from that represented by equation 5.11. However, in the absence of an equivalent formulation for the Hele-Shaw model, equation 5.11 was used to estimate the dispersion coefficient.

Probably a similar form of dispersion due to momentum variation occurs in a Hele-Shaw cell. In that regard, the layer of fluid at the vicinity of the vapor chamber moves relatively faster than the oil within the bitumen-bulk, which remains at the original viscosity. In addition, at any level away from the interface, a secondary momentum change is created from the center of the Hele-Shaw cell towards the walls of the cell. This concept is schematically shown in Figure-5.14. These together create a significant momentum change within the oil-phase and dispersion is formed. Although Taylor dispersion is essentially different than dispersion in porous media, it is a good analogue to explain the enhanced mass transfer within the Hele-Shaw cell.

In that regard, an effective diffusion coefficient, incorporating dispersion effects in Hele-Shaw cell was calculated, using intrinsic diffusivities at corresponding solvent concentrations and equation 5.11. The computed effective diffusion coefficient was later on inserted into equation-2.7 for analytical calculation of N_s parameter. It is important to mention that incorporation of Taylor dispersion is primarily intended to highlight the impact of non-uniform velocity distribution on the enhancement of mass transfer in

capillary tubes. However, the Taylor dispersion formulation in its original form cannot be directly used for calculation of dispersive mass transfer either in a Hele-Shaw cell or in porous media.

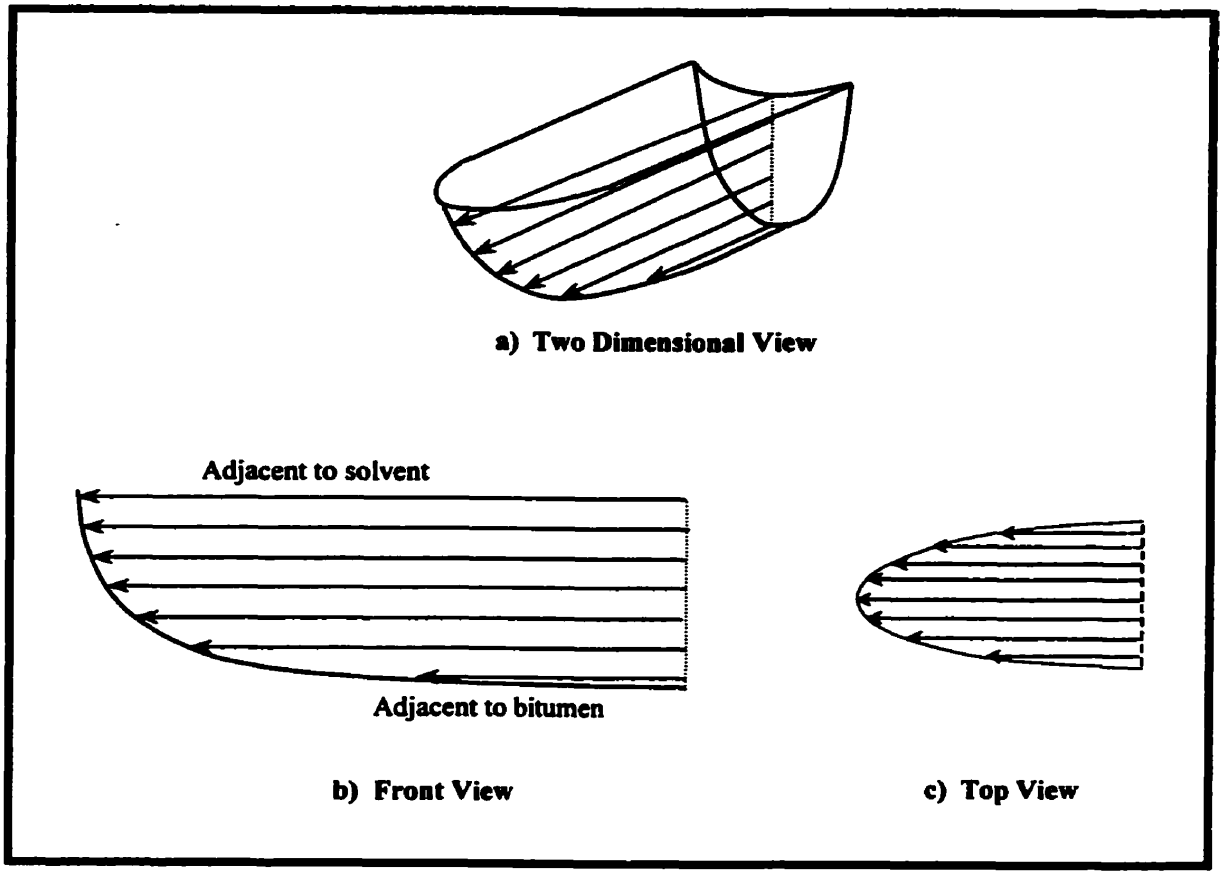

Figure-5-14: Schematic illustration of non-uniform velocity profile in Hele-Shaw Cell.

Figure-5.15 presents the experimentally derived N_s parameters versus those obtained by analytical techniques as explained above. The 45 degree dashed line is representative of a baseline where experimental and analytical N_s values are equal. Note that utilization of an effective diffusion coefficient incorporating the Taylor dispersion improves the estimated N_s parameter considerably.

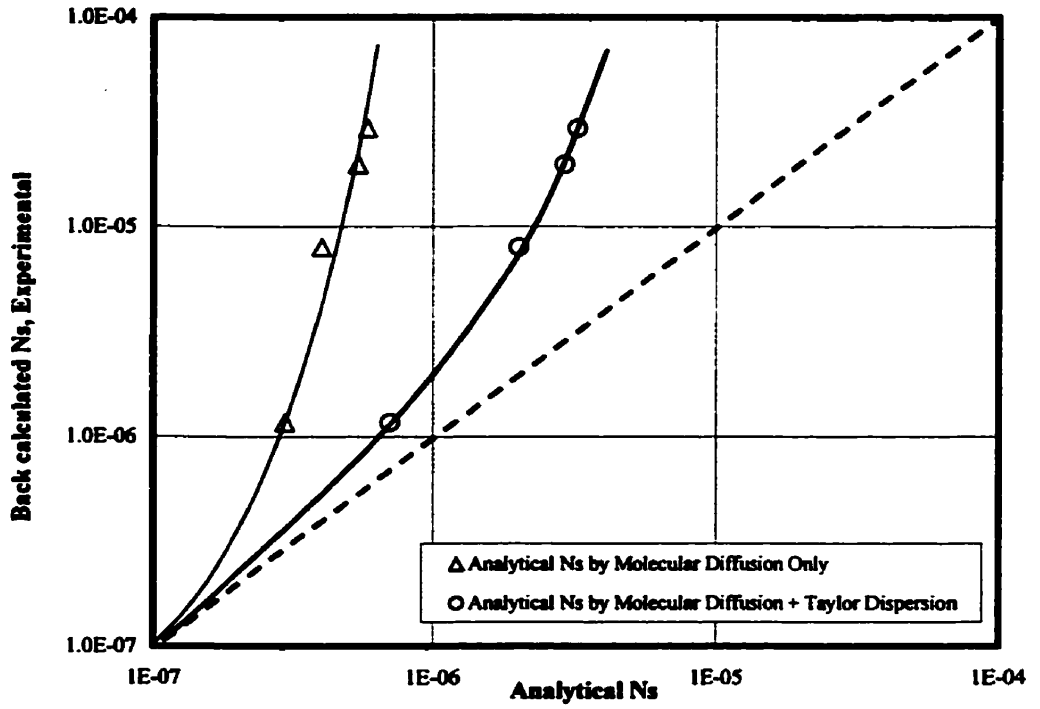

Figure-5.15: Comparison of analytical vs. experimental values of N_s parameter.

To establish a meaningful relationship, the ratio of the experimental to analytical N_s values were plotted versus Peclet number as shown in Figure-5.16. The Peclet numbers were calculated at the outermost layer of the diluted oil where solvent concentration is the maximum, viscosity is at its minimum and hence velocity is the maximum. Table-5.4 summarizes the results of this calculation.

Table-5.4: Calculated Peclet numbers for Propane/Bitumen experiments in Hele-Shaw cell (cell spacing b=10τ, k=5376 μm^2, cell width=7.6 cm, cell height=7.4 cm).

	$Ns_{\_Avg}/Ns$ [1]	$Ns_{\_Avg}/Ns$ [2]	Velocity, V (cm/S)	D_o (cm^2/S) @ Cs	Peclet Number, $N_{Pe}= b\ V/D_o$
Dover- 20 °C	3.90	1.65	0.00997	1.20E-05	21.16
Panny-10 °C	19.81	4.02	0.01156	1.30E-05	22.64
Panny-20 °C	36.56	6.82	0.01327	1.40E-05	24.10
Panny-23 °C	50.29	9.18	0.01377	1.43E-05	24.52

1- Analytical Ns based on molecular diffusion coefficient only.
2- Analytical Ns based on Taylor dispersion & molecular diffusion coefficient.

In the above table, column 2 and 3 represent the N_s ratio based on analytical values of N_s from column 8 and 9 of Table-5.3 respectively. Column 5 presents the intrinsic molecular diffusivity of solvent at maximum solvent concentration (at interface). Minor differences between the diffusivity values are due to viscosity variations of bitumens at the corresponding temperatures.

From figure-5.16, it appears that the discrepancy between experimental and analytical values of N_s increases as Peclet number is increased. The curve-fit to the above data suggest that at lower values of Peclet number (below 18), experimental and analytical N_s parameters become identical and the N_s ratio approaches unity. Although extrapolation outside the range of calculated values is speculative, the general trend of the curves is very similar to that observed by many authors investigating the dispersion in porous media. Due to existence of tortuousity in porous media, the ratio of effective diffusion to molecular diffusion coefficient (K/D_o) is slightly less than one (~ 0.7 in unconsolidated sands).

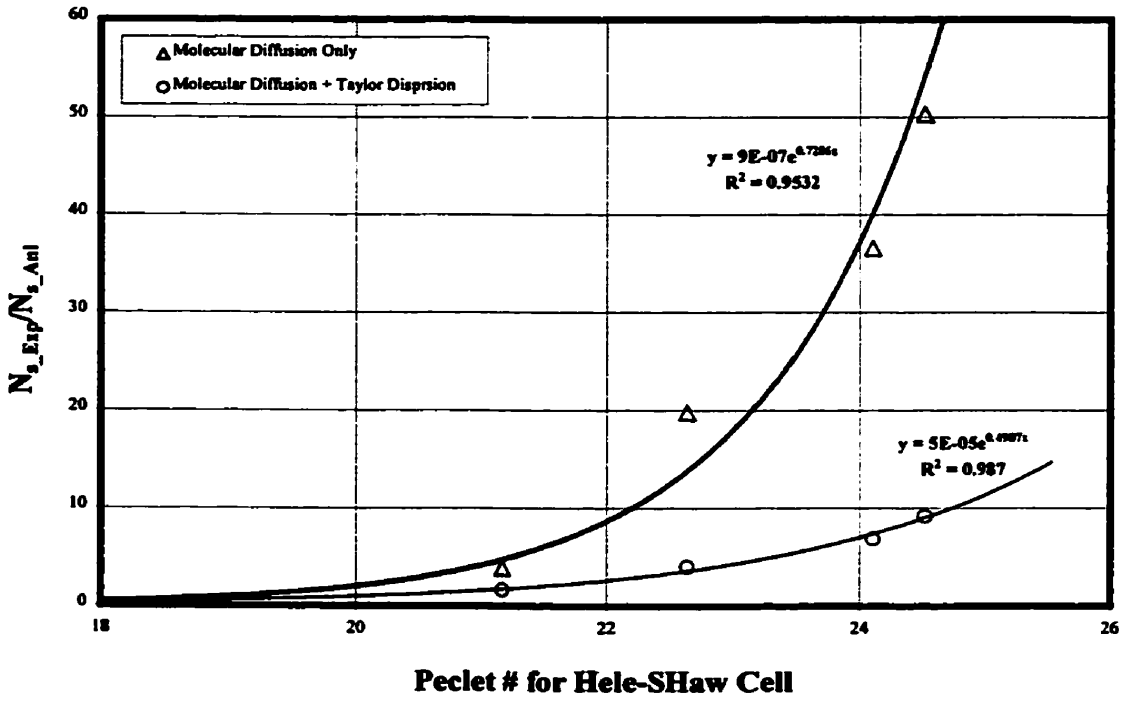

Figure-5.16: N_s Ratio vs. Peclet number for Hele-Shaw cell experiments.

Finally in order to have a better understanding of the factors controlling dispersion process in Hele-Shaw cell, the constant of Equation-5.11 (1/192) was modified through an optimization procedure. In that regard, a multiplier γ, was determined for each set of experiments such that the back-calculated Ns parameter becomes equal to the analytical Ns, incorporating diffusion and sipersion effects. Table-5.5 summarizes the results of this analysis.

$$K_l = D_o + \frac{V^2 a^2}{\gamma D_o} \tag{5.12}$$

Table-5.5: Calculated dispersion multipliers for Hele-Shaw cell experiments.

	γ	$1/\gamma$	μ_Bitumen (mPs)	μ_mixture (mPs)	Viscosity Ratio (μ/μ)
Dover-20 C	13.00	0.07692	543,796	4.01	0.0000074
Panny-10 C	10.03	0.09974	51,676	3.46	0.0000669
Panny-20 C	5.88	0.16994	8,971	3.01	0.0003357
Panny-23 C	4.36	0.22927	5,918	2.90	0.0004903

The viscosity ratio in the last column is the ratio of viscosity of diluted bitumen (at maximum solvent concentration) to the viscosity of undiluted bitumen. Viscosity ratio was used as a matching parameter for estimation of dispersion in Hele-Shaw cell. Figure-5.17 presents the plot of viscosity ratio vs. dispersion multiplier, γ.

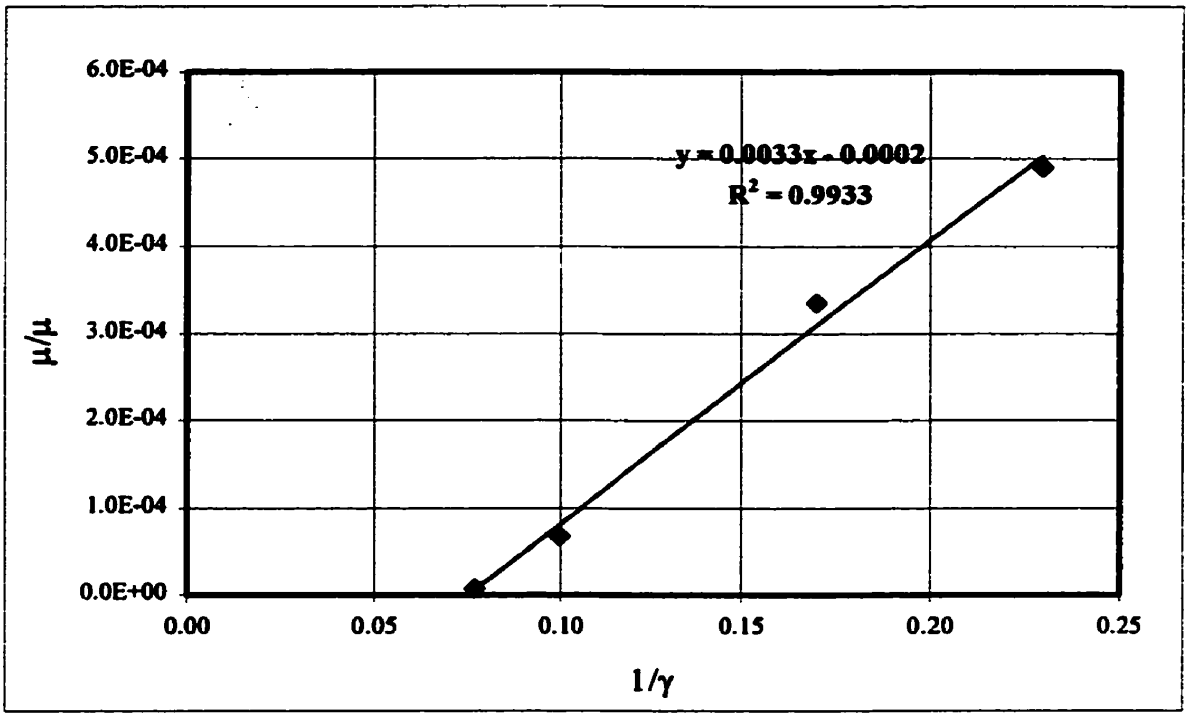

Figure-5.17: Dependency of viscosity ratio on γ multiplier in Hele-Shaw cell experiments.

CHAPTER SIX

INTERFACIAL MASS TRANSFER IN POROUS MEDIA

Dispersion process in porous media is essentially different than that in Hele-Shaw cell or capillary tubes. Development of Taylor dispersion due to non-uniform velocity distribution was discussed in previous chapter. Development of convective dispersion in porous media, in Vapex is probably a combination of momentum change due to viscosity contrast and influence of grain particles. Figure-6.1 represents the mechanism of transverse dispersion in porous media as proposed by Blackwell (1962). In this figure, tracers are initially flowing along distinct paths, Streamline-1, 2 and 3. However, after a short distance, the streamlines converge and share a common path (point-a and c), where part of the solute is transferred from one streamline to another. Therefore, the final effluent at individual streamlines will have different tracer concentrations than the initial values.

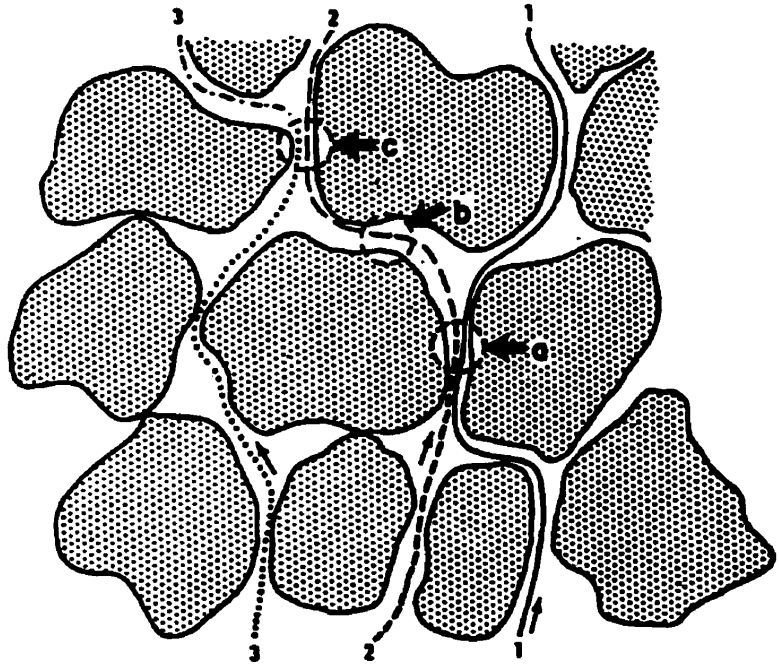

Figure-6.1: Schematic illustration of microscopic dispersion in porous media. (After Blackwell, 1962)

In the previous chapter the recovery of bitumen with propane in Hele-Shaw cell was discussed. Investigation of interfacial mass transfer in Hele-Shaw cell indicated that physical dispersion is a viable mechanism for enhanced mass transfer for Vapex process. However, in order to assess the role of diffusion and dispersion in porous media, experiments in sandpack were necessary.

The sandpack experiment in this work was conducted at room temperature, using Butane as solvent and Northstar-Panny heavy oil. Utilization of butane as solvent permitted lower operating pressure (120 KPag) which was well within the safe operating limit of the physical model. In two-phase flow, longitudinal dispersivity in a given phase rises substantially, as the saturation of that phase approaches residual values (Sahimi et al., 1982). Although solubility of butane in water is perceived to be small, to assure that presence of water would not complicate the process, connate water saturation was avoided and therefore, experiments were run under dry condition (Dry Vapex).

6-1 Experimental Set-up and Procedure

Figure-6.2 schematically illustrates the physical setup used for the experiments in porous media. The visual cell was made up of 3 cm thick reinforced phenolic panel at the back and around the edge, sealed against a transparent 2.5 cm thick plexiglass. The cavity inside the cell had the dimensions of 21.1cm x 3.25cm x 70.1cm and filled and vibropacked with 20-30 mesh Ottawa Sand. Since plexiglass tends to deflect at higher operating pressure, the cell was secured with two reinforcing steel bars in the front and the back of the cell. All the nuts and bolts were tightened at 50-lbf torque. The cell was mounted on a custom-built stand to provide a stand-off from the table. The true picture of the physical set-up is shown in Figure-6.3.

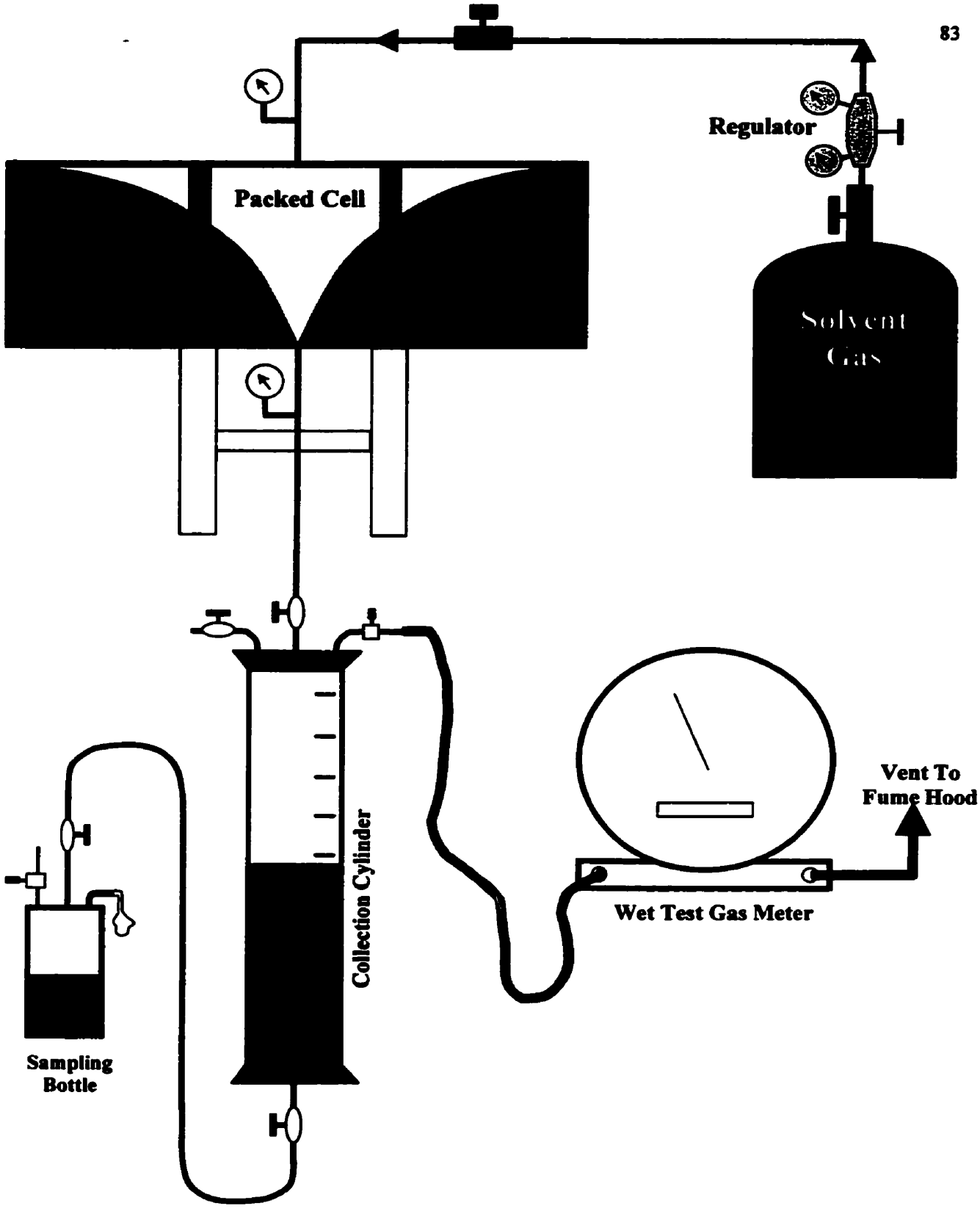

Figure-6.2: Schematic illustration of Sanpack set-up for Vapex experiment.

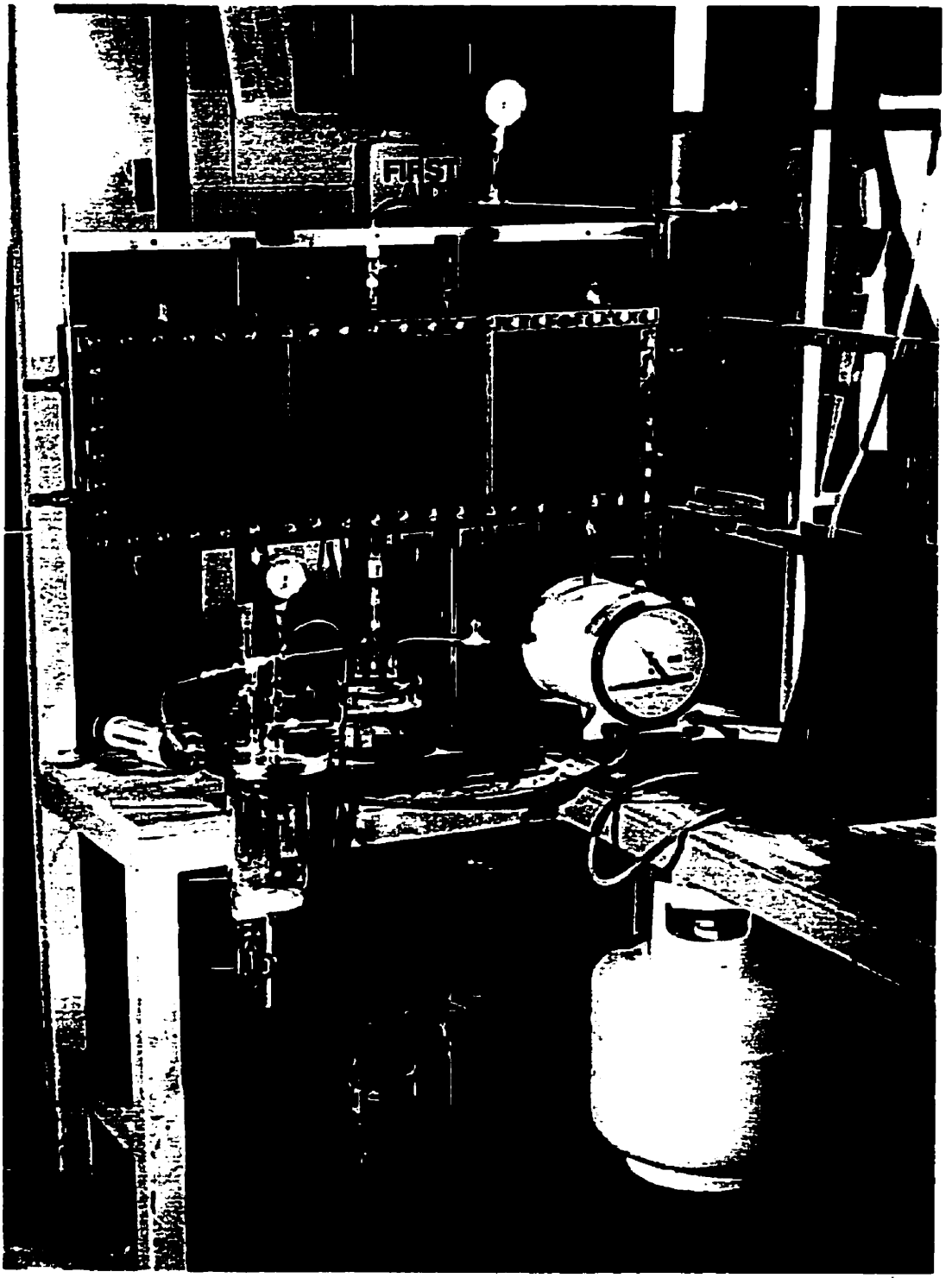

Figure-6.3: Photograoh of the physical model for sandpack experiments.

To examine the mechanical integrity of the empty cell, the cell was pressurized with Air to 205 KPa and the pressure was monitored for a 12 hours period. Once all the leaks were cured, the cell was held in upright position and filled with 20-30 mesh dry sand. A vibrating table with variable frequency was used to pack the sands in several stages. Additional sand was added to the cell as required until the packing was complete.

Once the packing was done, the cell was tested for permeability with respect to Air. In that regard, air was injected at constant pressure into one side of the cell and produced from the opposite side. The pressure drop across the cell was measured using two high-resolution pressure gauges and air injection was monitored using a Wet-Test Gas Meter, under steady-state flow condition. The cell permeability was determined to be 45 Darcy.

In order to fill the packed cell with oil, the cell was placed in a large oven and connected to a bottle containing Panny oil. To assure that no air bubbles are trapped in the cell, saturation was done very slowly, while maintaining the oven temperature at 50 °C. A small pressure (20-40 KPa) was applied to the oil bottle from the top and the oil was injected from the bottom into the packed cell. The connection ports at the top of the cell were left open to allow air to exit, while saturating the cell. After the entire visual cell was filled, a small amount of oil was allowed to overflow through the connection ports to assure that no air is trapped in the connection lines. The cell was disconnected from the bottle and all the ports were sealed and the cell was left at room temperature for 1 week to reach thermal equilibrium prior to the experiment. Knowing the density of oil, dimensions of the cell and the difference between the weight of the visual cell before and after saturation, the porosity of the cell was determined to be ϕ=0.318.

An instrument grade butane with a purity of 99.9% was used as solvent for the experiment. The butane cylinder was connected to the visual cell, from the top center port as shown in Figure-6.4, creating a symmetric vapor chamber within the cell.

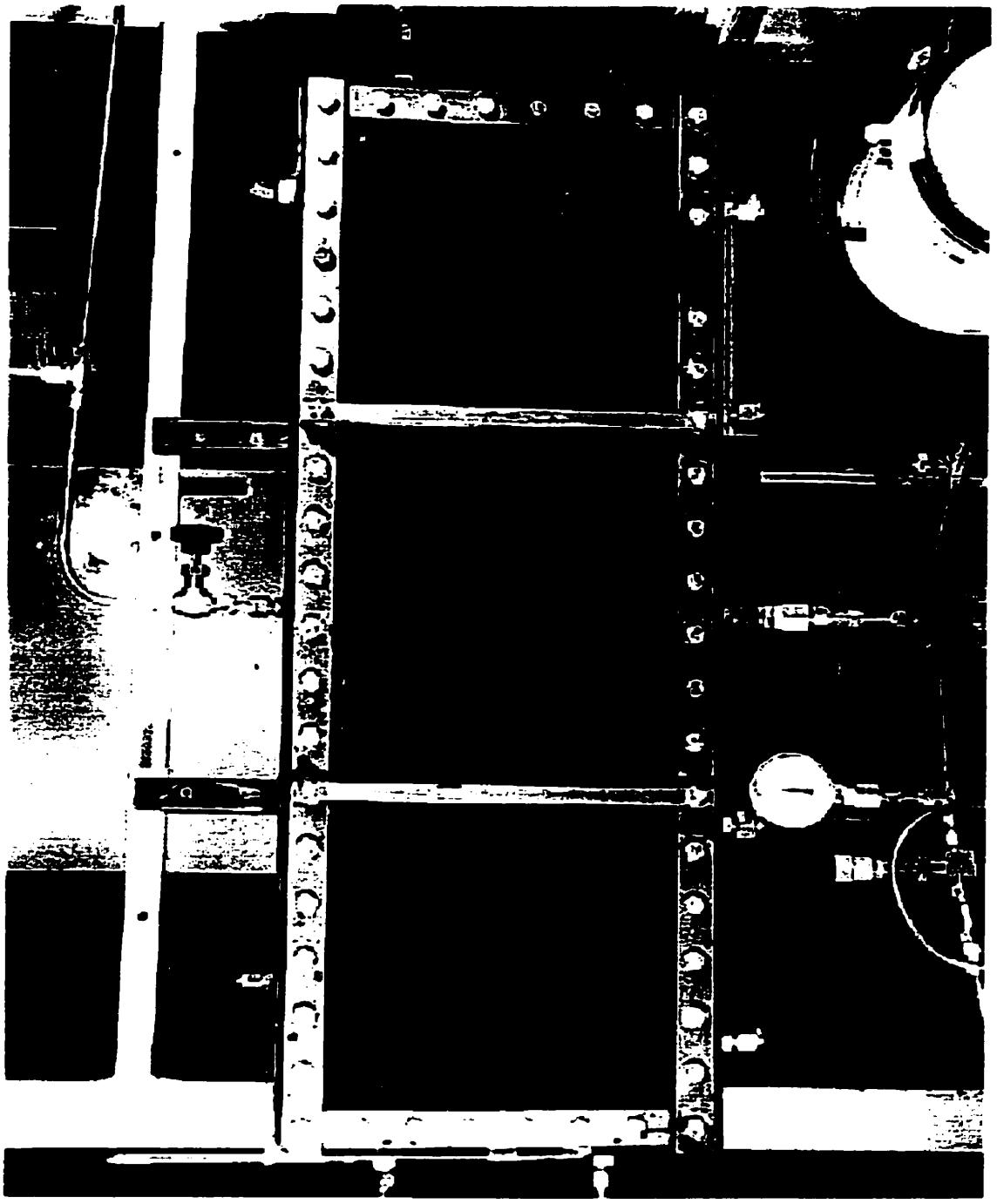

Figure-6.4: Creation of symmetric vapor chamber within the sandpack.

The production port was located at the lower side of the visual cell and right opposite the injection point. Prior to commencing the experiment, the graduated collection cylinder, which was connected to the production end, was pressurized by injecting butane. The main purpose of this procedure was to reduce the pressure surge within the cell at the start of the test and minimize the possibility of creation of viscous fingering. After pressurizing the cylinder, injection into the cell was started by gradually opening the valves at the injection and production ports.

During the experiment, the mixture of diluted oil and excess gas were directed to a graduated 1.1 liter transparent cylinder for collection as shown in Figure-6.5. The third port at the top of the collection cylinder was connected to a Wet Test Gas Meter, via a needle valve. The needle valve was adjusted such that a minimum pressure difference ($\cong$10 KPa) was established (across the sandpack) between the injection port (top) and production port (bottom). The outlet of the gas meter was connected via a flow line to the fume-hood for discharge. Therefore, the graduated cylinder was used as a separator to remove excess gas and provide the means for continuous monitoring of cumulative oil production.

The content of the graduated cylinder was transferred to a sampling jar by closing the valve at the top of the cylinder (inlet) and opening the drain valve at the bottom of the cylinder. A second needle valve was used on the sampling jar to release the solution gas. The sampling jar and auxiliary connections are shown in Figure-6.2 and 6.5. After desired volume of oil was removed, the experiment was continued by closing the valve at the bottom of the cylinder and reopening the valve at the top. A pressure regulator was connected to the butane tank to provide constant pressure (and hence concentration) boundary condition for the model. The regulator was adjusted such that downstream pressure was slightly less than saturation pressure of butane. The valve and regulator on the butane tank were left open during the entire experiment to provide continuous supply of solvent to the model.

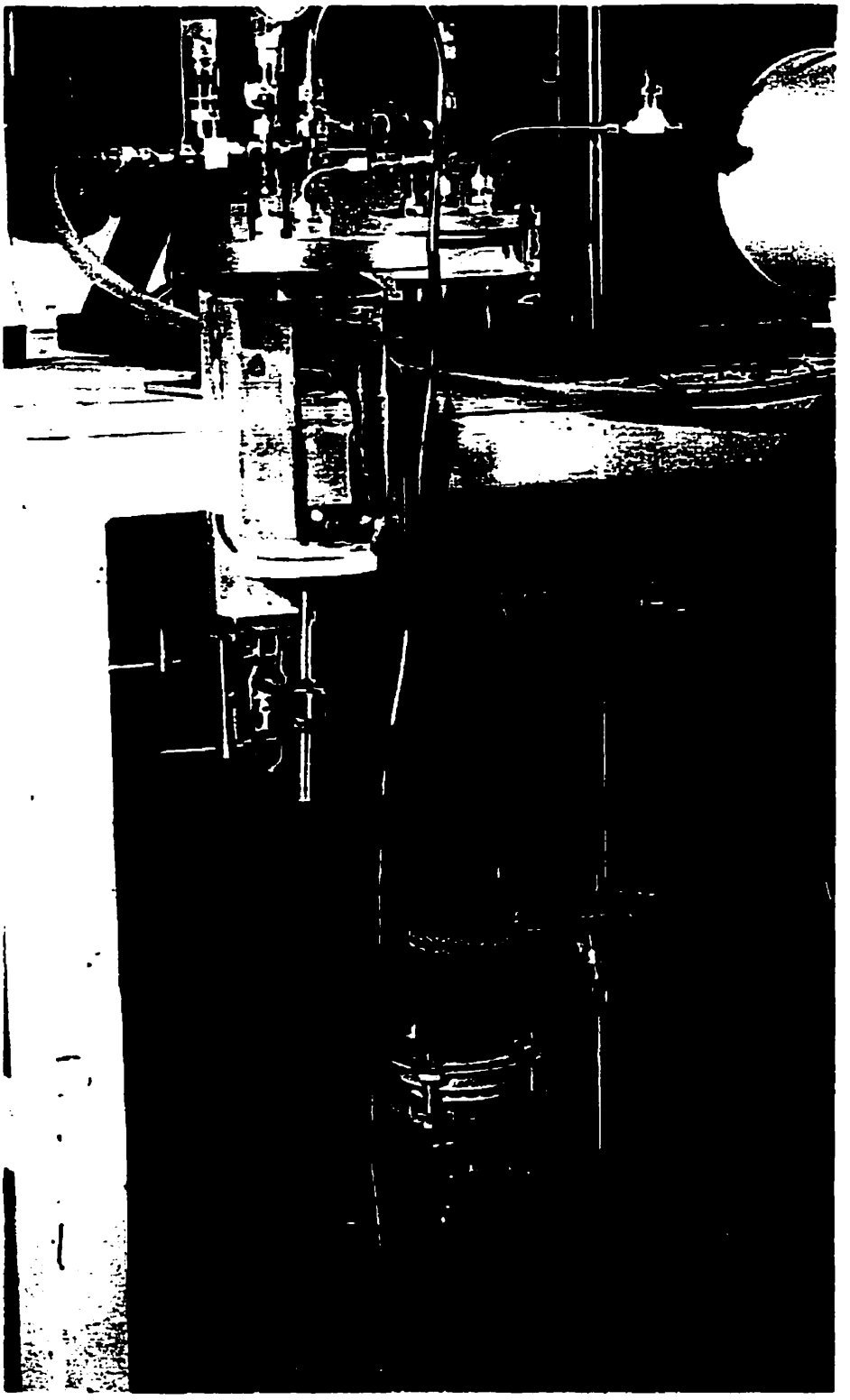

Figure-6.5: Graduated cylinder connected to production port in Sandpack.

The drainage rate of the recovery process was primarily calculated through direct measurement of produced oil from the graduated cylinder. However, still frames of the growing vapor chamber were used as back-up for calculation of flow rates. A programmable digital camera (Kodak DC290) was used during the experiments to record still frames of the process. During the experiment, 250 frames were taken at 20-minute time interval. The camera was placed on a special tripod facing the visual cell, and the cell was illuminated from the sides by three projectors.

6-2 Data Analysis

During experiments with Hele-Shaw cell, direct analysis of images was adequate to estimate the drainage rate by Vapex. In the case of sandpack models, the solute-solvent interface is not smooth and a transition zone exists between the vapor chamber and bitumen bulk. Moreover, visual examination of the outer most surface of the sand (contacted by Plexiglass) might not be representative of true interface position deeper inside the sand. Therefore, cumulative volume of produced oil was visually measured through the transparent graduated cylinder.

The drainage rates were calculated by taking the derivative of the cumulative oil production curve. Figure-6.6 presents the cumulative production and the calculated recovery rate during the process. The observed peak production rate (during the first 500-minute) is likely to be caused by inadequate level of pressure control. In that regard, until the gas break through occurs the recovery is partly influence by an immiscible gas displacement process. After the breakthrough occurs, the drainage is primarily gravity dominated. It is important to mention that both curves correspond to the diluted volume of oil. In order to determine the net production of bitumen, the above volumes were discounted for the solvent concentration, using the following relationship:

Net Bitumen = Produced Oil and Dissolved gas – Dissolved gas

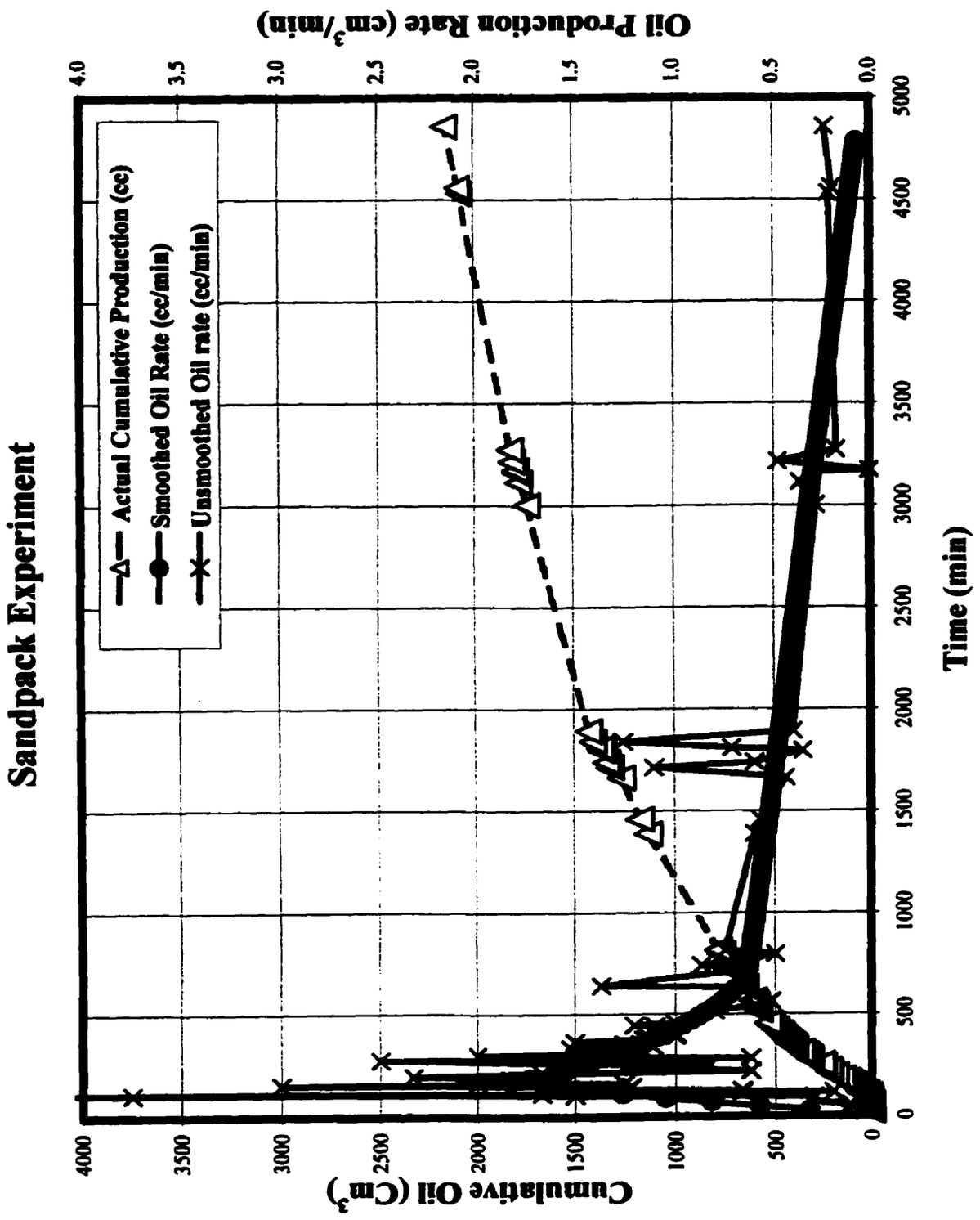

Figure-6.6: Cumulative production and instantaneous flow rate of diluted oil from sandpack experiment.

Table-6.1: Summary of calculation of butane solubility in Panny oil.

	Sample-1	Sample-2	Sample-3
Weight of Dead Oil + Bottle (g)	601.47	657.48	688.99
Weight of Empty Bottle (g)	354.41	356.74	354.78
Net Weight of Dead Oil (g)	247.06	300.74	334.21
Net Oil Volume (cm^3)	254.70	310.04	344.55
Volume of Oil + Dissolved Butane [1] (cm^3)	450	610	625
Butane Concentration (V/V)			

1- At the time of transfer

Solvent concentration was determined from the samples removed from the cylinder during the experiment. The dead oil weights were measured by exposing the sampling bottles to open air for an extended period of time to permit free liberation of the dissolved gas. The dead oil volumes were then calculated based on an average oil density of 0.97 g/cm^3 for Panny oil. The volume of dead oil was deducted from the live oil (at the time of transfer) and the volume fraction of solvent in oil was determined. The summary of this calculation shown in Table-6.1 indicates a maximum solvent concentration of 49% (V/V) with an average value of 46% (V/V). Therefore, in all the subsequent calculations, a maximum butane concentration of Cs=0.45 (V/V) was considered.

The average stabilized production rate of diluted oil during the experiment (600-1200 min.) is about 0.6 cm^3/min, corresponding to 36 cm^3/h. Dividing this number by the width of cell (3.25 cm) and multiplying it by oil concentration (55%), would yield a net areal rate of growth of vapor chamber equal to 6.09 cm^2/h. This number is further divided by 2, to represent the rate of growth of vapor chamber for one side of the cell.

Similar to the analysis presented in previous chapter, N_s parameter was back calculated from Equation-2.18, knowing the cell height and permeability. The N_s parameters were also computed analytically for comparison purposes using Equation-2.7 and assuming a maximum solvent concentration of C_s=0.45 (V/V). Table-6.2 summarizes the results of this analysis.

Table-6-2: Preliminary results of Sandpack experiment.

Stabilized diluted oil rate	(cm^3/min) (cm^3/h)	0.6 36
Thickness normalized diluted oil rate	(cm^3/cm/h)	11.08
Rate of growth of vapor chamber (Net bitumen production)	(cm^3/cm/h)	6.09
1-sided Rate of vapor chamber growth (Element of symmetry)	(cm^3/cm/h)	3.05
N_s, Back calculated	----	1.78E-04
N_s, Molecular Diffusion only	----	1.71E-07
N_s, Diffusion + Dispersion	----	1.83E-07

The dispersion effects were incorporated into N_s calculation in terms of an effective diffusion coefficient, using Equation-3.3 and 3.4. Note that the back calculated N_s term is almost three orders of magnitude higher than that calculated by molecular diffusion coefficient only. Moreover, incorporation of dispersion effect is only marginally improving the estimated N_s values. Therefore, in order to have a better understanding of dispersion effect in porous media, the reported experimental data from literature along with the results of this experiment were reviewed in detail, as discussed in the following section.

6-3 Comparison with Other Laboratory Experiments

Several experiments are available in the literature, which were primarily used to examine other characteristics of the Vapex process. However, it is still possible to utilize the data from the appropriate tests and use them for investigation of interfacial mass transfer. In doing so, emphasis was made in selecting the sandpack experiments of known porosity, permeability and cell dimension, where injector is on the top and producer on the bottom, solvent is Butane and no connate water saturation exists in the model (Dry-Vapex). The summary of the experiments in porous media by other investigators is shown in Table-6.3. The results of the experiment during this study are shown in the first row.

Table-6-3: Summary of experimental runs from previous works in porous media.

#	Experiment	Viscosity μ (mPa.s)	Maximum Rate [1] ($cm^3/cm/h$)	K (μm^2)	Back Calculated Ns, Experiments	Estimated Ns, Molecular Diffusion	Estimated Ns, Diffusion + Dispersion [2]
1	Panny	7,400	3.05	45	1.78E-04	1.71E-07	1.83E-07
2	Das, 1995 Peace River	126,500	6.31	830	3.61E-05	3.00E-08	1.13E-07
3			2.91	217	2.94E-05	3.00E-08	4.53E-08
4			1.26	43.5	2.73E-05	3.00E-08	3.15E-08
5			0.77	27	1.63E-05	3.00E-08	3.06E-08
6	Das, 1995 Lloydminster	7,000	12.19	830	1.35E-04	1.47E-07	6.69E-07
7			7.53	217	1.97E-04	1.47E-07	2.44E-07
8			4.78	43.5	3.95E-04	1.47E-07	1.57E-07
9			1.78	27	8.80E-05	1.49E-07	1.54E-07
10	Jiang, 1997 Lloydminster-1	7,400	3.83	43	2.78E-04	1.71E-07	1.82E-07
11			6.86	220	1.74E-04	1.71E-07	2.83E-07
12	Jiang, 1997 Lloydminster-2	7,000	4.97	43	4.69E-04	1.41E-07	1.50E-07
13			7.84	220	2.28E-04	1.41E-07	2.31E-07

1- Rates corrected for one side of the cell.

2- Dispersion is calculated from equation 3.3 and 3.4.

The flow rates tabulated in column 4 represent the stabilized average flow rates during the spreading phase of vapor chamber. Note that utilization of the coefficient of longitudinal and transverse dispersion (0.5 and 0.0157) as outlined in equations 3.1 to 3.4 is not capable to reconstruct the desired values of N_s parameter. Interestingly, all the experiments indicate that as the cell permeability increases, the reported flow rates increase as well. However, the same relationship does not hold for the back-calculated N_s parameters. For example, all the experiments with Lloydminster oil (with the exception of experiment # 9) indicate that increase in cell permeability results in reduced N_s values. On the other hand, experiments in Peace River bitumen indicate a direct relationship between permeability and N_s parameter.

Knowing that dispersion effects are directly related to convective forces (Peclet number), the ratio of back-calculated to analytical N_s values were plotted versus the Peclet number,

as shown in Figure-6.7. The analytical N_s in this plot are based on molecular diffusion coefficient only, and were computed using equation 2.7. Peclet number is calculated based on the maximum velocity of the diluted oil at solubility concentration limit as discussed in Chapter-5. It appears that the calculated values from experiment 5 and 9 are not in harmony with the observed trend in other experiments for the same crude. All other experiments using Lloydminster oil indicate an inverse relationship between the N_s-ratio and the Peclet number. Peace River bitumen, on the other hand indicates a direct relationship between N_s ratio and Peclet number. Earlier anticipation was that all the curves would exhibit the same characteristics as that observed for Hele-Shaw cell experiments as shown in Figure-5.16. With the exception of the Peace River bitumen, all the seven experiments on Lloydminster oil consistently indicate decreasing values of N_s-ratio vs. Peclet number. The discrepancy between the expected behavior and the observed trend is either due to human errors associated with measurement of experimental data or existence of a tertiary process in porous media, which is still overlooked.

To examine the quality of the data used in these calculations, the reported flow rates were normalized versus the thickness of the cell and plotted versus cell permeability, as shown in Figure-6.8. Theoretically, all the points are expected to pass through the origin. Interestingly, the experiments by Das (1995), particularly with Lloydminster crude, indicate a sudden reduction of recovery rate at the cell permeability of 27 μm^2. Das points out that in Lloydminster crude, the rate does not fall as fast as the square root of permeability. He attributes this behavior to the enhancement of the rate of mixing in the contact zone, as a function of reduced grain diameter. He suggests that this effect is greater for the less viscous Lloydminster oil than the high viscosity Peace River bitumen. However, he does not comment on the 27-μm^2 cell permeability. Although this behavior could be partly due to human error and/or other uncertainties of the experiment, it is unlikely that all other seven experiments on Lloydminster crude are subject to the same error. Interestingly, experiments by Jiang (1997) indicate more or less identical slopes to those by Das for Lloydminster bitumen. Therefore, attention was focused on the possibility of additional processes influencing the mass transfer in porous media.

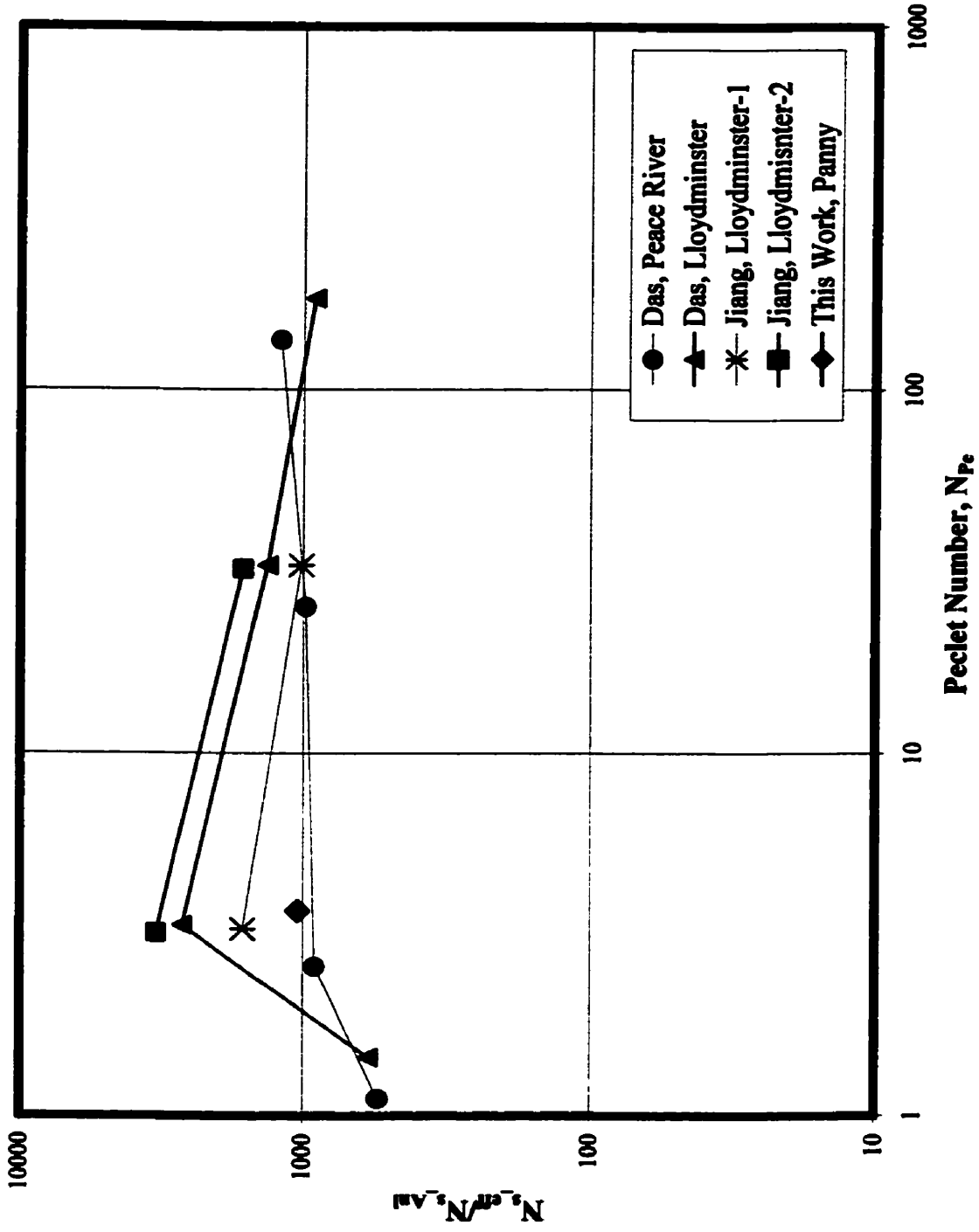

Figure-6.7: N_s Ratio vs. Peclet Number for sandpack experiments.

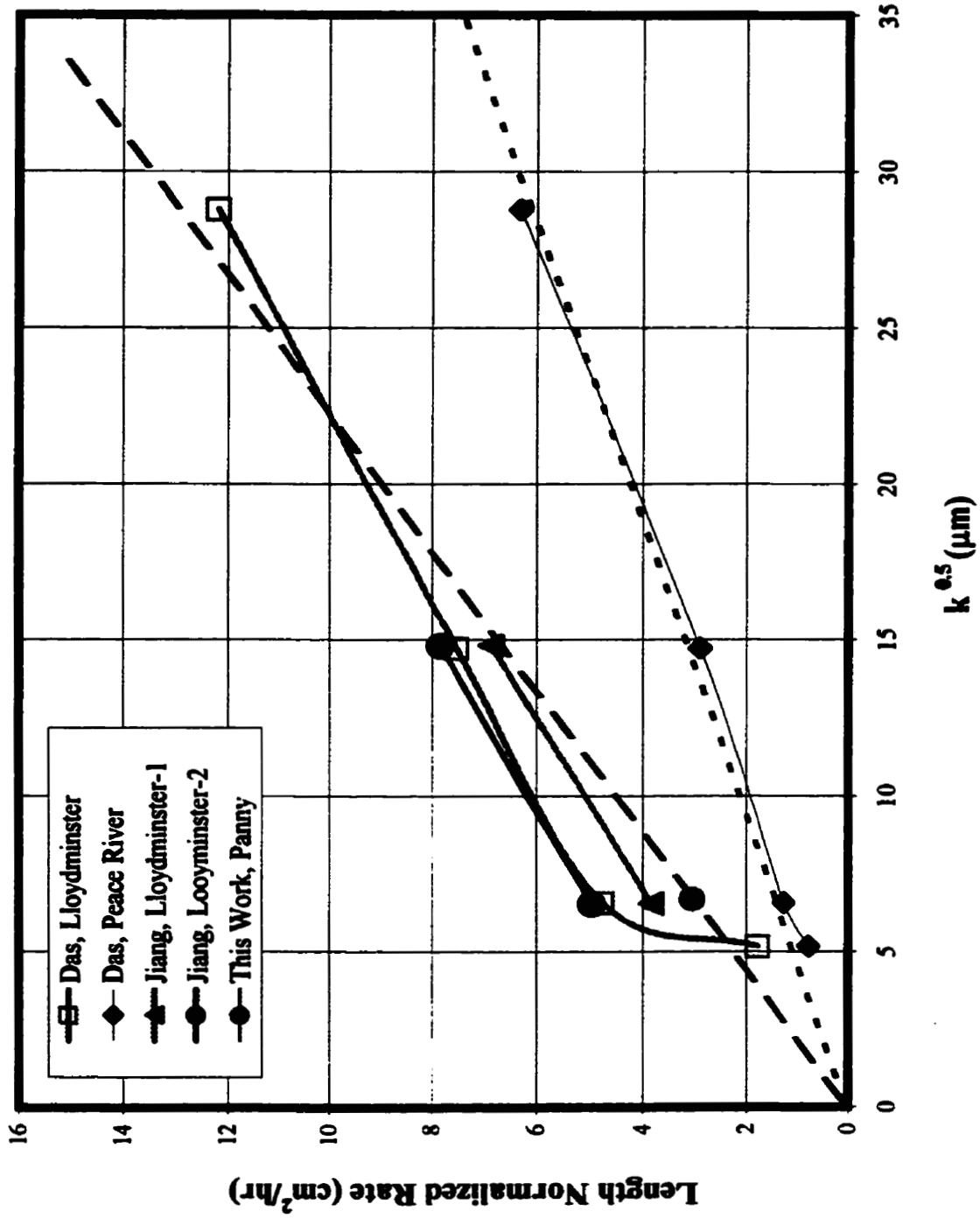

Figure-6.8: Comparison of estimated flow rates vs. square root of permeability.

6-4 Additional Processes in Mass Transfer

In order to address the discrepancy between the experimental rates and the estimated values by analytical models of Vapex in porous media, convective dispersion was looked into. Attempts in calculating an effective diffusion coefficient, using equation 3.1 and 3.2, were unsuccessful to provide the desired effective diffusion coefficient.

It is important to mention that the above formulation was primarily developed for systems under favorable viscosity ratio (Perkins & Johnston, 1963). Under favorable condition, the viscosity of the displacing fluid (zone of high solvent concentration) is expected to be higher than or equal to the displaced fluid (zone of low solvent concentration). However, the mass transfer mechanism in Vapex is different than the above processes for two main reasons. First, Vapex is essentially a non-displacement-type process, where flow is primarily under the influence of gravity. Therefore, apart from the head of the fluid, no additional pressure gradient is present in the system. Second, the viscosity of the more mobile fluid at maximum solvent concentration (leading front) is 2-3 orders of magnitude less than the viscosity of the bitumen bulk.

Brigham et al. (1961) experimentally showed that miscible displacement under unfavorable viscosity ratio results in enhanced mixing. They also noticed that effluent composition does not follow a smooth *S* shaped curve on error function plot, and instead a number of bumps and irregularities in composition are observed. They attributed these irregularities to creation of *fingers* of displacing fluid, run ahead of the bulk of the flood front. Although, Vapex process occurs under unfavorable viscosity ratio, no additional displacement force exists in the system and therefore viscous fingering is not prevalent (gravity stable). Although, some experiments in Vapex imply the possibility of viscous fingering, they could have been created due to poor level of pressure control. Therefore, there is a great likelihood that the multiplier of transverse dispersion (0.0157) is not capable to account for enhanced mass transfer in Vapex. Never the less, it is still possible to determine the combined effect of all the factors influencing the overall mass transfer in porous media, as a single parameter, β as shown in the following relationship.

$$\frac{K_t}{D_o} = \frac{1}{F\phi} + \beta \frac{V\, d_p \sigma}{D_o} \qquad (6.1)$$

In attempt to determine the β parameters, the original multiplier 0.0157, was modified by an optimization procedure, such that the analytical values of N_s (column-8, Table 6-3) became equal to the back calculated ones (column-6, Table 6-3). The results of such analysis are shown in Table 6-4.

It is important to mention that the velocity vector parallel to the interface was computed from the principal velocity vector, based on the assumption of an average angle of inclination of interface. The principal velocity vector is indeed the interstitial velocity of fluid, moving through the pore spaces under the influence of gravity. This velocity was computed by dividing the macroscopic flow rate to the cross sectional area available to flow from Darcy's equation, as shown below.

$$V = \frac{k\, g\, \Delta\rho}{\mu\, \phi} \qquad (6.2)$$

Calculation of the convective velocity vector parallel to the interface was based on the crude assumption that during the stabilized period of flow, the upper corner of the vapor chamber has traveled about 1/3 of the distance in X-direction. Therefore, it is possible to approximate the angle of interface from horizontal and define the projection of velocity, parallel to the interface. In reality, the angle of interface is dynamically changing as the vapor chamber is growing and the velocity parallel to interface is gradually decreasing. The influence of this approximation on the calculated recovery rate is far smaller than the "order of magnitude" discrepancy that we are after.

Table-6-4: Summary of calculated overall dispersion multiplier and Peclet number.

#	β_t	U_{cs} (cm/h)	$D_{o\_(C_s)}$ (cm^2/s)	dp (cm)	σ	σ dp V/D_o
1	223.10	0.948	9.01E-06	0.036	3.50	3.68
2	6.83	6.578	4.66E-06	0.100	3.50	137.24
3	30.06	1.720	4.66E-06	0.071	3.50	25.37
4	273.69	0.345	4.66E-06	0.036	3.50	2.59
5	380.10	0.214	4.66E-06	0.025	3.50	1.12
6	4.05	15.224	8.30E-06	0.100	3.50	178.28
7	32.03	3.980	8.30E-06	0.071	3.50	32.95
8	629.7	0.798	8.30E-06	0.036	3.50	3.36
9	324.90	0.495	8.30E-06	0.025	3.50	1.45
10	391.53	0.836	8.92E-06	0.036	3.50	3.28
11	24.44	4.275	8.92E-06	0.071	3.50	32.95
12	821.60	0.759	8.27E-06	0.036	3.50	3.21
13	39.73	3.881	8.27E-06	0.071	3.50	32.25

Figure-6.9 presents the estimated average β multiplier versus the calculated Peclet number. The β multiplier appears to be exponentially related to the Peclet number as shown in the following equation.

$$\beta = \alpha N_{pe}^{\theta} \qquad (6.3)$$

Note that as Peclet number increases, successively smaller β multipliers are needed to history match the experimental data. The coefficients and exponents of curve fit from this plot are listed in column 2 and 3 in Table-6-5. Note that, as the exponents of curve fit decrease the coefficients increase. Interestingly, the exponent of curve fit from Peace River bitumen (the most viscous sample) is the largest, while its multiplier of Peclet number is the smallest. This implies that there could be an inverse relationship between bitumen viscosity and α multiplier, and a direct relationship between viscosity and θ exponent.

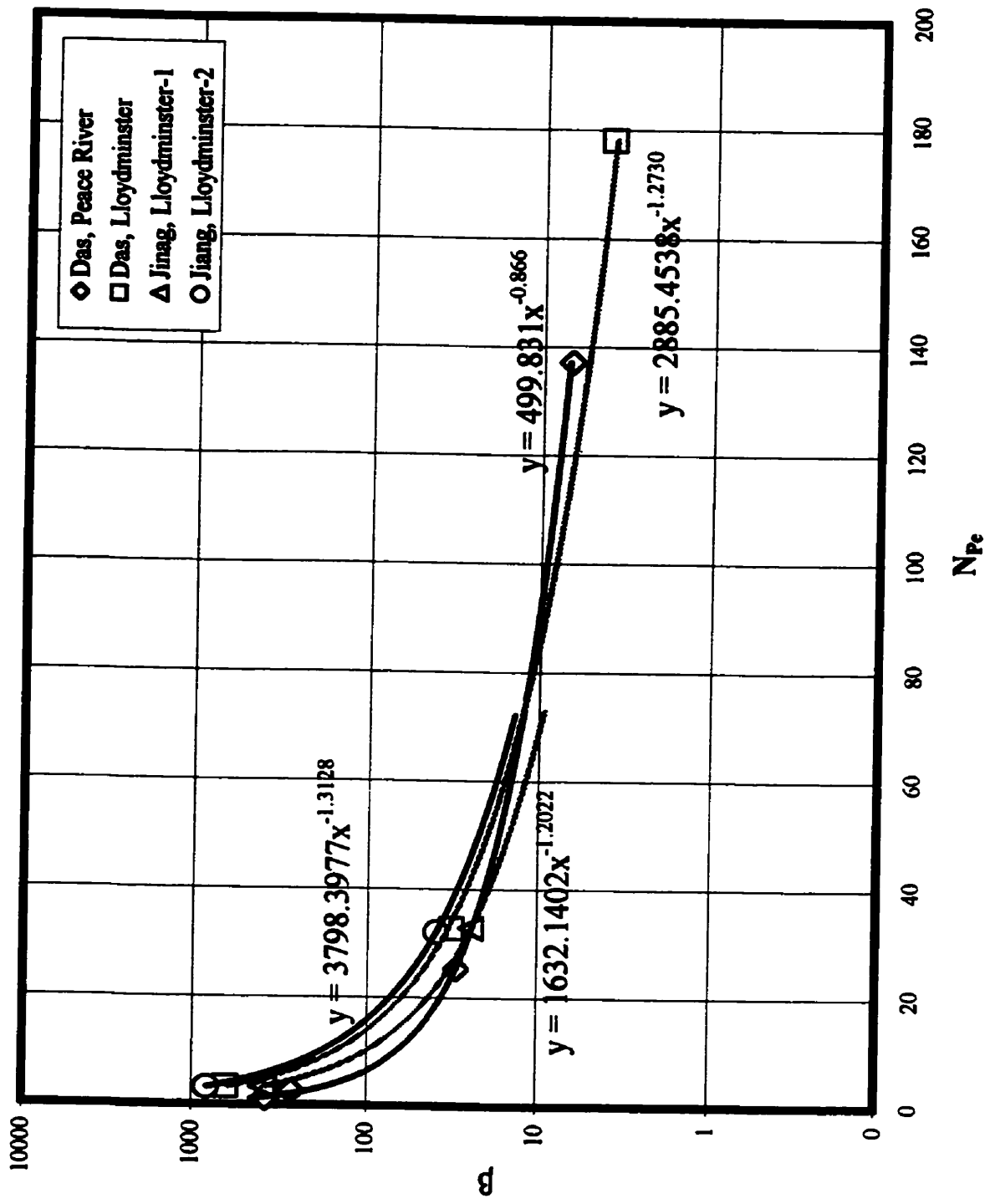

Figure-6.9: Overall dispersion multiplier β, versus Peclet number N_{pe}.

It is also important to mention that equation 3.1 and 3.2 suggest that if all other parameters are held constant, K/D_o decrease as particle diameter gets smaller. This is contrary to the reported experiments by several authors (Das & butler 1996, Dunn et al. 1989, Blackwell 1962, Perkins & Johnston 1963) where indeed dispersion effects tend to increase as particle diameter gets smaller. In order to examine the influence of particle size on dispersion effects, the β multiplier was plotted as a function of particle diameter, as shown in Figure-6.10. As expected, increase in particle diameter is accompanied with decrease in β.

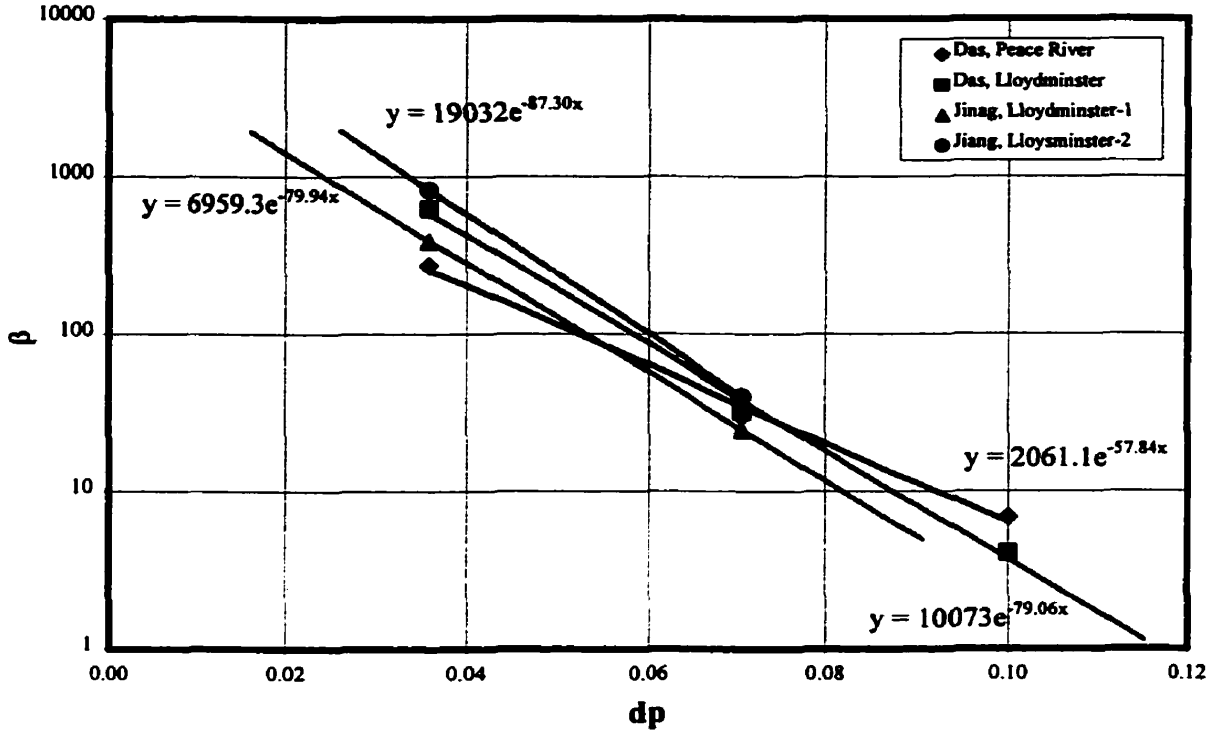

Figure-6.10: Sensitivity of β multiplier to particle diameter.

It is noteworthy that all the above mentioned experiments utilize identical sand particles, for the given cell permeability (mesh size). Therefore, it appears that differences between the experimental results could be primarily due to differences in the characteristics of the heavy oil used in the experiments, particularly viscosity.

Table-6-5: Summary of the curve-fit results to β vs. N_{pe} plot.

Sample	Coefficient α	Exponent θ	Original Viscosity μ (mPa.s)	Diluted Viscosity [1] $\mu_{\_Cs}$ (mPa.s)	Viscosity Ratio $\mu_{\_Cs}/\mu$
Das, Peace River	499.831	-0.8660	126,500	5.24	7.30E-05
Das, Lloydminster	1632.140	-1.2022	7,000	2.54	4.86E-04
Jiang, Lloydminster-1	2885.453	-1.2730	7,400	2.55	5.70E-04
Jiang, Lloydminster-2	3798.398	-1.3128	7,000	2.54	5.73E-04

1- Viscosity at solvent concentration of 50% (V/V) by Shu-Lederer correlation.

Experiments in Chapter 5 had highlighted that convective dispersion can be created under the influence of non-uniform velocity distribution in Hele-Shaw cell. It is anticipated that a similar form of dispersion due to velocity contrast would contribute to enhanced mass transfer in porous media. In addition, presence of grain particles in sandpack can further influence the dispersion process. Therefore, dispersive mass transfer formulation in porous media at least needs to incorporate the effect of viscosity and particle diameter explicitly.

Earlier researchers had presented relationships for estimation of dispersion coefficients in porous media, as a function of the Peclet number. Viscosity ratio is another dimensionless number, which can be related to dispersive mass transfer formulation as a matching parameter. Viscosity ratio in this context is the ratio of the diluted oil at maximum solvent concentration (leading front boundary layer) to the viscosity of undiluted oil at the bitumen bulk. The viscosity ratios for Lloydminster and Peace River bitumen are shown in Table-6-5. Note that the viscosity of Peace River bitumen is almost 17 times higher than that for Lloydminster oil, whereas the viscosity ratio for Lloydminster oil is 8.3 times larger than that for Peace River bitumen.

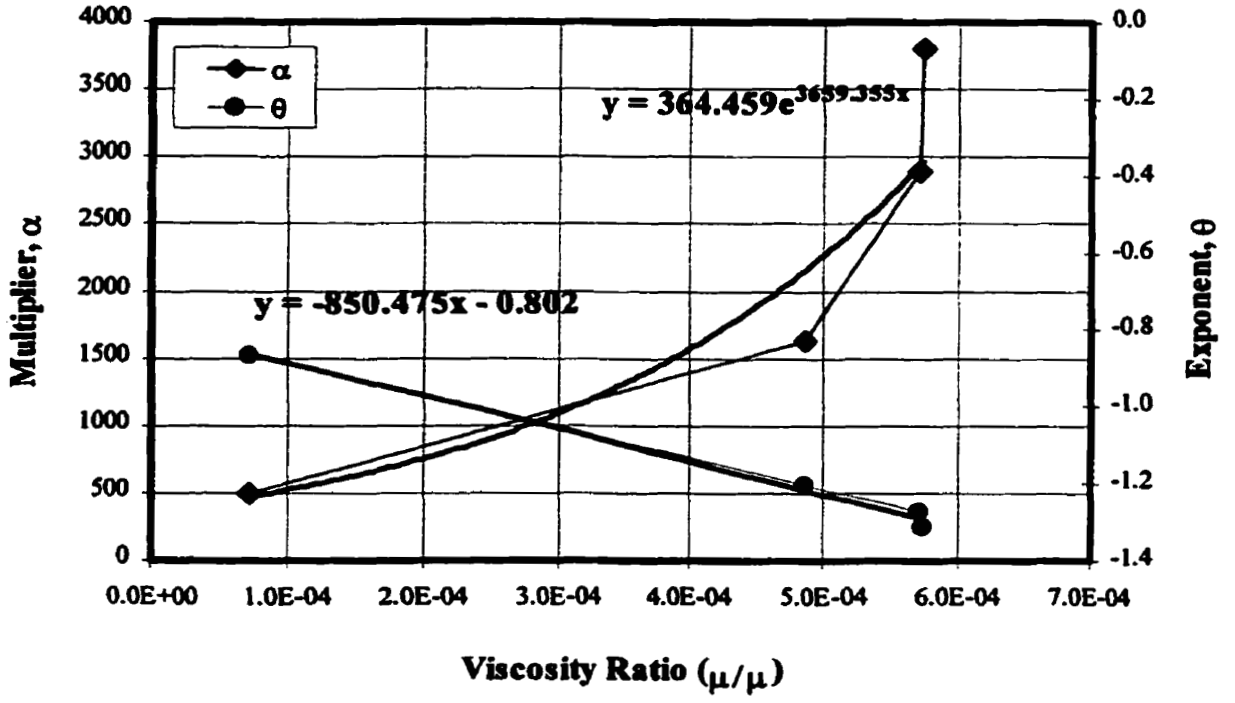

Figure-6.11: Dependency of α multiplier and θ exponent on viscosity ratio.

In order to examine the dependency of β multiplier on Peclet number, the coefficients and exponents of β in Table 6-5 were plotted as a function of viscosity ratio. The results of the best-fit lines in Figure-6.11 indicate the following relationships between the multiplier α, and the exponent θ vs. viscosity ratio.

$$\theta = -850.47\left(\frac{\mu_a}{\mu_b}\right) - 0.8016 \tag{6.4}$$

$$\alpha = 364.46\, e^{3659.36(\mu_a/\mu_b)} \tag{6.5}$$

Once equation 6.4 and 6.5 are inserted into equation 6.3, the following relationship between β and Peclet number is realized.

$$\beta = 364.46\, e^{3659.36(\mu_a/\mu_b)} N_{pe}^{-850.47\left(\frac{\mu_a}{\mu_b}\right)-0.8016} \tag{6.6}$$

Table-6.6: Calculated dispersion coefficients, using equation-6.7.

#	Average β	U_{cs} (cm/h)	$\beta.N_{pe}$ Back Calculated	$\beta.N_{pe}$ [1] Analytical	dp (cm)	$D_{o\,(Cs)}$ (cm^2/s)	σ dp V/D_o @ Cs	μ/μ
1	57.88	0.948	821.67	1629.66	0.036	1.22E-05	3.68	4.86E-04
2	1.76	6.578	937.80	931.05	0.100	6.89E-06	137.24	7.30E-05
3	7.73	1.720	762.57	739.68	0.071	6.89E-06	25.37	7.30E-05
4	71.31	0.345	708.71	541.97	0.036	6.89E-06	2.59	7.30E-05
5	97.30	0.214	424.24	483.24	0.025	6.89E-06	1.12	7.30E-05
6	1.43	15.224	721.99	664.96	0.100	1.13E-05	178.28	5.70E-04
7	10.58	3.980	1055.37	1078.41	0.071	1.13E-05	32.95	5.70E-04
8	201.58	0.798	2117.97	2073.16	0.036	1.13E-05	3.36	5.70E-04
9	105.09	0.495	471.06	2638.20	0.025	1.13E-05	1.45	5.70E-04
10	123.55	0.836	1283.77	1670.86	0.036	1.21E-05	3.28	4.86E-04
11	7.74	4.275	805.17	1017.88	0.071	1.21E-05	32.95	4.86E-04
12	258.30	0.759	2637.28	2118.82	0.036	1.13E-05	3.21	5.73E-04
13	12.49	3.881	1281.40	1087.48	0.071	1.13E-05	32.25	5.73E-04

Column-5 in Table-6.6 summarizes the calculated dispersion coefficients for all the experiments using equation 6.6. The dispersion coefficients, back calculated through history matching of experimental results are listed in column-4. Figure-6.12 compares the estimated dispersion coefficients by both techniques. Note that, majority of the data points are clustered around the 45-degree baseline. The adopted methodology for estimation of dispersive mass transfer for Vapex in porous media appears to be attractive. However, the author believes that additional experiments are necessary to verify and possibly improve the above mentioned relationships.

---

[1] $$\beta N_{pe\ Analytical} = 364.46\, e^{3659.35(\mu_{cs}/\mu_b)}\, N_{\mu}^{0.1984-850.47\left(\frac{\mu_{cs}}{\mu_b}\right)}$$

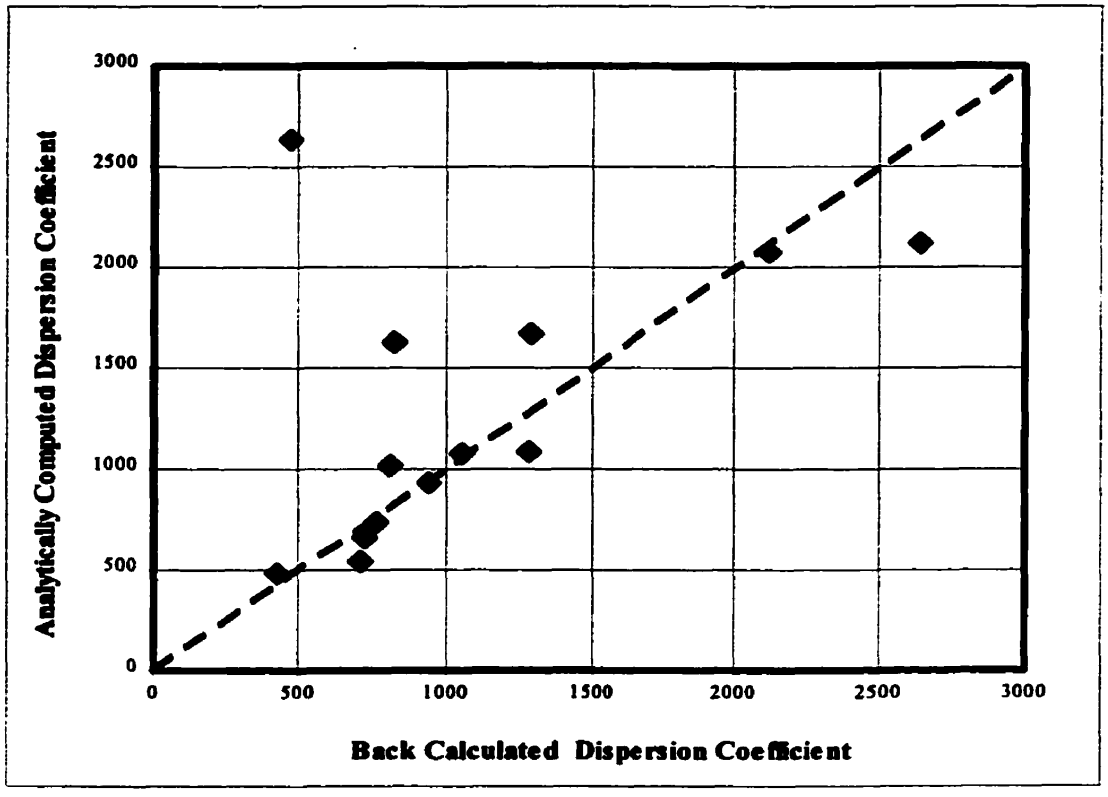

Figure-6.12: Comparison of analytical vs. back calculated dispersion coefficients.

In the light of the above discussion, it appears that it is possible to estimate the enhanced interfacial mass transfer for a solvent-bitumen pair, if the parameters controlling the dispersion, as defined by equation 6.3 are known. Although the exponents of α and θ are primarily derived from empirical observations, in the absence of additional information, they can still be used to provide a better estimate (than other methods) of the expected recovery rates for Vapex in porous media.

It is also important to mention that in addition to particle diameter and viscosity ratio, other parameters might be affecting the enhanced mass transfer in Vapex. Particle size distribution, particle sphericity, permeability heterogeneity and density difference between solute and solvent are among other parameters that could possibly affect the enhanced mass transfer in Vapex. Additional Dry-Vapex experiments are needed to clarify the current level of understandings on interfacial mass transfer in porous media.

CHAPTER SEVEN

EVALUATION OF USE OF GREENHOUSE GASES FOR VAPEX PROCESS

There is general agreement that increase in atmospheric concentration of Greenhouse gases (GHG's), such as CO_2, methane, nitrous oxide, etc., over the last hundred years or so, is due to human activity. The emitted greenhouse gases across the globe enter the atmosphere and large portions of them are accumulated at the top of the Troposphere. Solar energy in the form of radiation enters earth's atmospheric energy cycle. GHG's have high absorption capacity of infrared (IR) radiation and have positive contribution to radiative forcing. Therefore, by reflecting the radiated energy back to the earth, they act as a thermal blanket and decrease the escape of terrestrial thermal infrared radiation. It is thought that increasing GHG's would increase the energy input to the earth and hence global warming is thought to occur. It is perceived that this temperature increase would result in catastrophic climatological changes such as increased storm activity and flooding. In order to prevent or minimize the extents of such catastrophes in future, the levels of GHG emissions on a global scale have to be controlled. Although, some controversies are surrounding the issue of global warming (Robinson et al. 1998, Singer 1999, Keller 1999), most experts believe that GHG emission is a real threat to environment.

Utilization of greenhouse gases for improved oil recovery might have significant impact in reduction of atmospheric emissions. In this technique, the injected CO_2 dissolves in oil, reduces viscosity and interfacial tension, and hence improves the flow of oil to the production wells. This chapter elaborates with potential implications of CO_2 injection for Vapex process. Moreover, the produced oil provides a space for underground storage of CO_2. The technique can be extended to utilization of other greenhouse gases, once the uncertainties associated with the process are alleviated.

7.1 Greenhouse Gases

Among all gases emitted to atmosphere by different industrial units, CO_2, CH_4, N_2O, CFC and SF_6 are considered to have the most significant contribution to global warming. They have the capability to remain in the tropopause for considerably a long period of time (long lifetime). Carbon dioxide and other naturally occurring gases in the atmosphere do not absorb all infrared wavelengths. They are relatively transparent to radiation with wavelengths between 7 and 12 nm. Other GHG's such as CH_4, N_2O and the CFC's are powerful absorbers in this range. Table-7.1 summarizes the absorption capacity of infrared radiation by GHG's.

Table-7.1: Absorption capacity of greenhouse gases.

GHG	Absorption Capacity
CO_2	1.56 Wm^{-2}
CH_4	0.50 Wm^{-2}
N_2O	0.10 Wm^{-2}
CFC's	0.30 Wm^{-2}

Having the highest absorption capacity of radiative forcing and a very long atmospheric lifetime, CO_2 has gained considerable importance over other greenhouse gases. As the atmospheric lifetime of these gases are vastly different, their relative importance on global warming is measured through Global Warming Potential (GWP). GWP index is a measure of cumulative radiative forcing over time, per unit mass of emitted gas at time zero, relative to CO_2. Table-7.2 summarizes the global warming potential of some of the atmospheric gases (Norman, 2000). Note that NO_2 and CFC-12 have almost identical GWP at time zero. However, having a longer lifetime, the global warming potential of CFC-12 increases substantially over time. Although CFC-12 absorption capacity is not as high as CO_2 or methane, its increased concentration over time can considerably increase the cumulative radiative forcing of atmosphere and enhance the global warming.

Table-7.2: Global warming potential of greenhouse gases.

	Global Warming Potential (GWP)			
Life Time (years)	0	20	100	200
CFC-11	50	5000	4000	1400
CFC-12	102	7900	8500	4200
CH_4	14	62	24.5	7.5
N_2O	120	290	320	180
SF_6	3200	16500	24900	36500

7.2 CO_2 Effect

Compared to other GHG's, CO_2 has the greatest contribution to global warming. The effect of CO_2 is amplified by water vapor (high heat capacity) in withholding and absorbing this temperature increase. Interestingly, water vapor accounts for more than 90% of the radiative forcing. Carbon dioxide has increased in concentration from about 280 to 356 ppmv since the pre-industrial era (Robinson et al., 1998).

There are a lot of controversies surrounding the issue of global warming as a result of increased concentration of greenhouse gases in atmosphere (Robinson et al. 1998, Singer 1999, Keller 1999). Some scientists think that the Earth's average temperature might increase by about 0.30°C per decade over the next 100 years. A warming of this magnitude could significantly alter the Earth's climate. Storm patterns and severity might increase, a rise in sea level would displace millions of coastal residents and regional droughts and flooding could occur. As a result, Canada's agriculture, forestry and energy sectors could all be significantly affected.

7.3 Emission Trends and Inventories

Being the cheapest source of energy among other alternatives, fossil fuel consumption has substantially increased during the second half of the 20th century. On March 21, 1994 the United Nations Framework Convention on Climate Change (UNFCCC) entered into force. One of the fundamental objectives of this convention is to achieve stabilization of

greenhouse gas concentrations in the atmosphere at a level that would prevent dangerous anthropogenic interference with the climate system (Parties to the Climate Change Convention, 1996). Such a level should be achieved within a time frame sufficient to allow ecosystems to adapt naturally to climate change, to ensure that food production is not threatened and to enable economic development to proceed in a sustainable manner.

Figure-7.1 presents the estimated CO_2 emission and gross domestic product (GDP) for Canada since 1950 (Environment Canada Website). It's interesting that in spite of significant growth of GDP per capita, CO_2 emission per capita has remained relatively constant during the past 25 years. Figure-7.2 presents the greenhouse gas emission for Canada, in comparison to 1990 stabilization targets (Environment Canada Website). This indicates that gross GHG emission during the past decade has increased by 13%. Therefore, it appears that either Canada should slow the pace of industrialization, or a more realistic stabilization level, based on the foreseen rate of growth in gross domestic product and population might be necessary.

Figure-7.3 indicates that CO_2 contributes to more than 80% of the total GHG emission in 1995. The latest statistics by Environment Canada indicate that this percentage has remained more or less constant during the past few years (Neitzert et al., 1999). Table-7.3 and 7.4 summarize the estimated emissions of all greenhouse gas from 1990-1996 for Canada and Alberta respectively (Neitzert et al., 1999). A close review of these data indicates that Alberta accounts for almost 30% of total Energy related GHG emissions. Moreover, energy related emissions contribute to more than 78% of the total greenhouse gases.

On the sector basis, transportation related activities account for about 26 % of total GHG emissions. However, due to the nature of the process, collection of such emissions for sequestration purposes is not possible. The break-up of other major gas emissions for Alberta during 1996 is presented in Figure-7.4. The GHG emissions associated with electricity and steam generation as well as emissions by fuel dependent industrial units are the two main sources that could be possibly used for subsurface injection.

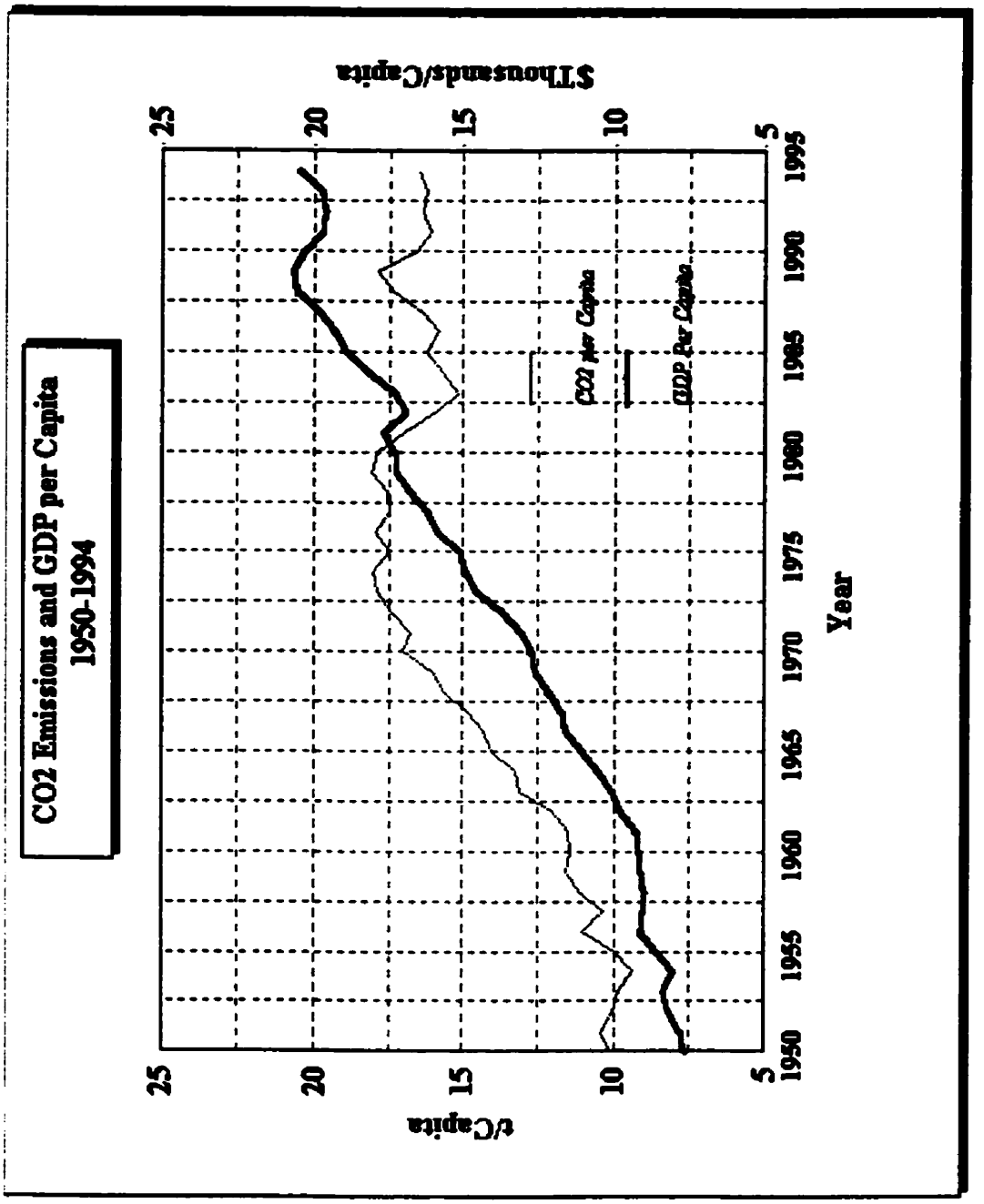

Figure-7.1: Historical trend on CO_2 emission and GDP per capita.

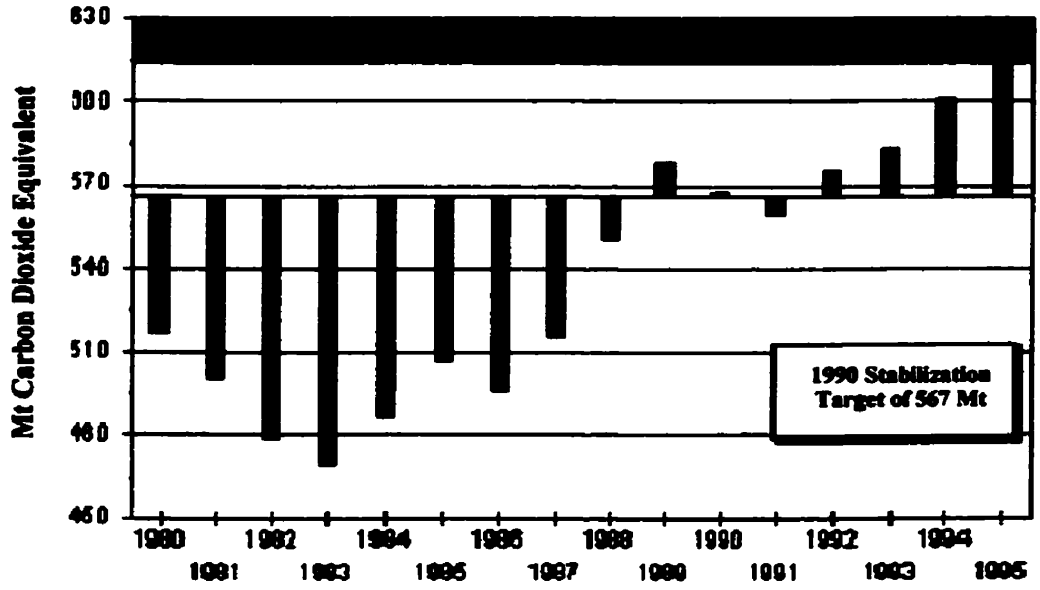

Figure-7.2: Greenhouse gas emissions in comparison to 1990 stabilization level.

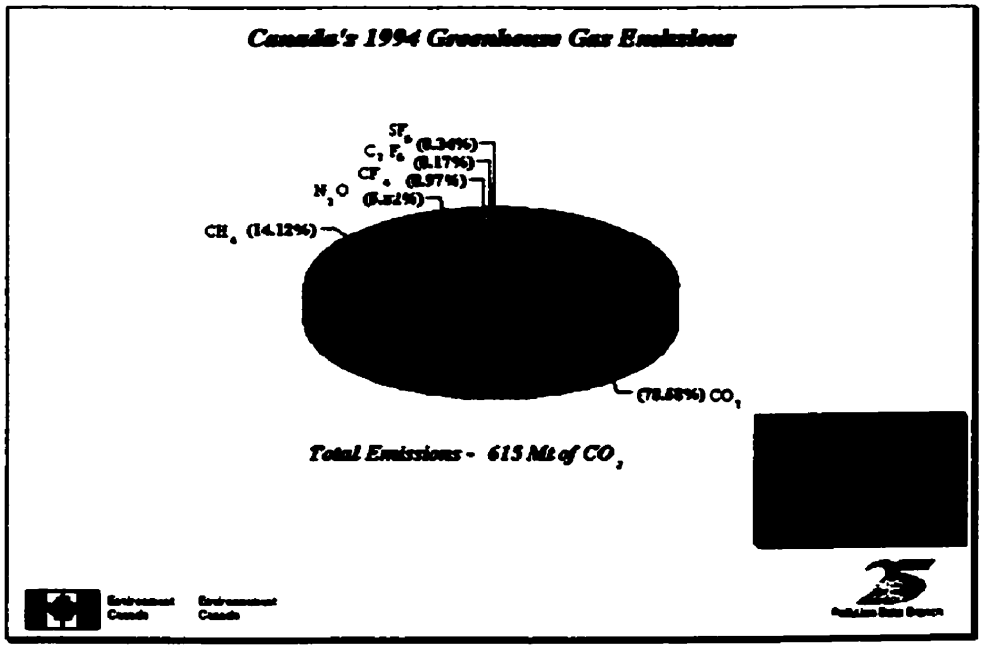

Figure-7.3: Greenhouse gas emissions summary, 1994.

Table-7.3: Alberta's greenhouse gas emission estimates from 1990 to 1996 (After Neitzert et al., 1999)

GHG Source and Sink Category	1990 kt CO2 eq.	1991 kt CO2 eq.	1992 kt CO2 eq.	1993 kt CO2 eq.	1994 kt CO2 eq.	1995 kt CO2 eq.	1996 kt CO2 eq.
ENERGY							
FUEL COMBUSTION							
Fossil Fuel Industries	21,200	21,900	22,300	23,400	23,800	22,400	21,500
Electricity & Steam Generation	40,100	42,100	45,100	45,500	48,900	49,000	48,900
Mining	4,340	3,730	3,340	5,270	5,540	7,330	8,760
Manufacturing	8,500	7,460	7,790	7,170	7,350	8,440	8,180
Construction	85	170	179	89	87	165	216
Transportation							
Gasoline Cars	5,630	5,150	5,070	4,940	5,200	5,040	4,660
Light Duty Gasoline Trucks	3,650	3,520	3,670	3,760	4,170	4,250	4,210
Heavy Duty Gasoline Trucks	651	697	796	881	1,040	1,120	1,090
Off Road Gasoline Vehicles	1,380	1,000	1,040	1,020	695	644	1,310
Diesel Cars	51	46	43	40	40	36	34
Light Duty Diesel Trucks	93	81	76	76	87	87	93
Heavy Duty Diesel Trucks	3,710	3,560	3,650	3,950	4,790	5,080	5,740
Off Road Diesel Vehicles	2,910	2,730	2,320	2,700	3,110	4,040	5,060
Propane and LNG Vehicles	491	538	542	473	576	639	747
Domestic Air	1,550	1,390	1,450	1,530	1,580	1,660	1,850
Rail	1,800	1,540	1,560	1,560	1,620	1,240	1,150
Vehicles SubTotal	21,900	20,300	20,200	21,000	22,900	23,900	26,000
Pipelines	1,230	1,320	1,860	2,040	2,520	2,580	2,690
Transportation SubTotal	23,200	21,600	22,100	23,000	25,400	26,500	28,700
Residential	6,590	6,460	6,400	6,620	7,250	7,550	8,700
Commercial and Institutional	5,050	4,630	4,340	5,010	5,370	6,020	5,250
Other	525	434	537	571	348	327	406
COMBUSTION SUBTOTAL	110,000	108,000	112,000	117,000	124,000	128,000	131,000
FUGITIVE							
Solid Fuels (ie Coal Mining)	240	250	270	270	270	300	290
Oil and Gas	25,000	26,000	28,000	29,000	30,000	32,000	34,000
FUGITIVE SUBTOTAL	25,000	26,000	28,000	29,000	31,000	32,000	34,000
ENERGY TOTAL	**135,000**	**135,000**	**140,000**	**146,000**	**155,000**	**160,000**	**165,000**
INDUSTRIAL PROCESSES							
Non Metalic Mineral Production	869	793	718	914	889	894	991
Adipic & Nitric Acid Production	660	650	660	660	650	660	670
Other Production	7,900	8,700	8,800	9,900	11,000	10,000	11,000
INDUSTRIAL PROCESSES TOTAL	9,400	10,000	10,000	12,000	12,000	12,000	13,000
SOLVENT & OTHER PRODUCTS	39	39	40	40	41	41	42
AGRICULTURE							
Enteric Fermentation	5,100	5,300	5,500	5,600	6,000	6,200	6,200
Manure Management	1,900	2,000	2,100	2,100	2,200	2,300	2,300
Agricultural Soils**	10,000	10,000	10,000	10,000	9,000	10,000	10,000
AGRICULTURE TOTAL	19,000	19,000	19,000	19,000	18,000	21,000	21,000
LAND USE & FORESTRY *	1,600	1,900	1,500	1,300	560	240	570
WASTE							
Solid Waste Disposal on Land	870	930	780	820	860	890	850
Wastewater Handling	140	140	140	140	150	150	150
WASTE TOTAL	1,000	1,100	920	960	1,000	1,000	990
PROVINCIAL TOTALS	**166,000**	**167,000**	**172,000**	**179,000**	**186,000**	**194,000**	**199,000**

Ammonia production emissions are under undifferentiated production at provincial level

* CH4 and N2O emissions from prescribed and other fires

** Only one significant figure shown due to high uncertainty

Note: due to rounding, individual values may not add up to totals

Table-7.4: Canada's greenhouse gas emission estimates from 1990 to 1996. (After Neitzert et al., 1999)

GHG Source and Sink Category	1990 kt CO2 eq.	1991 kt CO2 eq.	1992 kt CO2 eq.	1993 kt CO2 eq.	1994 kt CO2 eq.	1995 kt CO2 eq.	1996 kt CO2 eq.
ENERGY							
FUEL COMBUSTION							
Fossil Fuel Industries	38,600	37,300	38,900	39,100	40,000	40,200	39,900
Electricity and Steam Generation	95,200	96,500	104,000	93,800	95,600	100,000	101,000
Mining	7,650	7,210	6,850	9,930	10,900	12,000	13,000
Manufacturing	54,400	51,100	50,400	49,300	50,500	53,700	53,300
Construction	730	829	844	496	448	739	1,120
Transportation							
Gasoline Cars	53,800	51,200	51,600	51,800	52,200	51,200	50,100
Light Duty Gasoline Trucks	21,800	22,200	24,000	25,500	27,300	28,400	29,600
Heavy Duty Gasoline Trucks	3,170	3,380	3,820	4,200	4,650	4,970	4,990
Off Road Gasoline Vehicles	5,080	4,550	3,640	3,770	3,930	3,900	4,690
Diesel Cars	664	625	622	616	607	585	604
Light Duty Diesel Trucks	598	522	480	462	477	472	469
Heavy Duty Diesel Trucks	24,700	23,900	24,400	25,800	28,600	30,800	32,400
Off Road Diesel Vehicles	11,600	10,400	9,830	11,100	12,300	13,700	15,100
Propane and LNG Vehicles	1,730	1,920	1,940	2,150	2,370	2,480	2,590
Domestic Air	10,600	9,580	9,720	9,030	10,100	10,900	12,000
Domestic Marine	6,070	6,490	6,450	5,620	5,940	5,700	5,560
Rail	7,110	6,590	6,890	6,860	7,100	6,430	6,290
Vehicles SubTotal	147,000	142,000	144,000	147,000	156,000	160,000	165,000
Pipelines	6,690	7,410	9,590	10,100	10,500	11,600	12,100
Transportation SubTotal	154,000	149,000	153,000	157,000	166,000	171,000	177,000
Residential	46,500	44,700	44,800	49,100	49,600	48,100	53,300
Commercial and Institutional	26,100	25,900	26,400	28,700	28,200	30,000	30,200
Other	3,150	3,170	5,440	3,370	2,710	2,620	2,870
COMBUSTION SUBTOTAL	426,000	416,000	431,000	431,000	444,000	459,000	471,000
FUGITIVE							
Solid Fuels (ie Coal Mining)	1,900	2,100	1,800	1,800	1,800	1,700	1,800
Oil and Gas	36,000	38,000	41,000	43,000	45,000	48,000	51,000
FUGITIVE SUBTOTAL	38,000	40,000	42,000	44,000	47,000	50,000	53,000
ENERGY TOTAL	**464,000**	**455,000**	**473,000**	**475,000**	**491,000**	**509,000**	**524,000**
INDUSTRIAL PROCESSES							
Non Metalic Mineral Production	8,160	6,980	6,640	6,880	7,510	7,690	7,840
Ammonia, Adipic & Nitric Acid Production	15,000	14,000	14,000	13,000	15,000	16,000	16,000
Ferrous Metal Production	7,590	8,900	9,080	8,760	8,050	8,500	8,290
Aluminum and Magnesium Production	11,000	13,000	12,000	13,000	13,000	11,000	11,000
Other&Undifferentiated Production	10,000	11,000	12,000	13,000	13,000	13,000	15,000
INDUSTRIAL PROCESSES TOTAL	**52,000**	**54,000**	**54,000**	**55,000**	**57,000**	**56,000**	**59,000**
SOLVENT & OTHER PRODUCT USE	**400**	**400**	**400**	**400**	**400**	**900**	**900**
AGRICULTURE							
Enteric Fermentation	16,000	16,000	16,000	17,000	18,000	18,000	18,000
Manure Management	7,900	8,000	7,900	8,200	8,500	8,800	8,900
Agricultural Soils**	40,000	40,000	40,000	40,000	40,000	40,000	40,000
AGRICULTURE TOTAL	**62,000**	**61,000**	**60,000**	**61,000**	**63,000**	**63,000**	**64,000**
LAND USE & FORESTRY **	**2,500**	**3,200**	**2,900**	**2,800**	**1,500**	**2,100**	**1,700**
WASTE							
Solid Waste Disposal on Land	19,000	19,000	20,000	20,000	20,000	20,000	20,000
Wastewater Handling	1,200	1,200	1,300	1,300	1,300	1,300	1,300
WASTE TOTAL	**20,000**	**21,000**	**21,000**	**22,000**	**22,000**	**22,000**	**22,000**
TOTAL	**601,000**	**595,000**	**610,000**	**617,000**	**635,000**	**653,000**	**671,000**
CO2 from Land Use Change & Forestry**	-40,000	-60,000	-50,000	-30,000	-30,000	-20,000	-30,000

* CH4 and N2O emissions from prescribed and other fires

** Only one significant figure shown due to high uncertainty

Note: due to rounding, individual values may not add up to totals

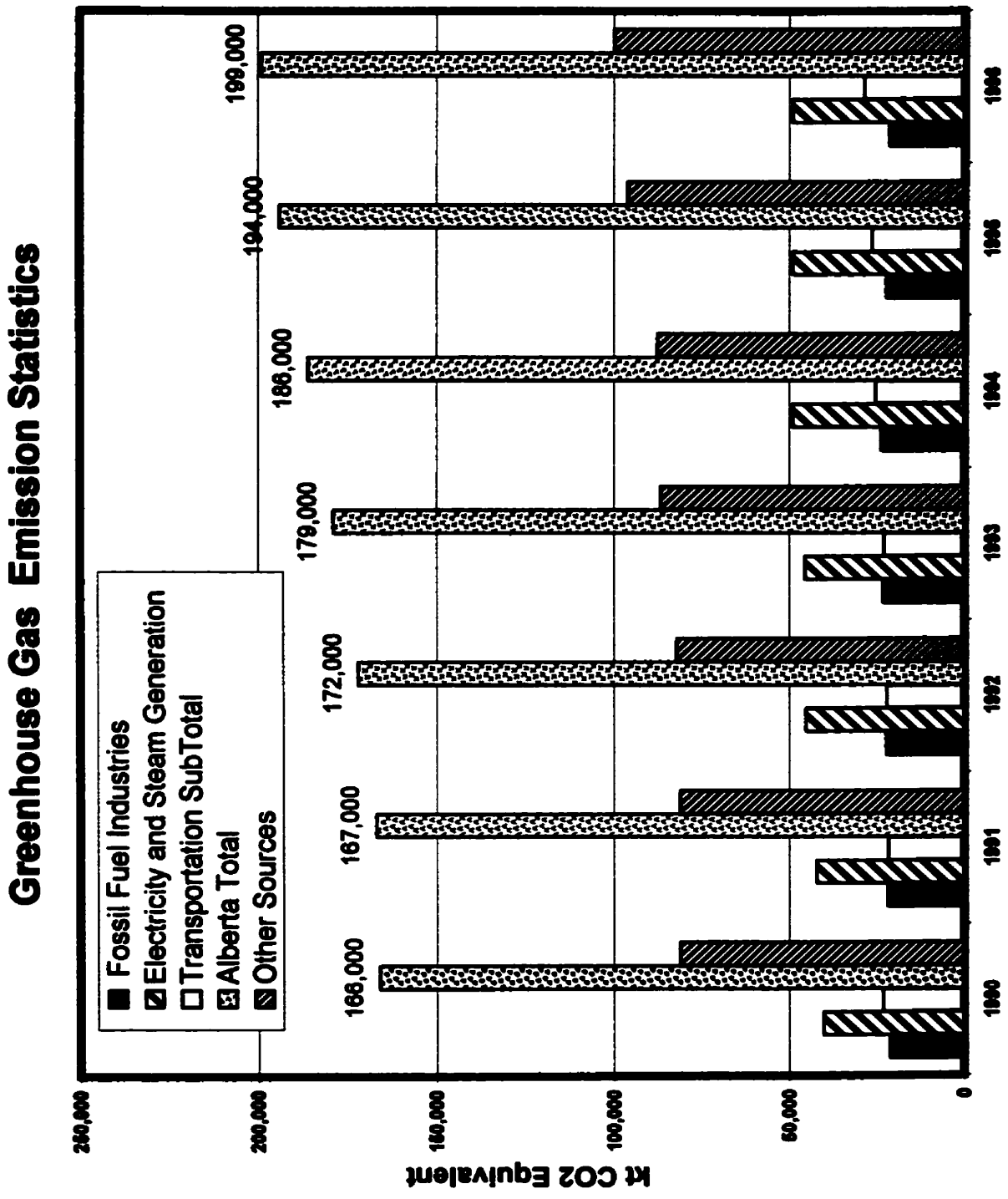

Figure-7.4: Major sources of greenhouse gas emission in Alberta, 1996 statistics.

7.4 Reduction of CO_2 Emission

Latest developments in design of combustion engines have significantly increased energy efficiency and fossil fuel utilization. However, increased demand for energy has remained extremely strong. Therefore, alternative solutions for coping with the increased GHG emissions must be sought.

There are four possible solutions for long-term disposal of CO_2. These include, biological immobilization, mineral immobilization, deep ocean disposal and disposal in geological media (Bachu, 1999). It appears that the most viable option for the Province of Alberta is disposal in geological strata. There are several ways to dispose of CO_2 in sedimentary formations.

- Use in Enhanced Oil Recovery (EOR) operations. This solution has limited capacity and lifetime since the CO_2 may be recovered back at the producing wells. However, there are certain advantages and merits in using this approach as explained in following sections.

- Disposal in depleted oil, gas and bitumen reservoirs; however, this solution requires that reservoirs be depleted first.

- Disposal in coal beds, where CO_2 would displace methane from the coal matrix because it has greater affinity to coal, at the same time producing a cleaner fuel.

- Disposal into deep aquifers (hydrodynamic entrapment).

Long-term effective CO_2 disposal is essential for reducing greenhouse effects. The most important element in assessing the viability of subsurface sequestration is that injected gas will not find a way out to surface or contaminate other subsurface strata. In that regard, permeability of the targeted formation and the trapping mechanism of target reservoirs are

of significant importance. Some of the potential solutions like coal bed or deep aquifer injection are at their preliminary levels of research and they might not be practically utilized before another one or two decades from now. Performing a regional-scale feasibility study for establishing the suitability of surface and subsurface locations for CO_2 disposal in Alberta requires significant amount of investment and time. Moreover, unlike enhanced oil recovery techniques, aquifer disposal of CO_2 is not economically a self-rewarding process.

7.5 Utilization of CO_2 in Vapex

One of the main problems of disposal techniques, is collection and gathering of the waste gases. After Ontario, Alberta is the second largest producer of greenhouse gases in Canada (Bachu, 1999). Unlike Ontario, where greenhouse gases are produced over widely distributed industrial heartland, majority of greenhouse gases in Alberta is rather produced at several major point sources. Most of these point sources in Alberta are the oil sands operations in the Fort McMurray, heavy oil production in Cold Lake area, coal-based power plants (in central Alberta near Lake Wabamun), and the petrochemical industry located in the Edmonton-Fort Saskatchewan and Red Deer (Joffre) areas. In that regard, the costs associated with shipment and layout of gathering pipeline network is significantly less than that for other provinces. Moreover, Oil deposits in Canada have been extensively studied by operating companies and their sedimentary strata are well understood. Therefore, investigation of these formations and characterization of the reservoirs is less labor intensive. However, prior to any long-term commitment or major investment for construction of the required infrastructure for collection and injection of such gases, the expected recovery rates by CO_2 injection in Vapex have to be evaluated.

Figure-7.5 presents the effect of pressure on the viscosity of CO_2 saturated bitumen. Note that increase in CO_2 pressure reduces the viscosity of saturated bitumen considerably. This is primarily due to increased solubility at elevated pressures. However, it is important to remind that due to small overburden pressures, shallow deposits of heavy oil in northern Alberta can hardly accommodate pressures in excess of 1.5-2.0 MPa. Figure-7.6 presents the estimated CO_2 solubility as a function of pressure, for various oil samples. Note that at an average injection pressure of 1.5 MPa, the maximum CO_2 concentration is between 3-4 weight percent. Therefore, it appears that for majority of the heavy oils in Canada, the extent of viscosity reduction by CO_2 injection will be significantly smaller than that by butane or propane.

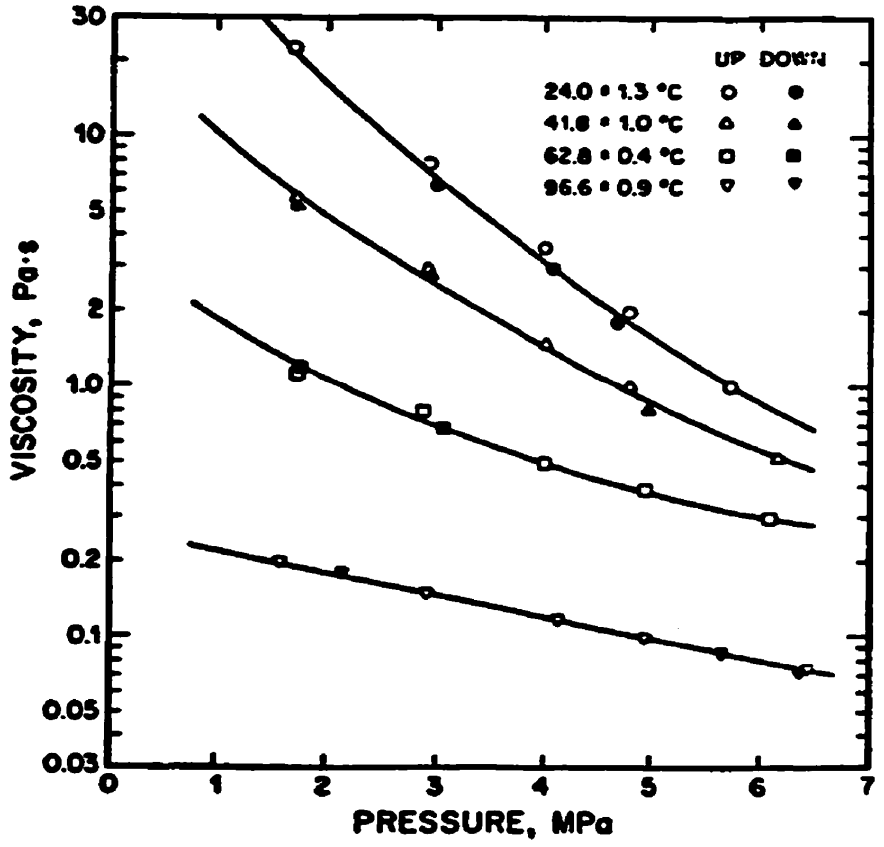

Figure-7.5: Viscosity-pressure isotherms for Athabasca bitumen saturated with CO_2. (After Svrcek & Mehrotra, 1982)

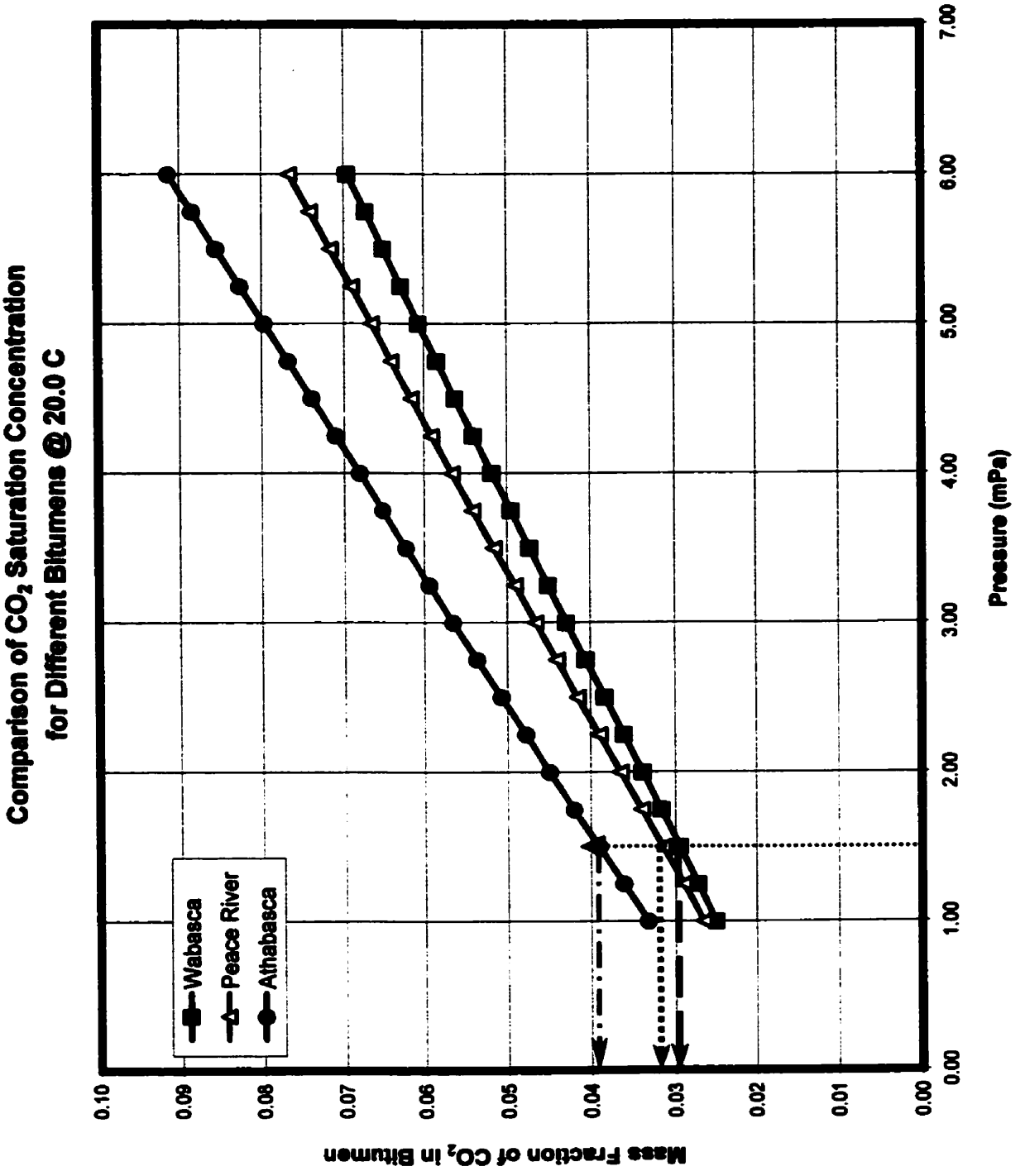

Figure-7.6: Estimated mass fraction of CO_2 vs. pressure for various oil samples. (After Upreti, 2000)

7.5.1. Estimation of Recovery Speed

In order to examine the speed of oil recovery through Vapex process by CO_2 injection, the interfacial mass transfer of CO_2 into bitumen was calculated. The Vapex parameter N_s was computed using the analytical techniques explained in previous chapters. The dependency of bitumen viscosity on CO_2 concentration was determined based on the correlation by Mehrotra (1992). In this technique a one-parametric mixing rule was utilized to estimate the viscosity of a binary gas-bitumen mixture. The calculated values presented in Figure7.7 indicate that bitumen at ambient reservoir temperature (10 °C) has a viscosity of 50,000 mPa.s in the absence of solvent and a viscosity of 2150 mPa.s at the maximum solvent concentration (i.e. the solubility limit of 4 wt%).

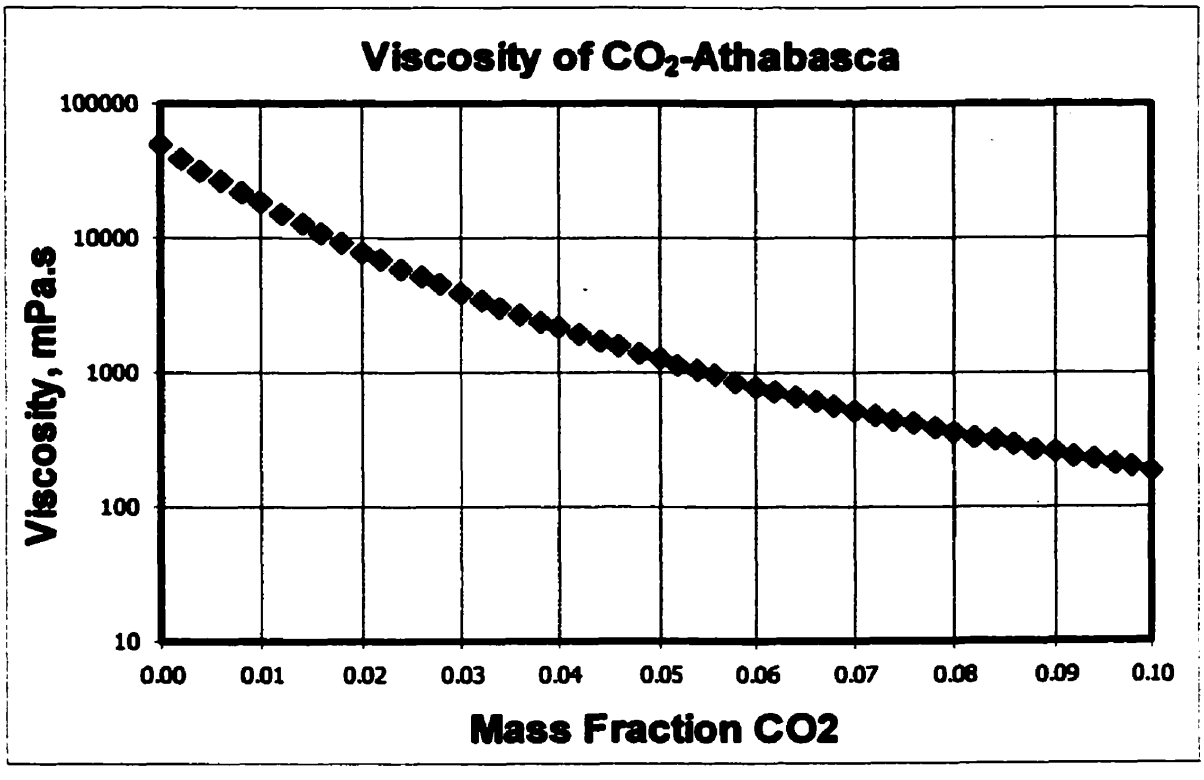

Figure-7.7: Estimated Athabasca oil viscosity vs. CO_2 concentration. (After Mehrotra, 1992)

The intrinsic diffusivity of carbon dioxide into bitumen as a function of solvent concentration was determined based on the experimental work by Upreti (2000), as shown in Figure-4.6. Figure-7.6 indicates that maximum concentration of carbon dioxide for typical heavy oils in Canada is about 4 wt%. This value corresponds to a solvent concentration of 5.6% by volume and was considered as the upper limit of integral in equation 2.7.

The N_s parameter in equation 2.7 was calculated by two different approaches. In the first technique, the viscosity, density and molecular diffusivity were computed as a function concentration and directly used in calculation of N_s parameter. In the second method, the molecular diffusion term was replaced by an effective diffusion, accounting for dispersion effects in porous media. Dispersion effects were incorporated in calculation of overall mass transfer by estimation of interstitial velocity of the mixture (diluted bitumen) at corresponding concentrations. In that regard, the effective diffusion term was computed as a direct summation of molecular diffusion and convective dispersion in porous media as explained in Chapter-6.

Table-7.5 summarizes the calculated N_s parameters and the corresponding flow rates based on a hypothetical reservoir, with an average formation thickness of 20 meter, porosity of 0.32, horizontal well length of 1000 m and a rock permeability of 10 Darcy.

Table-7.5: Calculated recovery rates for typical Athabasca bitumen at 10 °C.

	N_s parameter	Length-Normalized 1-Sided Oil Flow Rate (m^2/day)	2-Sided Oil Flow Rate (m^3/day)
Diffusion Only	2.82 E -10	4.87E-05	0.097
Diffusion + Dispersion	1.30 E –09	1.05E-04	0.210

Note that incorporation of dispersion effect is capable to improve the recovery rate twice larger than diffusion dominated process. However, the estimated recovery rates are not attractive enough to make the CO_2-Vapex process economically a viable project. This is primarily due to limited solubility of carbon dioxide at the operating pressure limit of 1.5 MPa. In that regard, the viscosity of diluted bitumen is only 25 times less than that for undiluted bitumen. Propane and butane are capable to reduce the viscosity of bitumen by 3 to 4 orders of magnitude and therefore have a far better chance to produce an economically viable project.

7.5.2 Underground Storage of CO_2

From the above discussion, it appears that due to limited solubility of carbon dioxide in heavy oil and small viscosity reduction, CO_2 is not likely to be an effective solvent for Vapex process. Moreover, since Vapex can not accommodate a significant amount of CO_2, (only 3 to 5% by weight of the mixture is comprised of CO_2), it has negligible impact on reduction of greenhouse gases. In spite of the above limitations, underground storage of CO_2 or other greenhouse gases in depleted oil and bitumen reservoirs is still possible as a complementing phase in Vapex process. In that regard, injection of hydrocarbon solvents can initiate the Vapex process. Towards the completion of the process where recovery rates approach the economic cut-off value, in-situ hydrocarbon gases can be blown down and CO_2 injection can be started afterwards.

One of the main parameters controlling the underground storage capacity of CO_2 is the maximum operating pressure limit of the reservoir. This limit is primarily set by the tensile strength of the formation and the cap rock. Usually, shallow deposits have small overburden pressure and hence the stresses confining the rock are limited. Therefore, these formations can not sustain high operating pressures, or otherwise they would be fractured. To assure safe underground storage of greenhouse gases, more detailed investigation of rock mechanics in the proposed formations is necessary which is beyond the scope of this research.

The following example is dedicated to examine the potential capability of CO_2 sequestration and reduction of greenhouse gases.

Most heavy oil deposits in Canada lie at temperatures in the range of 10 to 20°C. Assuming an average reservoir pressure of 1.5 MPa (which is typical in these formations), an average CO_2 solubility of 4% (wt) and a formation volume factor of B_{CO2}=0.055 m^3/scm can be expected. Experience from SAGD indicates that gravity drainage dominated processes can recover up to 50-60% of the original oil with a reasonable production rate. However, if only 20% of the 95 billion m^3 non-mineable bitumen in Alberta is produced by SAGD or Vapex, it would create an underground storage capacity to accommodate 345 billion scm of GHG, equivalent to 680 million ton CO_2. On the global scale, this number is extremely small and is just equal to the current annual level of GHG emission in Canada. At the same time, if we assume that 50% of the GHG emissions by electricity and steam generation plants in Alberta is captured and injected to such underground reservoirs, it can serve for only 27 years. Therefore, sequestration of carbon dioxide or other greenhouse gases into depleted oil and bitumen reservoirs is not likely to provide a long-term solution to GHG emission.

Diffusion of CO_2 into bitumen is a time dependent process. Therefore, unless the number of injectors/reservoirs involved (in sequestration of CO_2) are significantly increased, it is not likely that Vapex or any other EOR method would be able to capture even a small fraction of annual GHG emission in Canada. Therefore, it appears that the most effective long-term solution to the global warming problem, is direct reduction of such emissions.

CHAPTER EIGHT
CONCLUSIONS, IMPORTATNT OBSERVATIONS AND RECOMMENDATIONS

8.1 Conclusions

1. Experiments in Hele-Shaw cell indicate that incorporation of convective dispersion reduces the discrepancy between the experimental results and analytical models at identical values of Peclet number. It is important to mention that utilization of Taylor dispersion formulation (for computation of an effective diffusion coefficient) in it's original form is primarily for cursory examination purposes. However, the main objective of this analysis is to highlight that convective dispersion is an important phenomenon, which has been overlooked in the context of Vapex modeling, even in the Hele-Shaw cell.

2. Experiments in Hele-Shaw cell indicates that calculated effective diffusivity increases as the Peclet number is increased. This behavior is similar to the reported dispersion effects in porous media under favorable viscosity ratio. However, the same behavior was not observed during the analysis of Vapex experiments in porous media, where viscosity ratio is unfavorable.

3. The coefficients of longitudinal and transverse dispersion in porous media (0.5 and 0.0157) by earlier researchers are valid only in systems under favorable viscosity ratio. These conditions are not met in Vapex experiments and hence the corresponding dispersion coefficients are not valid. Additional experiments in porous media, dedicated to measurement of dispersion effect under unfavorable viscosity ratio at low velocity, are necessary.

4. Incorporation of viscosity ratio, as a matching parameter to the existing correlations for estimation of dispersion coefficient appears to improve the quality of history match for almost all the experiments, both in Hele-Shaw cell and Sandpack.

5. Investigation of CO_2 solubility in bitumen indicates that only 3 to 5% by weight of the diluted oil is comprised of CO_2. Therefore, the dissolved CO_2 in bitumen has negligible impact on temporary reduction of greenhouse gases.

6. The created vapor chamber in Vapex has some potential for underground storage of greenhouse gases. However, since the maximum safe injection pressure limit in such shallow reservoirs is very small, underground storage capacity of the created vapor chamber is not significant. Therefore, the created vapor chamber is unable to capture even a small fraction of the annual GHG emission in Canada. As the shrinkage factor of CO_2 and hence storage capacity is directly related to injection pressure, the maximum injection pressure limit of such formations have to be investigated through analysis of rock mechanics.

8.2 Important Observations

1- Experiments in Hele-Shaw cell at lowered temperatures resulted in asphaltene precipitation. This observation is similar to the results of experiments by previous investigators.

2- Enhanced interfacial mass transfer in Vapex process is directly related to the amount of solvent dissolving into bitumen. In a steady state process (if achievable), the rate of recovery in the 2-phase region has to be balanced with that in the leading front. Therefore, in a steady state process, mass transfer of the solvent at the leading front is the main limiting factor of the overall process.

3- At the leading front, mass transfer is exclusively controlled by diffusion and dispersion processes. Longitudinal dispersion develops along the solvent/bitumen interface (bulk flow direction), while transverse dispersion occurs perpendicular to this interface and towards the bitumen bulk. Incorporation of dispersion process into the mathematical model of Vapex can significantly improve the results. The combination of all the processes within the 2-phase region (increased surface area of contact, capillary imbibition and surface renewal, etc.) only tend to control the thickness of the 2-phase region, rather than influencing the rate of mass transfer.

4- The effective diffusivity used for computation of N_s parameter in these analyses is calculated based on coupling the intrinsic molecular diffusion coefficient of solvent in bitumen and dispersion processes in porous media.

5- Analytical correlations from literature (Hayduk et al. 1973, Hayduk and Minhas 1982) appear to provide adequate estimates of molecular diffusivity as a function of solvent concentration in bituminous systems. The correlation by Das & Butler (1996) is primarily based on matching the experimental recoveries in Hele-Shaw cell to an

equation similar to that proposed by Hayduk et al. (1973). Since the correlation by Das & Butler does not account for dispersion effects, it tends to overestimate the molecular diffusion coefficient, and underestimate the overall mass transfer, in terms of a coupled diffusion-dispersion process in porous media.

6- Analyses of data from Vapex experiments in porous media indicate a direct relationship between viscosity ratio and the β multiplier for a given Peclet number. In that regard, for a given particle diameter making up the porous media, the required dispersion multiplier needed to history match the experimental data increases, as the viscosity ratio increase.

7- Experimental data in porous media also indicate an inverse relationship between particle diameter and dispersion coefficient β (see equation 6.7), for a given viscosity ratio. This observation confirms the reported experiments by several authors that dispersion effects tend to increase as particle diameter gets smaller. Interestingly, earlier analytical models of dispersion (equation 3.1 and 3.2) were not capable to capture this behavior, even under favorable viscosity ratio.

8- The main difference between the Hele-Shaw cell and porous media is that flow in Hele-Shaw cell is not affected by grain particles. Analysis of data suggests that there is an inverse relationship between dispersion and particle diameter (see Figure 6.10). This dependency is captured in analytical correlation for estimation of dispersion effect, in terms of a negative exponent for Peclet number, as shown in equation 6.6.

8.3 Recommendations

1- In order to verify the viability of dispersion effects in Hele-Shaw cell environment, additional experiments with different cell spacing are recommended. In order to minimize uncertainties associated with estimated viscosity and diffusivity, identical solute/solvent pair should be used in several different cell spacing.

2- The Taylor-type dispersion in Hele-Shaw cell can be mathematically modeled. The starting point for this modeling is development of a momentum balance based on a two-dimensional velocity distribution, as explained in Chapter-5. The result of this modeling would provide a relationship for calculation of velocity distribution, replacing equation 5.7. This can be further linked with a solvent mass balance and subsequently solved with respect to appropriate boundary conditions. Our earlier attempt had indicated that due to non-symmetric velocity profile in Hele-Shaw cell, analytical modeling of the process is extremely complex and the resultant equation would be rather solved numerically.

3- Although laboratory experiments are extremely time consuming, measurement of diffusivity vs. concentration by these techniques provides more reliable results and are strongly recommended. Laboratory investigations (Oballa & Butler 1989, Upreti 2000) indicate that in some systems, intrinsic diffusivity reaches a maximum value at the intermediate concentration range. This behavior could be due to simplification of the solution mixture in terms of a binary system. Existence of asphaltenes, particularly in bituminous solutions, violates the assumption of a binary system and in turn might cause the observed peak diffusivity at intermediate concentration. Therefore, further refinement of the theoretical models for analysis of experimental data might be necessary.

References

1. Allen, J. C., "Gaseous Solvent Heavy Oil Recovery", Canadian Patent No. 1027851, (1974)

2. Archie G. E., "The Electrical Resistivity Log as an Aid in Determining Some Reservoir Characteristics", J. Pet. Tech., Vol.5, No. 1, January, (1942)

3. Aris R. and Amundson N. R., "Some Remarks on Longitudinal Mixing or Diffusion in Fixed Beds", AIChE Jour., Vol. 3, 280, (1957)

4. Bachu S., "Disposal and Sequestration of CO2 in Geological Media", AEUB – Alberta Geologic Survey, September, (1999).

5. Blackwell R. J., "Laboratory Studies of Microscopic Dispersion Phenomena", SPE J., p.1-8, March, (1962)

6. Bird R. B., Stewart W. E., Lightfoot E. N., Transport Phenomena, 7th Ed., John Wiley and Sons, Inc., New York, p. 150, (1966)

7. Brigham, W. E., Reed, P. W. and Dew J. N., "Experiments on Mixing During Miscible Displacement in Porous Media", SPE J., p. 1-8, March, (1961)

8. Brock J. R. and Bird R. B., "Surface Tension and The Principle of Corresponding States", AIChE Jour.,Vol.1, No. 2, p. 174-177, June, (1955)

9. Butler R. M., "Horizontal Wells For The Recovery of Oil, Gas and Bitumen", Petroleum Society Monograph No.2, CIM, Calgary, Alberta, p. 172-176, (1994)

10. Butler R. M., Thermal Recovery of Oil & Bitumen, Prentice-Hall Inc., Englewood Cliffs, New Jersey , p. 248-250, (1991)

11. Butler R. M., McNab G. S., Lo H.Y., "Theoretical Studies on The Gravity Drainage of Heavy Oil During In-Situ Steam Heating", Can. J. Chem. Eng., 59, (1981)

12. Butler R. M., Mokrys I. J., "A New Process (VAPEX) For Recovering Heavy Oils Using Hot Water and Hydrocarbon Vapor", JCPT, Vol.30, No.1, June, (1991)

13. Butler R. M., Mokrys I. J., "Recovery of Heavy Oils Using Vaporized Hydrocarbon Solvents: Further Development of The VAPEX Process", JCPT, Vol.32, No.6, June , (1993)

14. Butler R. M., Mokrys I. J., "Closed-Loop Extraction Method for the Recovery of Heavy Oils and Bitumens Underlain by Aquifers: The Vapex Process", Paper 1993-24, Fifth Petroleum Conference of South Saskatchewan Section, Regina, Saskatchewan, Canada, October 18-10, (1993)

15. Butler R. M., Mokrys I. J., "Solvent Analog Model of Steam-Assisted Gravity Drainage", AOSTRA J. Res., 5, p. 17, (1989)

16. Butler R. M., Stephens D. J., "The Gravity Drainage of Steam-Heated Heavy Oil to Parallel Horizontal Wells", JCPT, April-June , (1981)

17. Butler R. M., "Horizontal Wells For The Recovery of Oil, Gas and Bitumen", SPE Reprint Series, (1996)

18. Carman P. C., "Permeability of Saturated Sands, Soils and Clays", J. Agri. Sci., Vol. 29, 262, (1939)

19. Das S. K., "VAPEX: An Efficient Process for The Recovery of Heavy Oil and Bitumen", SPE J., September, p.232-237, (1998)

20. Das S. K., Butler R. M., "Mechanism of The Vapor Extraction Process For Heavy Oil and Bitumen", J. Pet Sci. Eng., 21, p.43-59, (1998)

21. Das S. K., Butler R. M., "Diffusion Coefficients of Propane and Butane in Peace River Bitumen", Can. J. Chem. Eng., Vol.74, No.6, p.985-992, (1996)

22. Das S. K., Butler R.M., "Extraction of Heavy Oil and Bitumen Using Solvents at Reservoir Pressure", paper No.95-118, Sixth Petroleum Conference of the South Saskatchewan Section, Regina, Canada , October 16-18, (1995)

23. Das S. K., "In-Situ Recovery of Heavy Oil and Bitumen Using Vaporized Hydrocarbon Solvents", PhD. Thesis, The University of Calgary, Alberta, Canada, (1995)

24. Das S.K., Butler R.M., "Effect of Asphaltene Deposition on the Vapex Process: A Preliminary Investigation Using a Hele-Shaw Cell", JCPT, Vol. 33, No.6, June, p. 39-45, (1994)

25. Dunn S. G., Nenniger E. H. and Rajan V. S. V., "A Study of Bitumen Recovery by Gravity Drainage Using Low-Temperature Soluble Gas Injection", Can. J. Chem. Eng., 67, p. 978-991, (1989)

26. Environment Canada Website, National Pollutant Release Inventory, Air Pollutant Emissions, http://www.ec.gc.ca/pdb/ape/cape_home_e.cfm

27. Fisher, D. B., Singhal, A. K., Das, S. K. and Golman, J., "Use of Magnetic Resonance Imaging and Advanced Image Analysis as a Tool to Extract Mass

Transfer Information from a 2D Physical Model of the Vapex Process", SPE 59330, SPE/DOE Improved Oil Recovery Symposium, Tulsa, Oklahoma, April 3-5, 2000.

28. Fu B. C., H., Phillips C. R., "New Technique for Determination of Diffusivities of Volatile Hydrocarbons in Semi-Solid Bitumen", Fuel, Vol. 8, (1979)

29. Hayduk W., Minhas B. S., "Correlations for Prediction of Molecular Diffusivities in Liquids", Can. J. Chem. Eng., Vol. 60, April, p. 295-299, (1982)

30. Hayduk W., Castaneda R., Bromfield H., Perras R. R., "Diffusivities of Propane in Normal Paraffin, Chlorobenzene, and Butanol Solvents", AIChE J. 19, p.859-861, (1973)

31. Hiss, T. G. and Cussler, E. L., "Diffusion in High Viscosity Liquids", AIChE J., Vol. 19, p 698-703, (1973)

32. Hayduk, W. and Cheng S. C., "Review of Relation Between Diffusivity and Solvent Viscosity in Dilute Liquid Solutions", Chem. Eng. Sci., Vol. 26, p.635-646, (1971)

33. Hayes M. J. , Park G. S., "The Diffusion of Benzene in Rubber", Trans Farad Soc., Vol. 52, p.949-955., (1956)

34. Hutcheon A. T., Kokes R. J., Hoard J. L., Long F. A., "Interdiffusion of Polyvinyl Acetate with a Series of Solvents", J. Chem. Phys, Vol. 20, No. 8, August, p.1232-1236, (1952)

35. Keller C. F., Reply to "Human Contributions to Climate Change Remains Questionable", EOS, Forum, August, (1999)

36. Lim G. B., Kry R. P., Harker B. C., Jha K. N., "Three-Dimensional Scaled Physical Modeling of Solvent Vapour Extraction of Cold Lake Bitumen", JCPT, Vol. 35, No. 4, April, p.32-40, (1996)

37. Mehrotra A. K., " Mixing Rules for Predicting the Viscosity of Bitumens Saturated with Pure Gases", JCPT, Vol. 70, February, p.165-172, (1992)

38. Mokrys I. J. and Butler R. M., "The Rise of Interfering Solvent Chambers: solvent analog model of steam-assisted gravity drainage", JCPT, Vol. 32, No. 3, March, p.26-26, (1993)

39. Monnery W. D., Mehrotra A. K., Svercek W. Y., "Viscosity Prediction of Nonpolar, Polar and Associating Fluids over a Wide $P_\rho T$ Range from a Modified Square Well Intermolecular Potential Model", Ind. Eng. Chem. Res., July 37, p.652-659, (1998)

40. Neitzert F., Olsen K., Collas P., "Canada's Greenhouse Gas Inventory 1997 Emissions and Removals with Trends", Greenhouse Gas Division, Environment Canada, PDB, APPD Report, April, (1999).

41. Nghiem L. X., Kohse B. F., Sammon P. H., "Compositional Simulation of the Vapex Process", Paper 2000-34, Canadian International Petroleum Conference, Calgary, Alberta, Canada, June 4-8, (2000)

42. Norman Ann-Lise, "Atmospheric Environment Chemistry; lecture notes on Environmental Science for Engineers", Atmospheric Science Division, Stable Isotope Group, The University of Calgary, (2000)

43. Oballa V., Butler R. M., "An Experimental Study of Diffusion in The Bitumen-Toluene System", JCPT, Vol. 28, No. 2, March-April, p. 63-69, (1989)

44. Parties to the Climate Change Convention, "Second Compilation and Synthesis Report of first national communications", United Nations Environmental Program, Doc. FCCC/CP/1996/12, (1996)

45. Perkins T. K., Johnston O. C., "A Review of Diffusion and Dispersion in Porous Media", SPE Reprint Series, Miscible Displacement, p. 77-91, (1963)

46. Reid, R. C., Prausnitz, J. M. and Poling, B. E., "The Properties of Gases & Liquids", Fourth edition, McGraw-Hill Book Co., New York, p.597-598, (1987)

47. Riazi M. R., "A New Method for Experimental Measurement of Diffusion Coefficients in Reservoir Fluids", J. Pet. Sci. Eng., Vol. 14, p. 235-250, (1996)

48. Robinson A. B., Baliunas S. L., Soon W., and Robinson Z. W., " Environmental Effects of Increased Atmospheric Carbon Dioxide", Oregon Institute of Science and Medicine, [info@oism.org], January, (1998)

49. Sahimi M, Heiba A. A., Hughes B. D., Davis H. T., Scriven L. E., "Dispersion in Flow Through Porous Media", SPE 10969, 57th Annual Technical Conference and Exhibition, New Orleans, LA September 26-29, (1982)

50. Schmidt T., Leshchyshyn T. H., Puttagunta V. R., "Diffusivity of Carbon Dioxide Into Athabasca Bitumen", 33rd Annual Technical Meeting of Petroleum Society of CIM, Calgary, Alberta, Canada, June, (1982)

51. Schmidt T., "Mass Transfer by Diffusion", AOSTRA Technical Handbook on Oil Sands, Bitumens and Heavy Oils, Hepler L. G. and Hsi C. (eds), AOSTRA Technical Publication Series No.6, Edmonton, Alberta, Canada, p.155-175, (1989)

52. Shu W. R., "A Viscosity Correlation for Mixtures of Heavy Oil, Bitumen, and Petroleum Fractions", SPE J., June, p.277-282., (1984)

53. Singer S. F., "Human Contributions to Climate Change Remains Questionable", EOS, Forum Article, April (1999)

54. Singhal A., Personal Communications, Petroleum Recovery Institute (PRI), Calgary, Canada, July (1999)

55. Svrcek W. Y. and Mehrotra A. K., " Gas Solubility, Viscosity and Density Measurements for Athabasca Bitumen", JCPT, July-August, p.31-38, (1982)

56. Taylor G. I., "Dispersion of Solute Matter in Solvent Flowing Slowly Through a Tube", Proc. Royal. Soc. Vol. 219, p.186-203, (1953)

57. Upreti S. R., "Experimental Measurement of Gas Diffusivity in Bitumen: Results for Carbon Dioxide", PhD. Thesis, The University of Calgary, Alberta, Canada, (2000)

58. Wilke, C. R. and Chang, P., "Correlation of Diffusion Coefficients in Dilute Solutions", AIChE J., 1, 264, (1955)

59. Zhang Y., Hyndman C. L., Maini B. B., "Measurement of Gas Diffusivity in Heavy Oils", 49th Annual Technical Meeting of Petroleum Society of CIM, Calgary, Alberta, Canada, June 8-10, (1998)